Fraunhofer
ICT

Fraunhofer Institute for Chemical Technology ICT

Manipulation of Carbon Nanoparticles in Composites for Improved Electrical Properties

Manuel Maria Vilão Cruz Gião Morais

Wissenschaftliche Schriftenreihe
des Fraunhofer ICT
Band 91

FRAUNHOFER VERLAG

Fraunhofer Institute
for Chemical Technology

Manuel Maria Vilão Cruz Gião Morais

Manipulation of Carbon Nanoparticles in Composites for Improved Electrical Properties

Wissenschaftliche Schriftenreihe
des Fraunhofer ICT
Band 91

FRAUNHOFER VERLAG

Editor:
Fraunhofer-Institut for Chemische Technologie ICT
Joseph-von-Fraunhofer-Straße 7
76327 Pfinztal (Berghausen)
Phone 0721 4640-0
Fax 0721 4640-111

Bibliographic information of the German National Library:
The German National Library has listed this publication in its Deutsche Nationalbibliografie; detailed bibliographic data is available on the internet at www.dnb.de.

D 90

Zugl.: Karlsruhe, KIT, Diss., 2020

ISBN 978-3-8396-1685-7

Print and finishing:
Fraunhofer Verlag, Mediendienstleistungen

The book was printed with chlorine- and acid-free paper.

Nobelstrasse 12
70569 Stuttgart
Germany
verlag@fraunhofer.de
www.verlag.fraunhofer.de

is a constituent entity of the Fraunhofer-Gesellschaft, and as such has no separate legal status.

Fraunhofer-Gesellschaft zur Förderung
der angewandten Forschung e.V.
Hansastrasse 27 c
80686 München
Germany
www.fraunhofer.de

Manipulation of carbon nanoparticles in composites with electric fields for improved electrical properties

Zur Erlangung des akademischen Grades eines
Doktors der Ingenieurwissenschaften (Dr.-Ing)

von der KIT-Fakultät für Maschinenbau des
Karlsruher Instituts für Technologie (KIT)
angenommene

Dissertation

von

MSc. Manuel Maria Vilão Cruz Gião Morais

Tag der mündlichen Prüfung:	2. Juni 2020
Hauptreferent:	Prof. Dr.-Ing. Frank Henning
Korreferent:	Prof. Dr.-Ing. Tim A. Osswald

Declaration

I hereby certify that, to the best of my knowledge, the intellectual content of this dissertation is the product of my own work and that all the assistance received in preparing it and sources have been indicated or acknowledged. This material has not been submitted for any degree or examination elsewhere.

Manuel Maria Vilão Cruz Gião Morais

To my family and friends...

Acknowledgements

This work is not only product of my own efforts but also from the many people that accompanied me along this journey. It was very challenging from the beginning both at a scientific and a personal level and it would definitely not have been possible without all the support I got along the way.
First of all my gratitude to Frank Henning for accepting me as his doctoral student, supporting and motivating me, and always believing in me. I was always sure that I had his full support and this really encouraged me to succeed. Thanks a lot to Tim Osswald for taking the time and interest to review my work and evaluate it, and all the suggestions for further investigations. I would also like to thank the chairman Prof. Volker Schulze for giving his time to the preparation and organisation of the exam.
In general I feel really grateful and lucky for the chance of working at the Fraunhofer Institute for Chemical Technology (ICT). There I met a lot of scientists with genuine interest, curiosity and pleasure about finding things out but also sharing their knowledge and helping the other, despite language barriers. Only in such a ecosystem would I be able to attempt such experiments from scratch and into so many questions and unknowns. So I would like to thank the ICT and all the colleagues with all my heart.
Some of the colleagues, however, truly deserve dedicated words. My deep gratitude to Christof Hübner. For believing in me since the very beginning, after he picked me up on the S-Bahn stop at the foot of the Hummelberg for my job interview. If I feel I grew up a lot in the last 5 years, much of it was thanks to Christof and his patience and guidance.
Even with all the support and guidance, none of the work would have been the same without Markus Schönwald. My deepest appreciation for your inter-

est and friendship, all the fruitful discussions and all the technical solutions that made the experiments possible.
To the students that helped me and supported my work: Elisabeth Ortelt, Nicolas Unger, Marco Marcellan, Robin Reidel and Nadine Sohn.
To Patrick Weiss, Irma Mikonsaari, Ralf Dreher and Burak Çağlar for all the discussions and support. To Birgit Eickershoff for all the time and ideas to find the nanotubes on the scanning electron microscope. To Ulrich Förter-Barth for the rheology experiments and the discussions around the results.
To Andrés Oliva-Avilés for his interest and time for working together, his guidance and contributions to this work.
Thanks to the European Commission for funding the TheLink project, under the Marie Skłodowska-Curie Grant Agreement no. 642890 (`http://thelink-project.eu`). To all the researchers involved in TheLink, for the exchange of ideas and motivation to carry on. To Milo Shaffer and Sandy Fisher for all the discussions and hosting me at the Imperial College London. To Imanol Recio Erquicia and Julio Gomez at Avanzare for the graphene nano-platelets. To Denis Ganin for all the trials, discussions and support. To Rosério Valente for the productive exchange of ideas, the motivation and inspiration. A big thanks to Miguel Matos for his support and collaboration that resulted in a publication together and greatly contributed to this work. And finally a special thanks to Carolyn Fisher for the organisation and motivation to make us learn and grow.
To all my remaining friends, who supported me, excused my absence and alienation during this time and in the end still want to remain friends.
To my family, in particular my mother Teresa, my father Pedro, my sister Maria, my brother Zé and my grandmother Rosa for their unconditional patience, support and belief.
To Anna Marcellan, for a whole lot of patience and support throughout this journey.

Abstract

The dispersion of electrically conductive nanoparticles in a polymer matrix enables the production of an useful class of materials: electrically conductive polymeric composites. However, tuning the electrical conductivity of the final conductive composite is not trivial: many variables play a role in view of the final particle network structure in the composite, which governs the electrical conductivity. In this work, the electrical properties of epoxy nanocomposites with carbon nanoparticles as conductive filler are investigated for different processing conditions.

Compared to a classical shaping process for epoxy materials, the application of electric fields during the curing process is used as an additional process parameter. Electric fields are applied to the nanocomposites during curing, influencing the electrical properties of the final material by inducing polarization and dipole interactions between the conductive particles (dielectrophoresis), leading to a new micro- and nanostructure of the conductive network. This phenomenon is studied for a system of single-wall carbon nanotube and the impact of processing parameters on the electrical response of the system is evaluated.

A scalable process based on resin transfer moulding for producing nanocomposites under electric fields is developed.

This processing technique presents promising results for enhancing and tailoring the electrical conductivity of polymer nanocomposites.

For a better understanding of the effect of electric fields on the rotation and interconnection of SWCNTs, the own findings are compared to simulations of cooperating scientists from Anáhuac Mayab University (Merida, Mexico) and Imperial College London (United Kingdom).

Zusammenfassung

Die Dispersion elektrisch leitfähiger Nanopartikel in einer Polymermatrix ermöglicht die Herstellung einer nützlichen Materialklasse: elektrisch leitfähige Polymerkomposite. Die gezielte Einstellung der elektrischen Leitfähigkeit des leitfähigen Komposits ist jedoch nicht trivial, da viele Material- und Verarbeitungsparameter die Partikel-Netzwerkstruktur im Komposit beeinflussen die letztlich für die elektrische Leitfähigkeit ausschlaggebend ist. In dieser Arbeit werden die elektrischen Eigenschaften von Epoxid-Nanokompositen mit Kohlenstoff-Nanopartikeln als leitfähigem Füllstoff für verschiedene Verarbeitungsbedingungen untersucht.

Im Unterschied zu einem klassischen Formgebungsverfahren für Epoxidmaterialien wird die Anwendung von elektrischen Feldern während des Aushärtungsprozesses als zusätzlicher Prozessparameter benutzt. Elektrische Felder werden während des Aushärtens an die Nanokomposite angelegt, wodurch die elektrischen Eigenschaften des Endmaterials durch Induktion von Polarisations- und Dipol-Wechselwirkungen zwischen den leitenden Partikeln (Dielektrophorese) beeinflusst werden. Diese führen zu einer neuen, und im Hinblick auf die elektrische Leitfähigkeit vorteilhaften Mikro- und Nanostruktur des leitfähigen Netzwerks. Dieses Phänomen wird für ein System von einwandigen Kohlenstoff-Nanoröhren in einer Epoxidharzmatrix im Hinblick auf den Einfluss verschiedener Verarbeitungsparameter auf die elektrische Leitfähigkeit des Systems untersucht. Darauf aufbauend wird ein skalierbares Verfahren auf der Grundlage des Harzinjektionsverfahrens zur Herstellung von Nanokompositen unter elektrischen Feldern entwickelt.

Für ein besseres Verständnis der Mechanismen, die der Wirkung elektrischer Felder auf die Rotation und die Verschaltung von SWCNTs werden

die eigenen Ergebnisse mit Simulationen kooperierender Wissenschaftler der Anáhuac Mayab University (Merida, Mexiko) und das Imperial College London (Vereinigtes Königreich) verglichen.

Table of Contents

List of Figures

List of Tables

Acronyms

AC alternate current

AFM atomic force microscopy

CB carbon black

CNT carbon nanotube

DC direct current

DIW deionised water

DMF dimethylformamide

DPSF dissolved polysulfone

FE finite element

GNP graphene nano-platelet

MR mould release agent

MWCNT multi-wall carbon nanotube

PTFE polytetrafluoroethylene

RMS root mean square

RT room temperature

RTM resin transfer moulding

RVE representative volume element

SEM scanning electron microscopy

SWCNT single-wall carbon nanotube

TEM transmission electron microscopy

UV ultra violet

Notation

Mathematical operators

(defined on variable ζ)

Δ	difference, $\Delta\zeta = \zeta_2 - \zeta_1$
$\bar{\zeta}$	homogenised/averaged
$Re[\zeta]$	real part

Lower case Greek letters

α^*	polarisation factor
β	CNT-to-CNT separation distance
δ	thickness of interphase layer
$\tan\delta$	loss factor
ϵ	electrical permittivity
ϵ_{CNT}	CNT electrical permittivity
ϵ_m	surrounding medium electrical permittivity
ϵ_{lay}	interphase layer electrical permittivity
η^*	complex viscosity
$\mid \eta^* \mid$	modulus of complex viscosity
μ	dynamic viscosity
ϕ	particle concentration
ϕ_c	percolation threshold
$\bar{\varphi}$	mean potential barrier
φ_0	potential barrier magnitude

ρ	volume resistivity
$\bar{\rho}$	composite homogenized resistivity adimensionalised
σ	electrical conductivity
σ_{CNT}	CNT electrical conductivity
σ_m	surrounding medium electrical conductivity
σ_{lay}	interphase layer electrical conductivity
θ_1, θ_2	deviation angles

Lower case Roman letters

a	CNT major semi-axis
a_R	distance from pins to edge of the sample
b	CNT minor semi-axis
d	distance between electrodes or sample thickness
d_{CNT}	is the CNT density
$d_{cut-off}$	cut-off distance
d_{min}	minimum distance separating CNT
e	charge of an electron
f	electric field frequency
h	Planck's constant
m	mass of CNTs
m_e	mass of an electron
s	CNT junction separation
s_R	distance between measuring pins (four-point method)
t	power law upper critical exponent
x_1,x_2	coordinates of centres of charge

1 Introduction

A polymer composite is a material composed of a variety of particles, platelets, short or continuous fibres embedded in an organic polymer matrix. This allows engineers to tailor the mechanical behaviour of the material system by combining different properties in only one final product. When the fibres, or functional fillers, have their size in the nanometre range (1×10^{-9} m), the material can be defined as a polymer nanocomposite. Unlike metals, which tend to have a defined conductivity depending on their elemental properties[1], electrically conductive polymer nanocomposites encompass a wide conductivity range, from insulator to almost metallic behaviour [3] (see figure 1.1). This is because the electrical conductivity arises from conductive nanoparticles, which can be added to virtually any polymer matrix in different concentrations according to the desired final electrical properties. Adding this electrical functionality to the other properties of the polymer matrix, together with versatile processing technologies, leads to two main industrial opportunities for electrical conductive nanocomposites:

- adding electrical functionality to existent non-conductive systems - expanding the possibilities for integration of sensing and connectivity capabilities
- replacement of metals for electrical conductivity - allowing the introduction of new materials in novel battery concepts (e.g. in bipolar plates for redox-flow batteries) and enabling considerable weight reduction in conductive components

[1] aluminium, gold, copper and silver have a conductivity in the range $3.8 \times 10^5\,\mathrm{S\,cm^{-1}}$ to $6.3 \times 10^5\,\mathrm{S\,cm^{-1}}$ [1, 2]

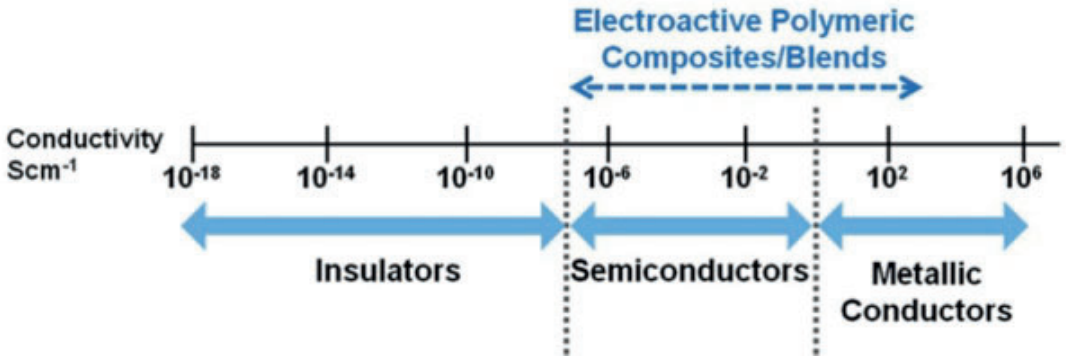

Figure 1.1: Conductivity range of conductive polymers and polymeric composites [3]

These two possibilities have motivated the use of electrically conductive polymer nanocomposites in diverse fields of application such as heating elements [4], electromagnetic interference shielding [5, 6], electrostatic dissipation [7], battery technology [8] and fuel cells [9]. Furthermore, their electrical response to external stimuli (e.g. mechanical, thermal, chemical) enables several kinds of sensing applications [3, 10], such as monitoring strain and damage for structural health monitoring systems [11], gas [12], or biodegradation [13], amongst others.

Amongst the large variety of nanoparticles available, carbon-based particles are a great example of multi-functionality, promising remarkable electrical, thermal and mechanical properties. These include carbon nanotubes (CNTs) and graphene nano-platelets (GNPs). Their electrical properties arise due to the carbon atomic structure, which allows for an electron conduction band resulting in metallic or semiconducting properties (depending on their chirality and wall structure in the case of CNTs) [14, 15]. Furthermore, their dimensions in the nanometer range, practically at the atomic scale, combined with very low density and aspect ratios (orders of 100 to 3000) lead to very high properties per unit weight. This enables considerable improvements in composites already by relatively low concentrations [15, 16]. An illustration of this effect is the transition from an electrically insulative state to conductive in polymer composites with less than 0.1 wt% CNTs [16].

However, tuning the electrical conductivity of the final conductive composite is not trivial. According to the percolation theory [17], for each material system there is a minimum concentration threshold that enables the flow of electrons through the material. Below this concentration, the material is electrically insulating, since there are no pathways for current to pass through. Then, at the percolation concentration, an abrupt increase of many orders of magnitude in the conductivity takes place. Around this concentration, only a few conductive paths exist and therefore the influence of contact resistance is more significant. Far above the critical concentration, adding more CNTs results in more parallel conductive paths, and therefore these pathways become the dominant conductivity mechanism [18, 19]. This is represented in figure 1.2. Nonetheless, it should be noted that this theory does not take the processing method used to produce the composite into account.
In literature it is possible to find numerous reports of percolation thresholds for different polymer-particle matrix systems [16, 19]. This value mainly depends on the particle shape and properties as well as on the matrix and the selected processing technique. Many variables play a role on the final parti-

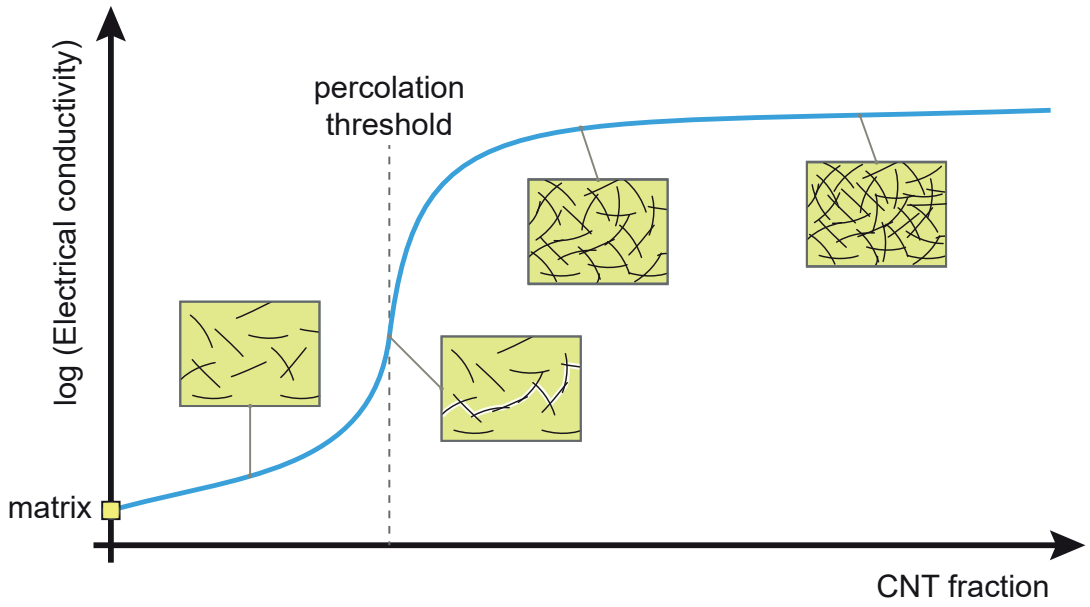

Figure 1.2: Evolution of electrical conductivity with CNT content in a composite - percolation behaviour

cle network structure such as the original state of agglomeration and geometry of the particles, viscosity of the matrix, processing parameters such as temperature and shear stresses undergone by the material [20, 21, 22]. For example, taking a thermoplastic-based composite and producing samples with compression moulding, usually leads to samples with a higher conductivity as their injection moulded counterparts, given the flow in the mould and the high shear stresses in the process [23].

Understanding the role of different processing parameters on the resultant nanoparticle network structure, and how this influences the final effective properties of the composites, is therefore of paramount importance for exploring their full potential and enabling their industrial widespread use. This will allow the concentration of particles required to be decreased, optimizing and improving the quality of processing and hence achieving commercial feasibility.

One convenient approach for influencing nanoparticles dispersed in liquid medium is the use of electric fields: inducing polarisation of the particles leads to dipole interactions between them in a phenomenon governed by the dielectrophoretic theory (see Figure 1.3). Since the pioneer reports of Yamamoto et al. [24, 25], the use of electric fields for CNT manipulation has been frequently addressed in the literature. However, up until the work of Martin et al. [26] in 2005, electric fields had only been applied to dispersions of nanotubes in different solvents such as ethanol and dimethylformamide. Following their experiments, dielectrophoresis has been reported to influence the network structure of CNTs in different polymer matrices and hence the electrical properties (see chapter 2).

The present study focuses on the improvement of the electrical conductivity of nanocomposites, namely in a system of epoxy and single-wall carbon nanotubes (SWCNTs). SWCNTs were chosen because of their extremely high aspect ratio (2777) and reported percolation at 0.01 wt% [27]. The goal here is to enhance the network by influencing the SWCNTs orientation within the polymer matrix and hence improve the electrical conductivity in the through-plane direction. Moreover, this improvement is to be achieved by modifying

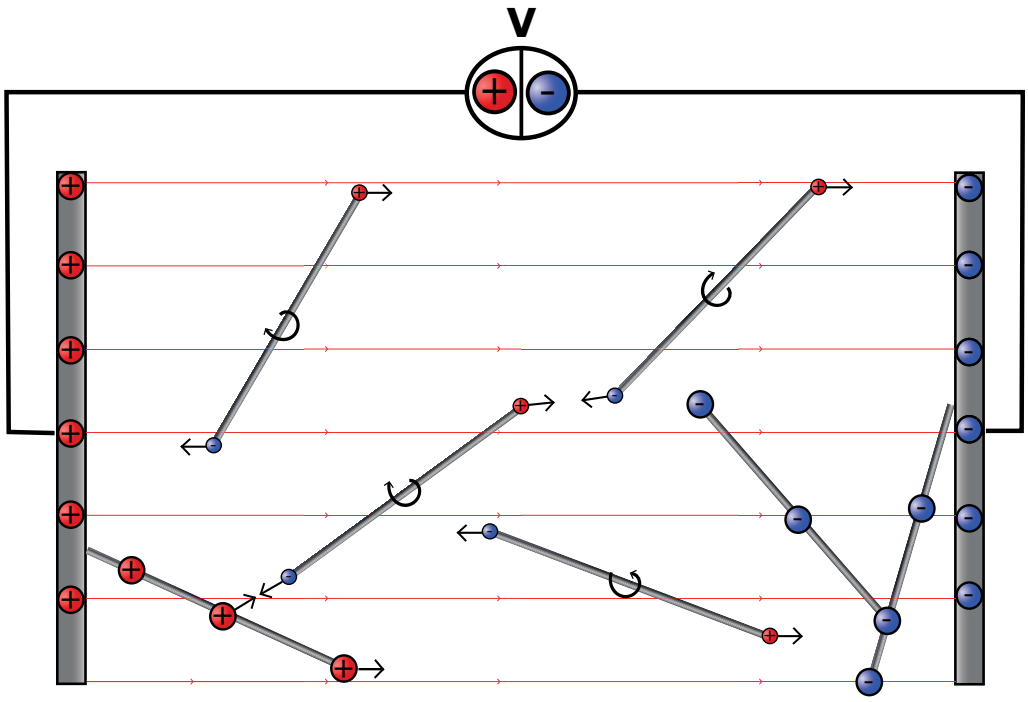

Figure 1.3: Randomly dispersed CNTs become polarized and orient under dielectrophoretic forces and torque, interact due to attractive and repulsive Coulomb forces, and assemble in conductive chains

the processing method for a specific composite part. This means developing a way of affecting the nanostructure of the CNTs during the moulding of the composite such that the process could be easily integrated with available technology. This will potentiate its industrial implementation.

The strategy employed to attain the aforementioned goals is to apply an electric field to the SWCNT/epoxy resin while it is still in the liquid form and then cure the composite. Experimental set-ups were therefore developed for this purpose and the effect of different electric field and process parameters on the final electrical resistivity of the composites was investigated. A decrease of up to more than tenfold in the electrical resistivity was verified. This suggests that the electric field improves the inter-particle contacts, therefore creating more conductive pathways between the electrodes and improving the conductive network for the same amount of nanoparticles.

In this work, an extensive experimental study was carried out, while complementary simulation studies were performed by Andrés Oliva-Avilés

(Anáhuac Mayab University, Mexico) and Miguel Matos (Imperial College London, United Kingdom) in order to support the interpretation of the experimental observations. In this context, Andrés Oliva-Avilés studied the influence of the electric field on the CNT rotation and interconnection by modelling the interaction between two SWCNTs using classical mechanics and dielectrophoresis theory. Furthermore, Miguel Matos explored the impact of the distance between adjacent CNTs in the bulk on the electrical properties using finite element analysis for a variety of particle concentrations, revealing resistivity changes compatible with the experimental observations.
Furthermore, the experimental methodology hereby developed was used to investigate dielectrophoresis of graphene nanoplates under electric fields in the same epoxy resin for different concentrations.

1.1 Motivation

Previous studies not only demonstrate the potential of dielectrophoresis for the manipulation of carbon nanotubes within a low viscosity polymeric matrix – promoting nanocomposites with improved particle networks and lower electrical resistivity – but also point out the challenging complexity of the process. Many parameters play a role in this phenomenon, such as electrode material and spacing, CNT type, the liquid medium, particle concentration, electric field voltage and frequency, and duration of exposure to the electric field (see chapter 2).
The dependency of this process on the electric field parameters (strength and frequency), as well as its limitations in terms of the range of particle concentrations where it can be applied (e.g. effectiveness below and above percolation) remain to be addressed. Moreover, there is no study that investigates the influence of the interface material between the electrodes and the nanocomposite.

This thesis aims to provide a clearer understanding of these questions and develop a technology allowing for its implementation in an industrial-relevant environment.

1.2 Objectives

The main objectives of this work are the following:

- Develop a scalable process for producing nanocomposites with carbon based nanoparticles utilizing electric fields
- Produce SWCNT and GNP nanocomposites with decreased electrical resistivity for the same filler ratio by influencing the nanostructure with electric fields
- Understand the role of the electric field parameters (strength and frequency) on the electrical resistivity of SWCNT/epoxy
- Understand the influence of SWCNT concentration on the improvement in resistivity of epoxy nanocomposites

1.3 Outline

This thesis has been divided in 6 chapters. The subject, motivation and objectives of the work have been introduced in Chapter 1. Chapter 2 presents the theory of dielectrophoresis and a review of the state-of-the-art of CNT dielectrophoresis. The experimental methodology is described in chapter 3. Chapter 4 presents the results and discussion of the experiments undertaken. Section 5.2 of Chapter 5 discusses the results of modelling the interactions between two SWCNTs in an electric field using classical mechanics and dielectrophoresis theory and section 5.3 explores the impact of the contact distance between adjacent SWCNTs influenced by these interactions on the composite bulk electrical properties using finite element simulations

of the SWCNT networks. Finally, the main conclusions from the work are drawn in Chapter 6.

2 State-of-the-art

The goal of this work is to create electrically improved nanoparticle networks in polymer composites during processing. The strategy to be followed for this purpose is the application of electric fields to polymer systems in liquid state containing carbon nanotubes.
The application of electric fields to a polymer/nanoparticle system in liquid state for influencing its electrical properties constitutes a complex system with many variables playing relevant roles that need to be considered. Therefore, such a problem requires a thorough understanding of the physical phenomena involved, which implies familiarity with different fields such as material and polymer science, electrokinetics and electronics. In addition, the engineering of nano-composites with particles like carbon-nanotubes is a quite recent practice, in constant development and with many open questions. Nevertheless, given the outstanding theoretical possibilities that this sort of composites promises, there has been a great academic and even industrial interest in the topic. Much literature on it has been produced, and one does not take too long before becoming overwhelmed and realize the disparity of results published.
In order to understand and develop experimental tools to pursue the objectives proposed in the work, this chapter starts by introducing some fundamental concepts of the field of electrokinetics (section 2.1) explaining polarisation and dielectrophoresis. Furthermore, pertinent literature on using electric fields to manipulate the orientation of carbon nanoparticles in liquid dispersions and influence the electrical properties of carbon-based nanocomposites is reviewed. Particular attention is given to the material system used (nanoparticle and matrix), the electric field parameters and the

electrical properties of the composites produced. The most relevant articles for this study are described in detail in section 2.2. Section 2.3 concludes with a summary of the fundamental theoretical concepts found in literature and which form the basis for the hypotheses investigated in this work.

2.1 Polarisation and dielectrophoresis

If an electric field is applied to a system composed by particles in a suspending fluid, electrical forces can act both on the particles and on the fluid. The most significant electrical forces acting on small particles are electrophoresis and dielectrophoresis [28, 29]. The former occurs when the electric field interacts with the net charge of the particles (i.e. the particles are charged). On the other hand, dielectrophoresis takes place when there are induced charges, leading to particle motion. As for the signal to generate the field, it can be either direct current (DC) or alternate current (AC).
When two opposite potentials (voltage) are applied on two non-contacting parallel electric conductors (electrodes) an electric field is established between them. This means that one of the electrodes is supplied with an extra amount of negative charges (electrons). Consequently, the other electrode lacks on electrons. Therefore, if a material sample is placed in between the electrodes, all the electric charges present within the material are attracted to the opposite poled electrodes. This phenomenon is called polarisation. The higher the voltage applied, the higher the amount of charges being placed on the electrodes, and the stronger the electric field and the polarisation. Such a material, containing charges which polarise upon the application of an electric field, is called a dielectric. The charges are bound in the material and are only able to travel limited distances when the field is applied, the positive and negative charges forming dipoles by moving in opposite directions. Figure 2.1 shows a scheme of a dielectric particle being polarised in a dielectric medium when subjected to a uniform electric field E.
There are basically four essential mechanisms for polarisation [29]:

- electronic - attraction of electrons surrounding each atom on the material and hence dislocation of the electron cloud charge centre in respect to the nucleus (depicted in figure 2.2)
- ionic (or atomic) - by acting on the ionic bonds in ionic molecules, which can be tensioned or compressed
- orientational - corresponding to the rotation and reorientation of molecules with permanent dipoles by nature (like water)
- interfacial - due to long-range charge transport, charges are trapped at internal interfaces or at the surface of the dielectric, leading to macroscopic distortion of the field

All non-conducting materials are capable of electronic polarisation. In contrast, ionic and orientational polarisation is only possible in materials that possess ions and permanent dipoles, respectively. Real systems are usually complex and consist of different dielectrics, each one with distinct electrical properties. Due to these differences, when the system is submitted to an electric field, surface charge gathers at the interfaces between the dielectrics leading to interfacial polarisation.
In order to understand the phenomenon of dielectrophoresis one needs to consider the charge distribution at the interface between two different ma-

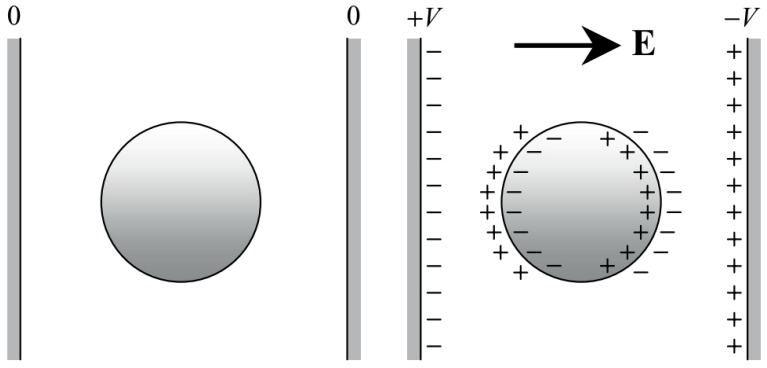

Figure 2.1: Schematic diagram of how a dielectric particle suspended in a dielectric fluid polarises in a uniform applied electric field [29]

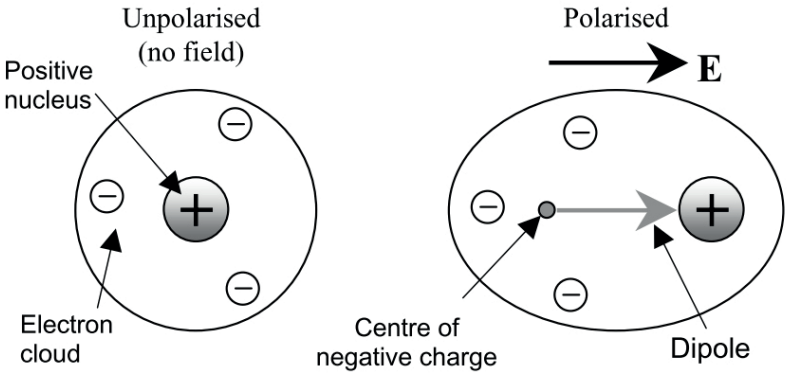

Figure 2.2: Electronic polarisation of an atom [29]

terials with distinct conductivity and/or permittivity. Conductivity (σ) is the measure of ease with which charges are able to flow through a material. Permittivity (ϵ) is the measure of the ability of a material/system to store energy in the polarisation of the medium [29]. At a local scale, polarisability is the ability of molecules to form dipoles, i.e. to react to a field (polarise). If we regard a simple spherical dielectric particle suspended in an electrolyte[1], then there are three cases to account for:

- The polarisability of the particle is much higher than the medium (Figure 2.3a) - more charges accumulate just inside the interface between the particle and medium rather than outside, leading to a difference in the charge density on both sides of the particle and hence to an induced dipole across it, aligned with the electric field. Examples of this situation would be a conducting particle (or with high permittivity) in an insulating liquid (or with low permittivity).

- The polarisability of the medium is much higher than the particle (Figure 2.3b) - more charges accumulate just outside of the interface rather than inside, also leading to an induced dipole in the particle but in opposite direction of the field. This would be the case of an insulating particle in a highly conductive medium (or with a high permittivity).

[1] a nonmetallic electric conductor in which current is carried by the movement of ions

- The particle and the medium have the same polarisability (not represented) - in this case there would be no induced dipole.

These schemes present the charge distribution in an equilibrium state only, i.e. some time after the electric field has been applied. If one would reverse the direction of the field and wait for a steady state to be achieved again, the same exact charge distributions would be found but in the opposite direction. After the field application, charges do not move instantaneously, but rather take some microseconds to reach a stable state [29]. If the electric field direction is changed at low frequency, all the free charges are able to follow up and reorganize. However, as the frequency is increased, a point is reached in which the charges cannot keep pace with the changing direction of the field. At high frequencies, polarisation of the bound charges (permittivity) becomes the dominant mechanism for charging the interface, instead of free charge mobility. An example is a high conductivity and low permittivity spherical particle suspended in a low conductivity and high permittivity electrolyte (e.g. pure water). At low frequencies, the dominant mechanism would be

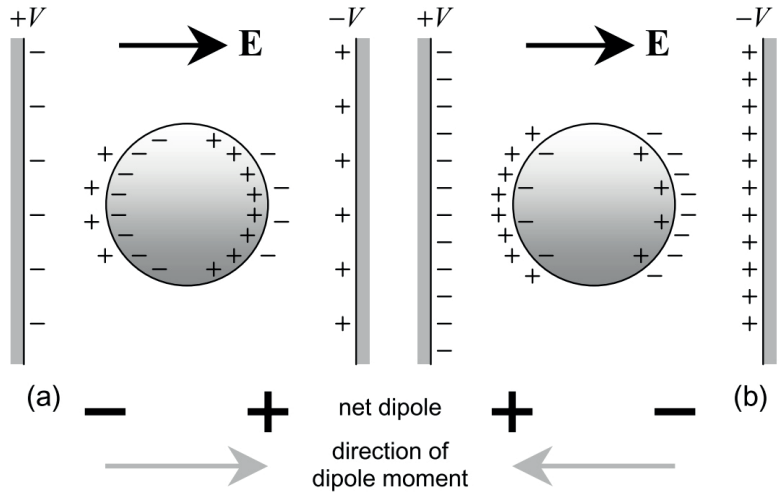

Figure 2.3: Scheme of polarisation for different dielectric particles when they have a much higher (a) or lower (b) polarisability than the suspending medium. When the particle polarisability is higher, more charges gather on the inside of the particle/fluid interface and a net dipole in the direction of the field forms across the particle. If the polarisability is lower, more charges are produced on the outer interface and the net dipole points in the opposite direction of the field [29]

conductivity, so the particle forms a dipole aligned with the electric field as depicted in Figure 2.3a. On the other hand, at high frequencies conductivities no longer play a role and so the interface polarisation is governed by permittivity, as in Figure 2.3b, i.e. the dipole with be in opposite direction relatively to the field. This example illustrates well the fact that interfacial polarisation and induced particle dipoles are also frequency dependant, which is related to the frequency-dependant nature of the different polarisation mechanisms, as depicted in figure 2.4.

If the material is solid, its constituent particles have only the restricted movement allowed by the packing of the molecules and molecular structure. This means that after a material has been polarised between two electrodes, like described, the removal of the electric field will lead do the discharge of the electrodes and therefore the return of the system to the previous state. This constitutes the idea behind the concept of a capacitor. However, if the material system is a suspension of dielectric particles in a dielectric fluid and there is mobility of the particles, then such an application of an electric field will promote migration of the particles according to their polarisation mechanism and the conditions of the electric field (electrophoresis and or dielectrophoresis).

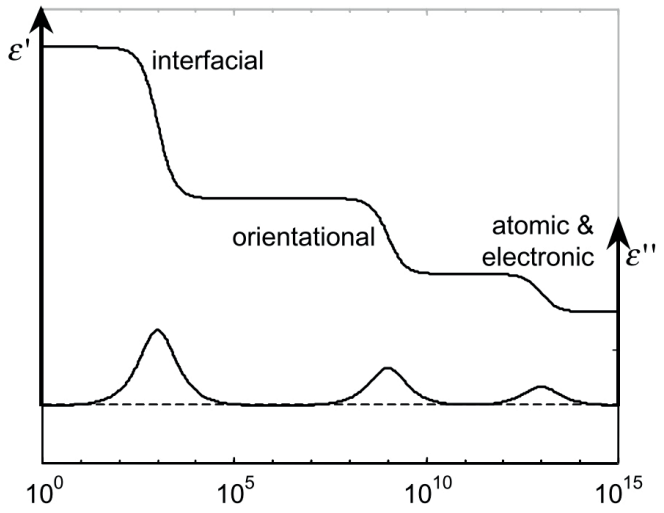

Figure 2.4: Frequency variation of the complex permittivity of a dielectric, considering typical relaxation mechanisms [29]

A higher voltage would simply result in stronger electronic interactions and forces, i.e., all the consequent phenomena would be accelerated, depending on the degree of mobility in that material state (which can be evaluated by the concept of viscosity for viscous fluids).

Due to the fact that particles with distinct electric and dielectric properties in a suspension behave differently when subjected to inhomogeneous electric fields, i.e. can form dipoles and migrate in different directions, dielectrophoresis is an interesting technique to align and/or separate uncharged particles in a medium, what can be used for several ends. Nevertheless, the case of CNTs in a liquid medium present a much more complex system than the simplified case of a single round particle in a homogeneous electric field. It is easy to imagine that long CNTs (with an aspect ratio of 200-3000) in an electric field will become polarised and form long dipoles. These dipoles could lead to particle motion (translation or rotation) depending on the electric field, which could theoretically lead to CNT alignment and dipolar (or Coulomb) interactions with one another. Since particle alignment is not the sole purpose of this work, but rather improving the electrical conductivity of CNT composites, the possibility of inducing dipolar interactions between CNTs presents itself as a promising method. Such interactions might theoretically lead to anchoring of the particles together and so contribute to the improvement of the electrical conductivity of the macroscopic system.

The next section presents a comprehensive review of scientific articles which have used electric fields to manipulate CNTs in different mediums. Most of them attempt to prove the phenomenon of *alignment* and some of them further explore the theory of dielectrophoresis applied to CNTs to explain the results. The focus of this literature study is to identify the potential of electric fields for improving electrical conductivity of CNT composites (not necessarily alignment) and understand what are the most interesting electric field parameters to be investigated.

For a more detailed description of the main theoretical concepts of dielectrophoresis see section 5.2.

2.2 Dielectrophoresis of CNTs

This work focuses on the manipulation of CNTs in a bulk matrix. This approach has the advantages of freedom of choice in terms of nanoparticles and matrix used, and potential scalability for composite parts with complex geometries. The following subsections present a detailed description of different studies where electric fields have been applied to CNTs in different mediums.

2.2.1 Solvents

A convenient approach for studying the influence of electric fields on nanotubes is their dispersion in a liquid solvent (such as ethanol and dimethylformamide) allowing for high mobility. Since Yamamoto et al. reported in 1996 [24, 25] the purification and orientation of CNTs dispersed in isopropyl alcohol under an alternating current field, the use of electric fields for CNT manipulation has been frequently addressed in literature, usually in the field of nano-electromechanical and sensor systems, where CNTs have been manipulated to bridge micro-electrode structures [30, 31, 32, 33, 34].
These are some of the very first reports on the effect of electric fields on CNTs, which induce polarisation of the particles, leading to dipole interactions between them in a phenomenon governed by the dielectrophoretic theory (further described in see section 5.2). CNTs were hereby deposited on top of interdigitated electrodes and the final arrangement was investigated with electron microscopy. Not only orientation of the CNTs was verified between the electrodes, but also induced interconnections between adjacent CNTs bridging the electrodes (figure 2.5). This effect, if also present in CNT dispersions in bulk material, could be used to enhance the contacting points in a CNT network and hence decrease the resistivity of the bulk composite.

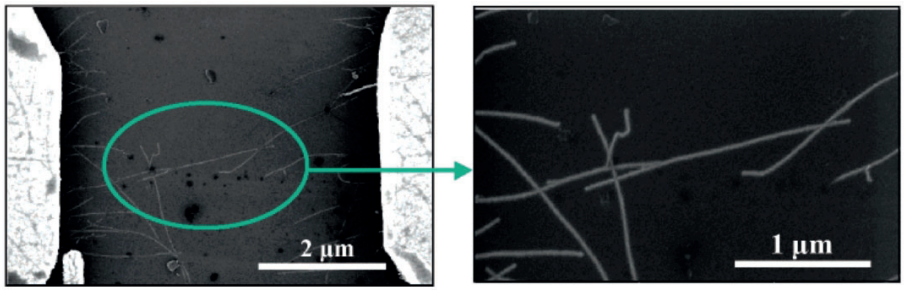

Figure 2.5: Interconnection of three SWCNT strands bridging two electrodes in dimethylformamide (DMF) dispersions under a 88 V_{RMS}/mm field @ 5 MHz (right-hand image is a closeup of the left one)[34]

2.2.2 Low viscosity reactive polymer systems

Martin et al. 2005 [26]

Up until the work of Martin et al. in 2005, electric fields had only been applied to dispersions of nanotubes in solvents. For this reason, the authors investigated the curing of an epoxy system based on a bisphenol-A resin and an amine harder filled with 0.01 wt% MWCNTs when subjected to DC and AC electric fields in an attempt to induce the formation of aligned conductive nanotube networks. Based on the previous trials with both SWCNTs and multi-wall carbon nanotubes (MWCNTs)s dispersed in isopropyl alcohol or ethanol [30, 35, 24, 25], the goal was to obtain more efficient networks that would render interesting anisotropic conductivities and optical properties.
For this purpose, MWCNTs were dispersed in epoxy resin using a dissolver disk. After this, the mixture was equilibrated at 60 °C and hardener was added. In order to observe the nanotube network formation *in situ*, electrodes were produced from optical microscopy slides sputtered with gold and placed with a spacing of 400 µm. These were then placed on a hot stage set at 80 °C, where droplets of the nanotube-epoxy dispersions were exposed to DC and sinusoidal AC electric fields of 10 V mm^{-1}. The alternate electric fields were applied with a signal generator with the frequency of 1 kHz. The formation of the networks with time was observed and recorded with a light

microscope coupled with a digital video camera, and the electrical current was measured.
Additionally, a distinct set of samples was cast in silicone rubber moulds to produce bulk nanocomposites. The same dispersion was in between two rectangular copper electrodes with a cross-sectional area of 2 cm^2 and a spacing of 1 mm, and this set-up was used to apply DC and AC fields of 5 $V\,mm^{-1}$, 10 $V\,mm^{-1}$ and 20 $V\,mm^{-1}$, while curing inside an oven for 4 h at 80 °C. The effects of loading fraction were explored with the production of bulk specimens with 0.005 wt% to 0.02 wt% nanotubes cured in DC and AC fields of 10 $V\,mm^{-1}$.
Both AC and DC fields have shown to induce the formation of oriented CNT networks during the curing of the epoxy, with the samples displaying a sharp improvement in current density with time. This was an indication of the formation of permanent electric field-induced networks.
When DC electric fields were applied, a migration of the nanotubes towards the anode, under electrophoresis, was observed, attributed to the presence of negative surface charges on the nanotubes in an epoxy matrix (supposed to be due to the basic character of the epoxy). When these nanotubes get close enough to the electrode to allow the transfer of charges, they discharge and adsorb onto the anode. Then, the tips of the nanotubes connected to the electrode become sources of high field strengths, constituting points for adsorption of more particles. The subsequent addition of more carbon nanotubes leads ultimately to a ramified network structure extending from the anode and reaching the cathode, providing conductive pathways throughout the specimen. Figures 2.6a and 2.6b display two transmission optical microscopy pictures of samples with 0.01 wt% nanotubes cured under a DC field of 10 $V\,mm^{-1}$. There, one can observe the dendritic structures at the anode after 5 min, and the final inhomogeneous nanotube structure formed after 240 min, respectively. Clearly, the particle network is denser in the area near the anode. These observations were confirmed with transmission electron microscopy (TEM) to thin sections of the bulk samples.

With alternate fields, more uniform and aligned nanotube structures were obtained, even though the initial onset was slower (around 10 min). The agglomerates were also ramified and extending along the electric field lines, and forming conductive connections between the electrodes, such as depicted in figures 2.6c and 2.6d. A similar phenomenon was observed in the bulk samples as well. The formation of such networks results from the polarisation of the CNTs, leading to an additional attractive interaction (dielectrophoresis) between the individual dispersed particles and/or the already formed network branches.

In situ current density measurements revealed pronounced changes with time, as it can be seen in Figure 2.7a, where also the viscosity of the mixture is plotted, to evaluate the progress of the curing reaction. After 600 s, the sample cured in a DC field displays a progressing increase in current den-

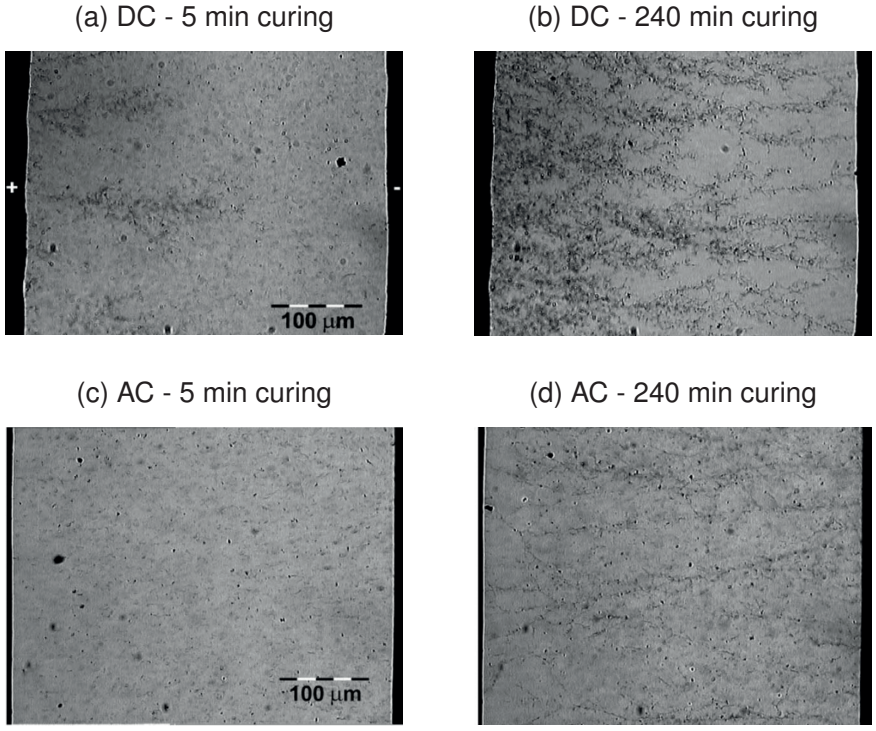

Figure 2.6: Transmission optical microscopy images of epoxy/MWCNT 0.01 wt% during curing at 80 °C under (a)(b) DC field of 10 V mm^{-1} and (c)(d) AC field of 10 V mm^{-1} @ 1 kHz [26].

sity. On the other hand, in the AC field cured sample, the nanotube network formation occurred earlier due to the reason that it grew from both the electrodes, despite the fact that the onset for agglomeration was slower. Since the AC fields render a more homogeneous final network structure, the maximum current density was higher than for the DC fields.

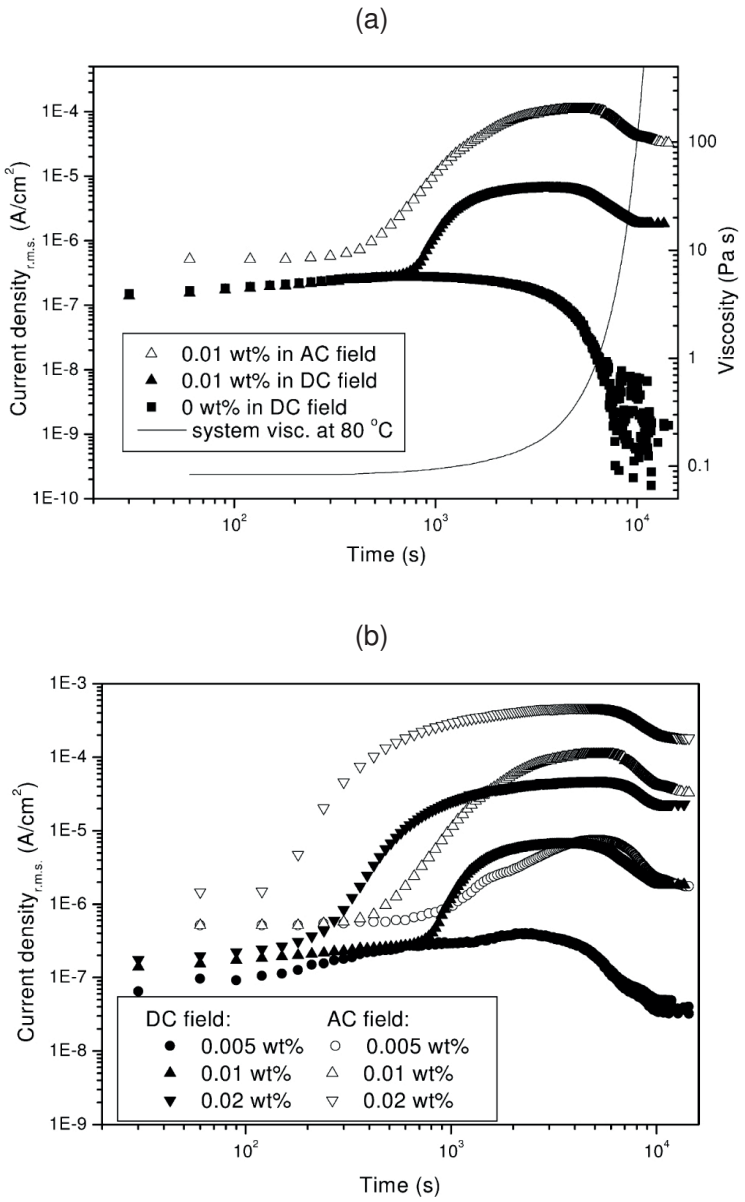

Figure 2.7: *In situ* current density of bulk epoxy/MWCNT systems during curing at 80 °C under a AC (@ 1 kHz) and DC fields of 10 V mm^{-1}, (a) comparing to pristine epoxy (viscosity as a function of time at 80 °C as a reference) and (b) For different weight fractions of MWCNTs [26]

Furthermore, increasing the loading fraction has led to an earlier onset of network formation, given the higher chance of nanotube contacts and agglomeration, leading to a higher number of pathways for the current and thus a higher maximum current density. This can be observed in Figure 2.7b. After an initial step increase in current density, it reached a plateau behaviour for all the specimens. This is an indication of stability of the networks in spite of the incompletion of curing. Additionally, all of them also displayed a step decrease in the final conductivity, as the curing cycle was finished. This can be attributed to the shrinkage associated with the final cross-linking of the epoxy matrix, distorting the nanotube network.
Increasing the electric field strength also proved to enhance the electrical properties of the composites produced, leading to a rise of the specific bulk conductivity. Here it is also evident that AC fields lead to conductivity values of up to an order of magnitude higher than DC fields, confirming the results of the in-situ observations.
In a concluding remark, the authors indicate that even though the resulting specific conductivity of the bulk epoxy/MWCNTs is suitable for electrostatic dissipation, it is still considerably low compared to the conductivity values for pure multi-walled carbon nanotubes, indicating the presence of polymer barriers that hinder the contact between each other. In addition, they mention that the conductivities obtained are still lower than the maximum conductivities achievable for the same weight fraction of nanotubes when randomly dispersed in optimized processing conditions for epoxy composites. A possibility for this, according to them, is the efficiency of the ramified network, whose dendritic structure might lead do the production of a large number of dead ends.

Park et al. 2006 [36]

Later on, in 2006, Park et al. presented a novel method for controlling the orientation of SWCNTs in a photopolymerizable monomer solution by processing it under an alternate electric field, adjusting its strength, frequency and

application time. They used sonication in order to disperse 3 wt% nanotubes in a solution of UDMA/HDDMA[2] and cured it in a 1 mm deep micro-cuvet cell with electrodes on two narrow sides, spaced at 2.3 mm. The impact of alternate field parameters was investigated by varying voltage from 10 to 250 $V_{p\text{-}p}$ (2.2 to 54.3 $V\,mm^{-1}$) as a step function for a time range from 1 min to 60 min and changing its frequency from 1×10^{-3} to 1×10^{5} Hz.

A strong dependency of the degree of alignment on the electric strength was found, which became noticeable at 75 $V_{p\text{-}p}$ (16 $V\,mm^{-1}$). Increasing the applied voltage led to an improvement of the alignment up to the value of 200 $V_{p\text{-}p}$ (43.5 $V\,mm^{-1}$), after which a skewed form of alignment was obtained close to the electrodes, perhaps due to excessive thermal energy. For voltages higher than 300 $V_{p\text{-}p}$, Joule heating led to temperatures higher than 100 °C, promoting local disruption or bending of the aligned nanotubes. In order to understand the time component on this phenomenon, a 200 $V_{p\text{-}p}$ and 10 kHz field was applied for different durations. Alignment was reported to begin almost immediately, increasing with time up until saturation after around 12 min. In addition, increasing frequency was shown to improve the degree of alignment, with saturation at 100 Hz.

High-resolution SEM enabled the investigation of aligned SWCNT microstructures for samples cured under an AC field of 200 $V_{p\text{-}p}$ and 10 Hz for 10 min, where clusters aligned along the field direction, with a length of several hundred micrometers, can be found. These clusters seemed to be composed by smaller SWCNT clusters ranging from tens of nanometers to a few micrometers, with some of them lying parallel to each other and connected with aligned clusters, described as a coarsening effect, which is stated to be due to lateral migration among the aligned nanotubes, leading to conductive percolation paths at loadings as low as 0.03 wt%. The anisotropic nanotubes structure was confirmed by the images obtained when the samples where microtomed perpendicular to the electric field direction: round SWCNT clusters were reported, likely to be the cross sections of the aligned clusters observed.

[2] urethane dimethacrylate/1,6-hexanediol dimethacrylate

For a 100 Hz field applied during 10 min, it was observed that it improved marginally up to 50 $V_{p\text{-}p}$ (1.4×10^{-12} S cm^{-1}), increasing considerably at 100 $V_{p\text{-}p}$ (3×10^{-9} S cm^{-1}) and saturating at around 150 $V_{p\text{-}p}$ (1×10^{-7} S cm^{-1}) - the latter corresponding to an electric field of 65.2 V mm^{-1}. This constitutes an increase in 6 orders of magnitude when compared to the unaligned composite, with only 3.3×10^{-13} S cm^{-1} (not even an order higher than the conductivity of the pristine resin, 1.4×10^{-13} S cm^{-1}). It is important to recall that these samples were produced with a low content of 0.03 wt% of nanotubes, which was selected because it was expected to be below the percolation threshold. Moreover, the relatively constant conductivities at frequencies below 100 Hz indicated a metallic behavior for the samples produced under electric fields above 100 $V_{p\text{-}p}$. The frequency of the electric field also played a crucial role, having being compared for samples produced with a voltage of 200 $V_{p\text{-}p}$ for 10 min. This revealed a transition from insulating to metallic at 1 Hz, with the conductivity increasing from 3.3×10^{-13} S cm^{-1} (no field) to 4.6×10^{-9} S cm^{-1}. At 10 Hz it increased to 1.4×10^{-7} S cm^{-1}, reaching a plateau of 1×10^{-6} S cm^{-1} at 100 Hz, and eventually saturating at higher frequencies. They suggest that this might be an indication that at very low frequencies the misaligning forces (like Brownian motion and electrophoretic force), prevail over the aligning dielectrophoretic one, hindering the alignment. On the other hand, for frequencies higher than 1 Hz electrophoresis becomes insignificant and the aligning dielectrophoretic force dominates, saturating above 100 Hz.

The phenomenon of enhancing the conductivity due to increase in nanotube alignment can be further explained by interactions between the aligned SWCNTs, increasing the effective aspect ratio of the CNT groupings. Additionally, it is also probable that the lateral contacts between aligned clusters contribute to the conductive network. This can be concluded from the conductivity measurements in the direction perpendicular to the electric field alignment direction, which also increased about two orders of magnitude, indicating that the aligned clusters are also attracted to each other laterally.

This coarsening effect might contribute to a substantial improvement of the overall conductivity.
Furthermore, Park et al. also performed dielectric measurements of the aligned samples, obtaining results consistent with the conductivity and concluding that the dielectric constant of the composites can be simply adjusted over three orders of magnitude by controlling the frequency and strength of the alternate electric field applied.

Zhu et al. 2009 [37]

In 2009, Zhu et al. have been able to obtain anisotropic properties with aligned MWCNT networks in epoxy composites by applying an electric field during the photopolymerization of a thermosetting resin with ultra violet (UV) light. The main goals of this paper were to address two issues from former investigations [38, 39]: the undesired agglomeration of the CNTs in suspensions, forming thick bundles; and the fact that up until that time the nanocomposite samples produced with electric fields were usually too small to perform macroscopic tests or measurements, hindering their macroscopic application.
In order to produce the samples, with 0.1 wt% and 0.5 wt% CNT content, they used a macro-layer-by-layer method by first dispersing the nanotubes in liquid epoxy using ultrasonication and then pouring the suspension into a teflon mould (base interior area of 25×50 mm) with two copper electrodes on opposite side walls, applying an electric field for around 10 min to the suspension. Then, UV light was set to irradiate the samples in order to cure the suspension for an additional 10 min, after which a new layer of suspension was added and the process repeated five times.
This strategy was used in order to achieve a fast curing of the matrix in an attempt to preserve the aligned CNT structure. In addition, they have also decided to study the effect of amine functionalization of the nanotubes in order to not only improve compatibility between the MWCNTs and matrix, but also promote their repulsion between each other and thus retard their

agglomeration. This is due to the charging of the nanotubes because of the functional groups introduced to their surface, causing them to repel each other.

The electric field applied to the composite was always the same, with an AC voltage of 2 $kV_{p\text{-}p}$ at 2 kHz during approximately 10 min. Since the spacing in between the copper electrodes was of 25 mm, this means that a field of 80 V mm^{-1} was applied. Furthermore, liquid state viscosity of the epoxy was around 100 Pa s. Optical photographs taken to the alignment process at different stages clearly demonstrate the formation of nanotubes network, as seen in Figure 2.8.

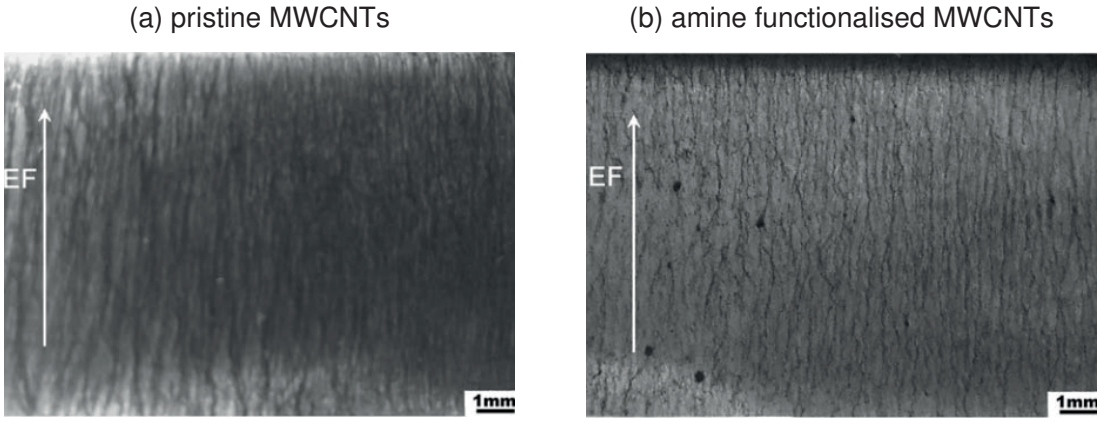

Figure 2.8: Optical photographs of 0.1 wt% MWCNT networks in epoxy after cure with UV light under AC field 80 V mm^{-1} (@ 2 kHz) [37]

Additionally, they measured the storage modulus of the produced specimens in a rheometer, concluding that its value was considerably larger when it was measured parallel to the electric field, comparing with perpendicular to the field and without field. This denotes anisotropy in the dispersion of the nanotubes due to the electric field application. Conductivity measurements at a series of different frequencies were done in a wide frequency LCR meter. Interestingly, while the samples without exposure to the electric field exhibit a typical dielectric behaviour, with conductivity increasing linearly with the frequency (as the pure epoxy), the same was not verified with the samples processed under the electric field, displaying nearly constant conductivities

in the low frequency range. This effect becomes more evident for higher frequencies in the direction parallel to the electric field, when compared to the perpendicular direction, which is an indication of conductivity anisotropy, and alignment. Such result goes in agreement to the measurements done by Park et al [36]. Moreover, they measured a conductivity of about two orders of magnitude higher on the composites produced with pristine MWCNTs to the ones with functionalized MWCNTs. They suggest that this effect was likely due to two reasons: firstly, the significant length reduction of the nanotubes during chemical functionalization, particularly the oxidation process, which then hinders the formation of the conductive network required for the flow of electrons; and secondly, the possibility of functional groups having an impact on the geometry and electrical conductivity of the nanotubes. Another possibility, not considered by the authors, is that the repulsion effect introduced by the amine groups, intended to prevent agglomeration, might also prevent physical contacts between the nanotubes, much required for the conduction of electric current.

Oliva-Avilés et al. 2012 [40]

In spite of the fact that these results appear to be promising for the alignment of carbon nanotubes within a low viscosity polymeric matrix, they do not provide clear insight into the dependency of the phenomenon on the characteristics of the medium/polymer. In [40], Oliva-Avilés et al. looked further into this matter, together with the influence of electric field parameters. They did this by investigating the effects of magnitude and frequency of the field on the network formation in two different systems: a liquid solution of deionised water (DIW) and dissolved polysulfone (DPSF), with room temperature (RT) viscosities of 1×10^{-3} Pa s and 30 Pa s, respectively.
The setup used consisted of a custom-made glass mould with aluminium electrodes separated by 30 mm. In different experiments, continuous and alternate voltages were applied, both of which were amplified by a high-voltage power amplifier. DC voltages of 50 V, 100 V and 200 V were ap-

plied, corresponding to electric field strengths of 1.6 V mm^{-1}, 3.3 V mm^{-1} and 6.6 V mm^{-1}, respectively. For the AC fields, the voltage was applied in steps of 50 $V_{p\text{-}p}$ from 50 to 400 $V_{p\text{-}p}$, yielding magnitudes of the field in range of 0.6 V_{RMS}mm^{-1} to 4.7 V_{RMS}mm^{-1}.In addition, the frequency was also varied from 10 Hz to 100 kHz. While applying the fields, electric current between the electrodes was measured in series with the system, in order to obtain curves of the current versus time. Composites for the electric field alignment were prepared with low concentration (0.1 wt% to 0.5 wt% by dispersing the nanotubes in solutions using an ultrasonic bath followed by mechanical stirring. Furthermore, MWCNT/PSF solid composites were produced under the influence of fields, and their final properties investigated.

In agreement to the previous works, the application of a DC electric field to the composites proved to be rather infeasible for the final particle distribution, since it led to migration of the nanotubes towards the negative electrode due to electrophoresis. On the other hand, when subjected to an AC field, the nanotubes have preserved their dispersion state, forming an electro-induced chained system similar to the ones reported earlier, as depicted in Figure 2.9.

According to the macroscopic observations, the formation of an aligned network in the CNT/PSF composites occurred for electric fields higher than

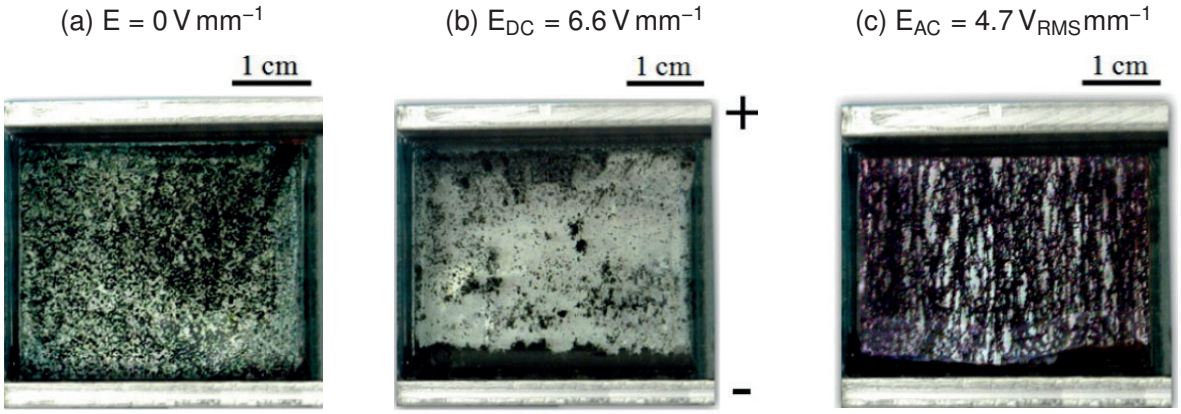

Figure 2.9: Optical photographs of MWCNT/DIW solutions under application of electric fields [40]

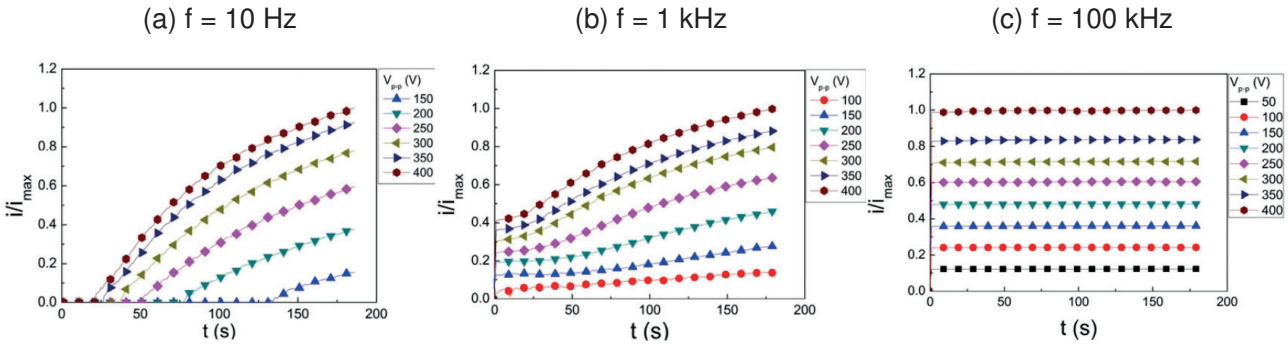

Figure 2.10: Time dependency of normalised electrical current measured *in situ* during AC electric field application to MWCNT/DPSF solutions at different field frequencies. (i_{max}) is the maximum current measured reached after 3 min at the maximum voltage (400 V_{pp}), for each frequency [40]

1.8 $V_{RMS}mm^{-1}$ (150 V_{pp}), and it got faster with the increase of field frequency. For frequencies of 1 kHz and higher, an almost instantaneous alignment was observed. *In situ* current measurements provide valuable insight into the timings of this phenomenon, strongly dependent on the characteristics of the field, as it can be observed in Figure 2.10. Here, the electric current was normalized with the maximum current measured (i_{max}) for each frequency, reached after 3 min at the maximum voltage (400 V_{pp}). Interestingly, it can be seen that increasing the field frequency leads especially to a faster reach of the final state for the higher field strengths, while actually enabling current flow for the lower voltages. This can be exemplified by the fact that at 10 Hz the voltage of 400 V_{pp} allows the current flowing to almost reaching its final value after 3 min, while this happens almost instantaneously for the frequencies of 10 and 100 kHz. On the other hand, for the low voltage of 50 V_{pp}, there is only measured current crossing the samples when the frequency of the field is higher than 10 kHz. The currents measured were on the order of µA. The authors suggest a relation between the minimum voltage required to promote an immediate effect on the nanotube network and the electric field screening effects among the MWCNTs within and among the bundles, referring to [41].

In these graphs (Figure 2.10) it is also noticeable that the voltage applied determines the final magnitude of the electrical current flowing in the system. Current increases with the voltage for all the frequencies, with nearly linear (ohmic) changes, particularly for higher frequencies.

In order to investigate the role of the fluid viscosity on the alignment of the MWCNTs, these experiments were repeated but using deionized water. In this case, it was observed a similar electrical current behaviour for the whole frequency range, so they have presented only the curves for the lowest and highest frequencies (10 Hz and 100 kHz, respectively). Remarkably, for all the measurements performed, there was an instant response of the current across the electrodes as soon as a voltage was applied, suggesting a very fast formation of the conductive network. This is a clear indication that viscosity plays a key role such that when it is very low (like water, 1×10^{-3} Pa s), there is an immediate reaction to the field at any frequency, while for a more viscous solution (in this case DPSF - 30 Pa s), the time required for the phenomenon of alignment and network formation depends highly on the field frequency.

Additionally, MWCNT/PSF solid composites produced under an electric field of 4.7 $V_{RMS}mm^{-1}$ (400 V_{pp}) and different frequencies were investigated. Even though macroscopically aligned nanotube networks were achieved for the whole range of frequencies, a more aligned network was obtained for 1 kHz and higher. Figure 2.11 shows optical micrographs to composites with 0.5 wt% MWCNTs produced with 10 Hz and 1 kHz where this fact is evidenced.

At last, the electrical anisotropy of the samples produced was investigated through DC electrical conductivity measurements to the MWCNT/PSF solid composites with different particle concentrations measured in parallel (σ_{par}) and perpendicular (σ_{perp}) directions with respect to the electric field direction. For 0.1 wt%, there was an increase of 11 orders of magnitude in σ_{par} and of 7 orders of magnitude in σ_{perp} with respect to the conductivity of the neat polymer (1×10^{-15} S m^{-1}). An interesting result found was that this anisotropy persisted until 0.3 wt%, but was lost for the MWCNT concentra-

tion of 0.5 wt%. Apparently, this means that above a certain critical network density, the separation gaps between parallel nanotubes become negligible, and so the electrons can flow easily in both directions.
In what comes to the physical mechanisms involved in this phenomenon of electric field alignment, the theory proposed by this group will be addressed further on in section 5.2, together with a model developed within a cooperation for the work in this dissertation.

2.2.3 High viscosity liquid polymer systems

In two publications in 2014 and 2015 [42, 43], O. Osazuwa contributed to the limited work on alignment of CNTs in thermoplastic melts that had been done so far. He investigated the network formation of MWCNTs in composites with EOC[3], a matrix with MFI[4] 1g/10 min at 190 °C and a melt temperature of 60 °C, under the application of AC electric fields and studied the conductivity of the resulting samples. In addition, the effect of non-covalent functionalization with HBPE[5] was also analysed.

[3] ethylene-octene copolymer
[4] Melt flow index
[5] hyperbranched polyethylene

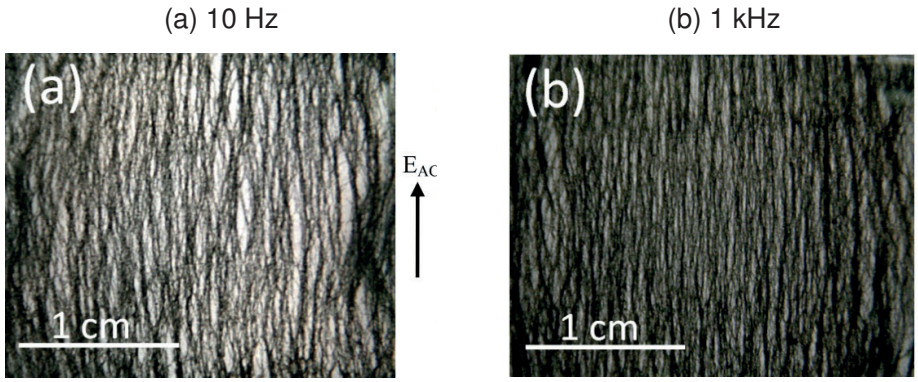

Figure 2.11: Optical photographs of 0.5 wt% MWCNT networks in PSF cured under AC field of 13.3 V/mm [40].

A custom-made mould was developed in order to apply the electric field while the melt was kept at a temperature between 160 and 200 °C with the aid of a heating plate. It consisted of two stainless steel electrodes spaced by a perforated teflon sheet with a thickness of 500 µm to get a thin film of 6 cm diameter. Polymer and MWCNTs were mixed together in a micro-compounder at 150 °C at a screw speed of 90 rpm for 10 min. Composites were then melt pressed into thin films to fit the mould (600 µm). Samples with a MWCNT content ranging from 0.1 wt% to 3 wt% were produced.
As for the electric field, it was provided by a function generator coupled with a high power amplifier generating an AC field of magnitudes from 50 to 600 $V_{p\text{-}p}$ at the frequency of 1 kHz. The effect of the field on the sample was monitored *in situ* through the measurement of voltage drop across it.
Resistivity measurements were made with a multimeter, by calculating it based on the resistance, area of contact surface and thickness. The application of an electric field of 212.1 V mm^{-1} led to a drop in resistivity from around 8 (0.5 wt%) to 4 (3 wt%) orders of magnitude. SEM pictures to these specimens show, in accordance, the typical chaining phenomenon resulting in columnar structures aligning in the direction of the applied electric field.
The increase in electric field intensity and MWCNT loading were reported to decrease the insulator-to-conductor transition times. On the other hand, and has expected, higher viscosities had the effect of increasing these times. It can be noticed that the viscosity range tested was relatively high, with values from 1×10^4 Pa s onwards. This is likely to be the reason for such the long durations obtained, when compared with [40]. In fact, the authors suggest that the process of network formation might take hours to be completed: it is possible to see a great difference between samples treated for 20 min and 6 h, something that would not be expected following the work in [40]. In addition, the fact that specimens annealed for 6 h present better conductivity than the ones subjected to 212.1 V mm^{-1} electric fields remains unexplained. Unfortunately, O. Osazuwa et al. did not focus on the aspects considered fundamental on the previous work of A. Oliva-Avilés, namely the viscosity of host polymer and frequency of the electrical field applied. Therefore, some

results diverge considerably. The former have also put some effort on the attempt to model the complete process. However, rather than starting from a force equilibrium perspective, such as done in [40, 44], they derived several scaling relations and made order-of-magnitude calculations. For example, in order to estimate the translational motion driven by nanotube attraction, they referred to an expression derived by Monti el al. [45], which had actually been calculated based on measurements with single-walled carbon nanotubes in a DC electric field. Given the differences verified so far in the behaviour of carbon nanotubes according to the type and characteristics of the applied electric field, care should be taken with the conclusions arising from the comparison of such relations with the experimental results. Despite that fact, their theory for the assembly of nanotubes based on the contributions of the electric field applied and the Brownian motion constitutes an interesting approach to explain the dynamics of this phenomenon.

2.3 Concluding remarks on electric field manipulation of nanoparticles in composites

Through the examples hereby presented, it was shown that alignment of carbon nanotubes with electric fields under dielectrophoresis has successfully worked for improvement of electrical properties of composites with this sort of nanoparticles. Table 2.1 presents relevant data from some of the work done until now on the alignment of carbon nanotubes in composites, comparing different attempts in terms of the many parameters that play a role in this phenomenon such as: CNT type, liquid medium, particle concentration, electrode material and spacing, electric field voltage and frequency, and duration of exposure to the electric field. Several researchers have accomplished it by trying different strategies, and from these works some initial conclusions can already be drawn:

- Under the influence of an electric field inside a viscous medium, carbon nanotubes undergo distinct effects:

  - migration towards an electrode (electrophoresis)
  - alignment in the direction of the field (dielectrophoresis-induced torque)
  - chaining with other nanotubes (due to Coulombic interactions)

- Due to the electric fields, the resistivity of CNT composites has been reported to decrease up to 5 orders of magnitude, which is expected to result from the formation of improved conductive networks
- As expected from the dielectrophoresis theory, the frequency of the field plays a role - in [40] there was a clear improvement on the dynamics of the network forming for higher frequencies (for more than 1 kHz, the process was almost instantaneous)
- AC electric fields appear to be more indicated for the chaining effect - DC fields lead to migration of the nanotubes to the electrodes, which is something to be avoided if one is aiming at a uniform network
- Viscosity of the host matrix is crucial - only with enough mobility will the CNTs be allowed to rotate and change their configuration

These results not only demonstrate the potential of dielectrophoresis for the manipulation of carbon nanotubes within a low viscosity polymeric matrix, but also point out to the challenging complexity of the process. Although some effects appear to be quite intuitively explained, such as the viscosity of medium (inversely proportional to the mobility of the particles) and the electric field strength (dielectrophoretic force is proportional to the force square), others appear to be highly system dependent, given the disparity of results. Clear insight into the dependency of this process on the electric field frequency, as well as its limitations in terms of range of particle concentration where it can be applied (e.g. effectiveness below and above percolation) are questions which remain to be addressed. Moreover, no mention has been found about the effect of the electrode material used for applying the field.

Table 2.1: Overview of previous studies on electric field manipulation of CNTs and experimental conditions

Source	Materials	Concentration [wt%]	Sample	Electrode material	Spacing [mm]	Strength [$V_{RMS}mm^{-1}$]	Frequency [Hz]	Time [min]	Resistivity decrease	Comments
Bubkte et al. 1997 [35]	Low purity CNT in ethanol	-	No sample produced	Aluminium	-	25-225 (AC), 250 (DC)	300 and 1×10^4	0.0125-0.5	-	Anisotropy of dispersion observed w/ TEM
Chen et al. 2001 [30]	SWCNT in ethanol	-	No sample produced	Gold on Si/SiO_2 substrate	0.025	85-141	5×10^3 to 5×10^6	15	-	Alignment observed w/ SEM
Krupke et al. 2003 [31]	SWCNT in deuterium oxide	10 mg L^{-1}	No sample produced	Gold on p-type silicon substrate	-	3.5	1×10^6	10	-	Alignment observed w/ Raman spectroscopy
Chung et al. 2004 [46]	MWCNT in ethanol	-	No sample produced	Aluminium on Si/SiO_2 substrate	0.004	0-1590 (AC) 0-2500 (DC)	5×10^6	-	-	Alignment observed w/ SEM
Kumar et al. 2004 [32]	SWCNT in DMF	2.1×10^{-8} to 1.3×10^{-5}	No sample produced	Titanium/gold on gallium arsenide and Si/SiO_2	0.002-0.004	0-1590 (AC), 0-2500 (DC)	10 to 1×10^6	3	-	Alignment observed w/ SEM
Li et al. 2005 [33]	SWCNT in isopropanol	2.5×10^{-6}	No sample produced	Titanium/gold on Si/SiO_2	0.001-0.004	530-2120	1×10^6	0.5-6.7	-	Alignment observed w/ AFM
Martin et al. 2005 [26]	MWCNT in epoxy	0.005-0.02	$30 \times 1 \times 1$ mm	Copper	1	5-20 (AC,DC)	1×10^3	240	5 orders magnitude	Bulk samples produced by dipping in epoxy solution
Chen et al. 2005 [34]	SWCNT in DMF	-	No sample produced	Gold	0.005	88	5×10^6	20	-	Interconnection of CNT observed w/ SEM
Park et al. 2006 [36]	SWCNT in UDMA: HDDMA[a]	0.03	$1 \times 2.3 \times 1$ mm (casting in microcuvet)	-	2.3	1.5-38	1×10^{-3} to 1×10^5	1-60	6 orders magnitude	Alignment observed w/ optical microscope and SEM

[a] Urethane dimethacrylate (UDMA) and 1,6-hexanediol dimethacrylate (HDDMA) [b] Ethylene-octene copolymer [c] Polyvinylidene difluoride [d] Highly ordered pyrolytic graphite
[e] Highly structured carbon black

Continuation of Table 2.1

Source	Materials	Concentration [wt%]	Sample	Electrode material	Spacing [mm]	Strength [$V_{RMS}mm^{-1}$]	Frequency [Hz]	Time [min]	Resistivity decrease	Comments
Zhu et al. 2009 [37]	MWCNT in epoxy	0.1-0.5	50×25mm section	Copper	25	28	2×10^3	10 per layer (5 layers)	4 orders magnitude	Layer-by-layer UV curing Alignment observed w/ optical microscope
Sarker et al. 2011 [47]	SWCNT in water	-	No sample produced	Chromium, Paladium on Si/SiO_2	>0.025	70	3×10^5	0.5	-	Alignment of CNT array for organic field effect transistor
Sun et al. 2011 [48]	MWCNT in epoxy	0.05	$150 \times 150 \times 0.4$ mm film	Tungsten wire	10	177	4×10^3	10	3 orders magnitude	Interdigitated wire electrodes for in-plane aligned CNT
Felisberto et al. 2012 [49]	MWCNT in epoxy	0.06-0.5	30 mm diameter, 3 mm thick disks	-	3	83	50	3333	5 orders magnitude	Alignment observed w/ optical microscope
Oliva-Avilés et al. 2012 [40]	MWCNT in water and DPSF	0.1-0.5	$30 \times 30 \times 25$ mm (liquid) 15×9 mm (film)	Aluminium	30	1.6-13 (AC), 1.6-6.7 (DC)	10 to 1×10^5	3	-	Solid films produced by solution casting Anisotropic properties measured
Romyen et al. 2012 [50]	SWCNT in polyimide	0.5	Film	Glass	1	15-60 (DC) + 2 T magnetic field	DC	7	-	Electric + magnetic field Orientation verified w/ Raman spectroscopy
Monti et al. 2012 [45]	SWCNT in epoxy	0.025	-	-	1	800 (DC)	DC	12	-	Extensive modelling but only for DC case
Osazuwa et al. 2014 [42]	MWCNT in EOC[b]	0.1-3	60 mm diameter, 0.6 mm thick film	-	0.5	35-424	1×10^3	0-360	Up to 8 orders magnitude	Melt compounding and film pressing

[a] Urethane dimethacrylate (UDMA) and 1,6-hexanediol dimethacrylate (HDDMA) [b] Ethylene-octene copolymer [c] Polyvinylidene difluoride [d] Highly ordered pyrolytic graphite
[e] Highly structured carbon black

Continuation of Table 2.1

Source	Materials	Concentration [wt%]	Sample	Electrode material	Spacing [mm]	Strength [$V_{RMS}mm^{-1}$]	Frequency [Hz]	Time [min]	Resistivity decrease	Comments
Wu et al. 2015 [51]	GNP in epoxy	0.27-1.08 vol%	-	Aluminium and carbon fibre composite	2	25	1×10^4	0-60	Up to 3 orders magnitude	Fracture toughness improvement
Remillard et al. 2016 [52]	MWCNT in water	0.002-0.01	Coating on PVDF[c]	Titanium	5	0-22	3×10^5	5	-	Combination w/ vacuum filtration for membrane coating
Nguyen et al. 2016 [53]	HOPG[d] in water	-	No sample produced	Copper wires	0.150	20 (AC) + 240 mT magnetic field	1 to 70×10^6	15	-	Measurement of rotational Brownian motion of individual particles
Knite et al. 2017 [54]	HSCB[e] in silicon oil	0.0125-0.8	$20 \times 20 \times 10$ mm	-	20	10	DC	10	Up to 3 orders magnitude	Investigation of viscosity effect

[a] Urethane dimethacrylate (UDMA) and 1,6-hexanediol dimethacrylate (HDDMA) [b] Ethylene-octene copolymer [c] Polyvinylidene difluoride [d] Highly ordered pyrolytic graphite
[e] Highly structured carbon black

3 Experimental Methodology

3.1 Materials

3.1.1 Carbon nanotubes

For this investigation, SWCNTs were chosen given their high aspect ratio (in comparison with MWCNT) which allows for significant changes in the electric properties of a composite at very low concentrations (already at only 0.001 wt%). Commercial pristine SWCNTs TUBALL in powder form provided by Ocsial were used as received. Figure 3.1 shows two SEM images of these SWCNT and table 3.1 presents their properties.

(a) (b)

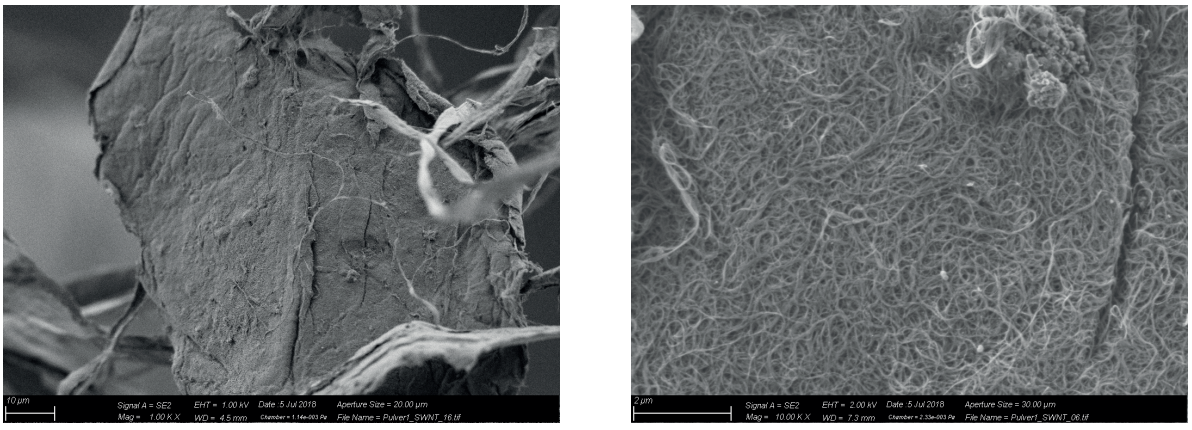

Figure 3.1: SEM images of SWCNTs in powder form as received

Table 3.1: Properties of SWCNTs used in this work [55]

Carbon content $[\mathbf{wt\%}]$	> 85
CNT content $[\mathbf{wt\%}]$	$\geq$ 75
Number of walls	1
Mean diameter $[\mathbf{nm}]$	1.6 ± 0.4
Length $[\mathbf{\mu m}]$	> 5
Metal impurities $[\mathbf{wt\%}]$	< 15

3.1.2 Graphene nano-platelets

Graphene nano-platelets (GNP) were also used for experiments with electric fields. A research grade (TL-E1-B, properties in table 3.2) was provided from company Avanzare (Spain), partner of TheLink consortium[1].

Table 3.2: Properties of GNPs used in this work (info provided by Avanzare)

Production	oxidation, exfoliation, reduction
Lateral size $[\mathbf{\mu m}]$	40
Thickness $[\mathbf{nm}]$	> 2
Layers	5 to 6
Oxygen content $[\mathbf{\%}]$	1
BET[2]surface $[\mathbf{m^2\,g^{-1}}]$	280-350

[1] This project (TheLink, www.thelink-project.eu) has received funding from the European Union's Horizon 2020 research and innovation programme under the Marie Skłodowska-Curie Grant Agreement no. 642890.

[2] Brunauer-Emmett-Teller (BET) surface area analysis provides a specific surface area evaluation by nitrogen multilayer adsorption measured as a function of relative pressure using an automated analyser

3.1.3 Epoxy resin

Epoxy resin Epikote MGS RIMR426 and curing agent Epikure RIHMH433 were obtained from Lange-Ritter GmbH (properties in table 3.3). This epoxy system is normally used in industry for injection in processes for glass, carbon or aramid fibre composites and has been chosen for its low viscosity, to allow for mobility of the nanoparticles. The amine curing agent was selected among the available ones for its relatively fast curing time.

3.1.4 Surfactant

A non-ionic surfactant, TritonX-100 ($C_{14}H_{22}O(C_2H_4O)_n$) was added to SWCNT/composites for investigating its effect on the final electrical properties of samples produced.

Table 3.3: Properties of epoxy resin used in this work [56]

Specification	Resin RIMR426	Curing agent RIMH433
Density[3] $[\mathbf{g\,cm^{-1}}]$	1.14-1.18	0.930-0.965
Viscosity[3] $[\mathbf{mPa\,s}]$	500-900	5-40
Epoxy equivalent weight[3] [g/equivalent]	158-172	-
Refractive index[3] [-]	1.5530-1.5560	1.4830-1.4860
Amine value[3] [mg KOH/g]	-	750-800
Pot life[3] [**min**]	25-55	
Tg midpoint [**°C**]	$\geq$80	
Mixing ratio	100 : 26$\pm$2 (weight) 100 : 32$\pm$2 (volume)	

[3] Measured at 25 °C

3.1.5 Mould release agent

To prevent the attachment of epoxy samples to the electrodes in the mould, 3 distinct materials were used as interface between the electrodes and the nanocomposites:

1. mould release agent 1 (MR1) - mechanical grease (calcium sulfonate Ceran XM 220, Total)
2. mould release agent 2 (MR2) - mechanical grease with carbon black (CB) (Printex CB80)
3. mould release agent 3 (MR3) - silver paint (RS Components)

3.2 Processing of CNT dispersions

The experimental procedure for production of bulk epoxy nanocomposites was done in the following steps:

1. Dispersion of nanoparticles in the liquid resin (with three roll mill)
2. Addition of the curing agent in the correct stoichiometric amount (manually)
3. Feeding the mould, setting the electric field and the curing temperature
4. After reaction completion, removal of the field and retrieval of the samples

Given the initial agglomerate state of the CNTs in powder form [16, 19, 27], the first mixing step is absolutely crucial to guarantee that the CNTs are sufficiently dispersed in the resin and ensure reproducibility of results. This was the motivation to use a three roll mill (Exakt 80E, Germany). Comparing to other dispersion techniques (such as ultrasonication or ball milling), it provides more process control in the mixing, which constitutes a great advantage in what comes to reproducibility in sample production. This is

achieved by fine tuning of the rotation speed of the rolls together with the gaps between them. Moreover, it is a scalable production method because the mixing energy does not depend on the amount of material, in contrast with other dispersion technologies like ultrasonication, for example, and so it is more relevant for industrial applications.

3.2.1 Three roll mill

A three-roll mill (rolls of 80 mm diameter and 200 mm length made of chemically neutral silicon carbide) throughput capacity of 20-20000 cm h^{-1} and a minimum gap between rolls of 5 µm, was used to disperse nanoparticles in the epoxy resin. As depicted in figure 3.2, the mill is composed of three rolls coupled together to operate at distinct velocities: the set speed is given for the apron roll, while the centre and feed rolls follow with 3 and 9 times slower, respectively. The suspension is fed on the feed roll, that forces it to pass through the first gap while undergoing shear forces generated by the rotation at different speed of the centre roll. The suspension then goes through a second smaller gap (usually set to be three times smaller than the first gap) and is finally collected by a sharp blade in contact with the apron roll, ending a cyclic process hereby called *pass*. For this study, the speed of the apron roll was set to 180 rpm (argued to be more suitable to preserve a longer aspect ratio of the CNTs in [21, 22]). The number of mixing passes

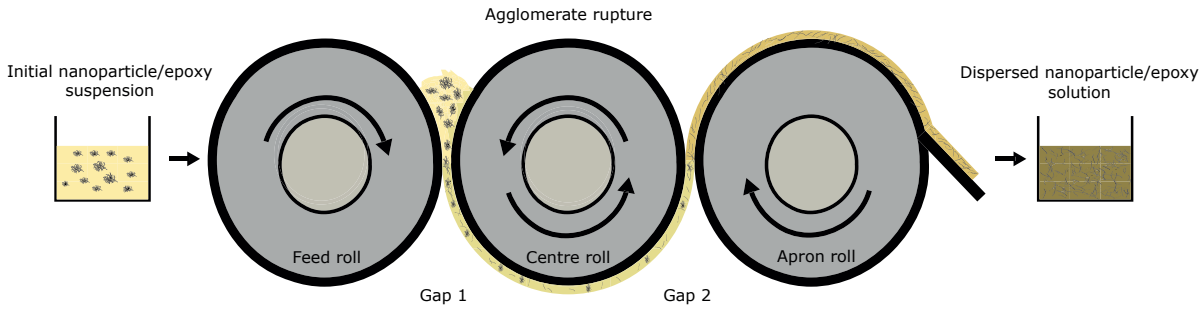

Figure 3.2: Dispersion of the nanoparticles in the three-roll mill - nanoparticle/epoxy suspension is poured between the feed and center rolls (gap 1), passes through the two adjustable gaps and is collected on the apron roll

and influence of the gap distances between the rolls on the electrical resistivity of different dispersions was investigated and is presented in section 4.1. The goal was to obtain the lowest electrical resistivity (indicator of optimised dispersion) and, as important, a stable and reproducible electrical response of the samples produced. Only so it is possible to take conclusions from the electric field experiments performed later on with the composite resin.

3.3 Experimental procedure and set-ups

3.3.1 Optimisation of dispersion

For understanding and improving the dispersion of nanoparticles in view of electrical properties, the influence of gap configuration between the rolls and number of passes was investigated. Therefore, epoxy/nanoparticle dispersions were used to produce bar-shaped samples ($5 \times 2 \times 40$ mm) in a silicone mould (mould A). For each experimental configuration, the electrical resistivity of 6 samples was measured using the four-point method (described in section 3.5.1). The results of this investigation are presented in chapter 4.1. The presence of air voids was tested by comparing samples made from the same suspension treated in two different ways after the curing agent hand-mixing:

- resting for 10 min and then curing in the oven at 80 °C
- degassing under vacuum for 10 min and then curing in the oven at 80 °C

No visible air holes nor differences in resistance measurements were observed, so that a careful slow mixing of curing agent and suspension was taken as a standard procedure while the degassing step was left out.
As for the experimental set-ups for the application of electric fields on the CNT dispersions, two types were developed:

- Mould B - for curing of two vertical plates ($22.5 \times 12 \times 1.65$ mm) (figure 3.3)

- Mould C - Resin transfer moulding arrangement for curing of multiple plates (3.4)

3.3.2 Mould B - Silicone moulds for electric field application during curing of epoxy nanocomposites

A silicone mould containing an aluminium heating block between two sample gaps (figure 3.3) was used for the application of electric fields to composites during curing. Two specimens ($22.5 \times 12 \times 1.65$ mm) were simultaneously produced under the same curing conditions but only one of them was under the influence of the electric field by connecting the electrodes to the voltage source (the other was used as a reference, i.e. without electric field). Gold-coated copper plates with dimensions $24 \times 14 \times 1.5$ mm were used as electrodes for field application. The electrodes were covered with silver paint as an electrically conductive mould release agent, i.e. to be able to recover the samples after the reaction.
The following procedure was executed for each experiment: ca. 2 g of epoxy resin filled with SWCNTs (previously dispersed in the three-roll mill) were hand-mixed with the curing agent in the weight ratio 100:26, and fed into the two spaces between the electrodes (figure 3.3) with a volumetric pipette. The

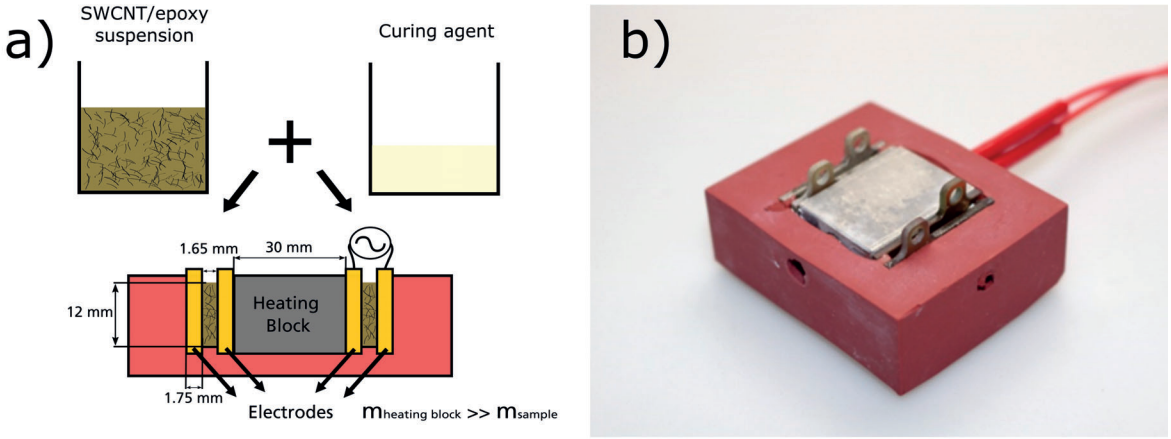

Figure 3.3: For sample production: a) the SWCNT/epoxy suspension was mixed with the curing agent and then fed into the two sample forms, b) silicone mould (B) used

electrode of the test sample was then connected to the voltage supply. The desired electric field parameters were set (strength and frequency) and, as soon as the power supply was on, the temperature was set on the heating block (around 1 min to reach in the case of 80 °C). After approximately 1 h, the voltage was shut down and, as soon as the samples had cooled down to room temperature, the electrical resistance of both (test and reference) was measured by attaching a multimeter to the two respective electrode pairs (*ex situ* measurement, explained in section 3.5.1).
Using this set-up, the following effects were investigated on SWCNT/epoxy composites: electric field strength and frequency, curing temperature, and SWCNT concentration. Results are presented in section 4.2.

3.3.3 Mould C - Resin Transfer Moulding with electric field

A set-up for simultaneous production of multiple disk samples was developed inspired on resin transfer moulding, depicted in figure 3.4.
A silicone form for six disk samples of 20 mm diameter and 1.5 mm thickness (3 in fig. 3.4) was placed between two gold-coated electrodes (2 in fig. 3.4). Together with another layer of silicone (4 in fig. 3.4), which served as sealing, the four layers were placed between two steel plates (1 in fig. 3.4). The outer plates were fitted with four nuts screwed together and used for clamping the structure. The inner arrangement was additionally fixed with 3 guiding pins, in order to prevent slipping or warping of the silicone form and thus avoiding the clogging of the narrow flowing channels between the disk moulds.
After mounting the system together, two hose couplings (5 in fig. 3.4) were screwed on the top plate, each then connecting a feeding tube (6 in fig. 3.4) fastened with a tightening nut (7 in fig. 3.4). One of the hoses was closed with a clamp, the other one connected to a syringe with double sealing ring. With the syringe a negative pressure is generated in the mould. Particular attention had to be paid to the torque with which the nuts of the steel plates were tightened. If they were too tight, it was possible that the negative pressure generated by the syringe was not present in the entire mould cavity, i.e.

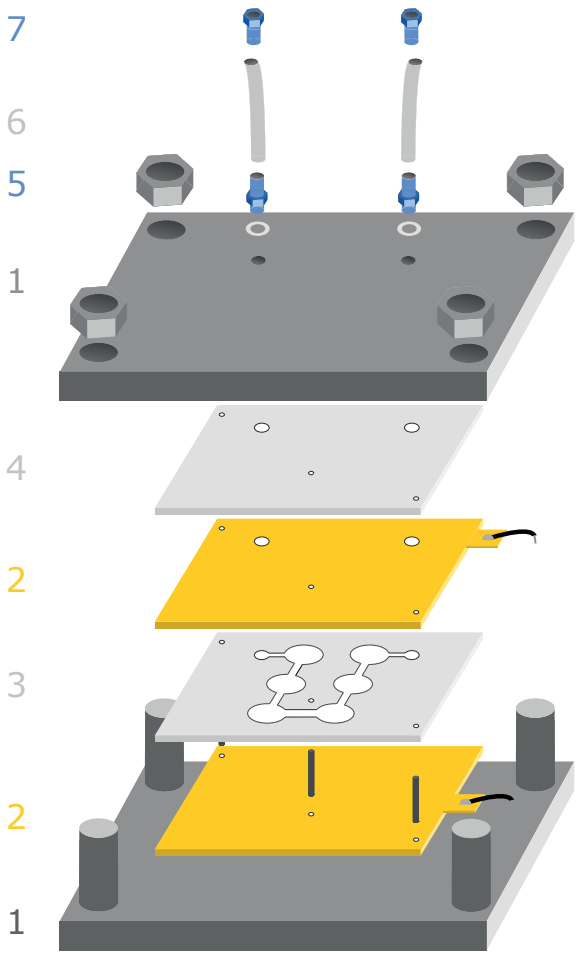

Figure 3.4: Mould C - RTM set-up for application of electric fields during resin curing

that some of the flowing channels got closed by a dislocation of the silicone. On the other hand, if they were too loose, the cavity was not airtight, which could lead to leakage.

Subsequently, the epoxy dispersion was mixed with the curing agent and, in order to avoid air bubbles in the samples, degassed under vacuum in a desiccator. The composition was then filled into a second syringe, connected to the feeding tube and fed to the cavity until it emerged from the other tube. The electrodes were connected to the voltage source through a temperature resistant silicone coated cable. Finally, the complete mould was placed on top of an aluminium heating plate set to the desired curing temperature.

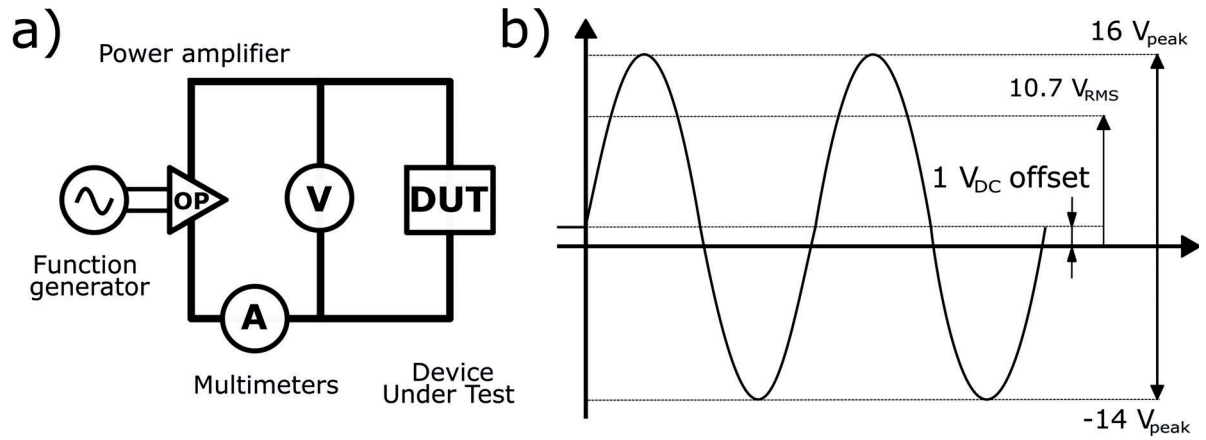

Figure 3.5: Schematic of: a) the electrical setup, and b) the respective AC signal used for the experiments: a DC offset of 1 V was added to the 30 V_{pp} sinus, allowing measurement of the resistance improvement *in situ*

In order to be able to remove the samples from the electrodes, mould release agent had to be used. Standard mould release agent is either silicone or polytetrafluoroethylene (PTFE) based and so electrically non conductive. For this reason, experiments were performed with conductive silver paint, mechanical grease and carbon black filled grease.

3.4 Electric field

To generate the electric field, a voltage of up to 60 V_{pp} and frequency of up to 10 MHz was applied. A DC offset of 1 V_{pp} was used for *in situ* resistance measurements, as illustrated in figure 3.5. For each experiment, the wave (input) signal was defined in the function generator (Agilent 33250A) by setting the desired voltage and frequency, which was then connected to the high frequency power amplifier (Tabor 9260). This amplifier is able to increase the voltage signal by either a factor of 10 (up to 36 V_{pp} in normal mode or a factor of 20 in differential mode), with a current of up to 1 A.
One commonly used definition for AC time varying sinusoidal voltages is the root mean square (RMS), also denoted by effective value for the fact that it can be used for comparison with an equivalent DC circuit which would

generate the same electrical power (fig. 3.5a). For the peak voltage of V_{peak}, one can easily calculate V_{RMS} through: $V_{RMS} = \frac{V_{peak}}{\sqrt{2}} = 0.707 \times V_{peak}$. In case there is a superposition of an AC voltage with a DC offset, the total RMS voltage is computed with $V_{RMS} = \sqrt{V_{AC}^2 + V_{DC}^2}$ [57].
The *in situ* DC voltage and current were tracked with two Metrix MTX 3283B Multimeters (V and A in fig. 3.5a, resp.). In addition to the electrical settings, also the distance between the electrodes plays a crucial role in the experiments since it defines the electric field strength according to $E = \frac{V_{RMS}}{d}$, where V_{RMS} is voltage and d distance. For an average sample thickness of 1.65 mmand a voltage of 10.7 V_{RMS}, the effective electric field over the samples is 6.5 V_{RMS}/mm.
With mould C, the amplifier was used in differential mode and so a voltage of 21.2 V_{RMS} was applied to samples of an average thickness of 1.5 mm. This equates an effective electric field of 14.1 V_{RMS}/mm. To prevent undesired high frequency-related inductive effects, frequencies above 10 MHz were not tested.

3.5 Characterisation

3.5.1 Measurement of electrical properties

Four-point method

The four-point method (also known as Kelvin sensing) is an electrical impedance measuring technique that uses two separate pairs of electrodes: the outer ones supply current and the inner measure voltage, as shown in figure 3.6. The method works on the simple principle of the Ohm law: if a determined quantity of flowing current is assured and the voltage is sensed using a different high impedance voltmeter it is possible to calculate the electrical resistance. This allows to make more accurate measurements than the simpler two-terminal sensing: separation of current and voltage pins eliminates contact resistance from the measurement, which is an advantage for measuring low resistance values.

A comparison of resistance values measured with the four-point method for a fixed sample geometry gives insights into the relation between material, process parameters and electrical properties. However, to calculate the actual resistivity of the processed material and to compare results with other shaped samples, geometrical correction factors have to be taken in consideration. This is discussed in annex A.1.

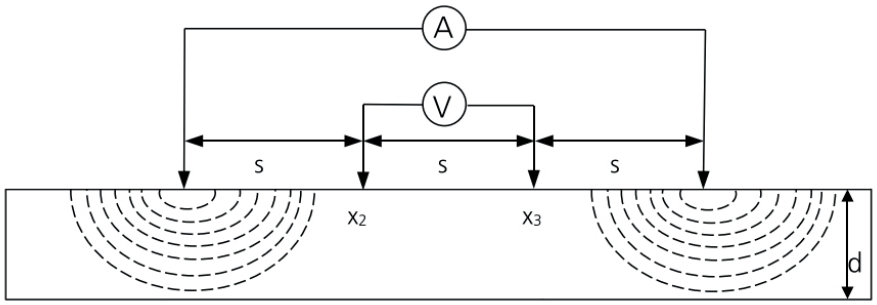

Figure 3.6: Schematic of four-point method for resistance measurements [58]

Through-plane resistivity of samples cured under electric fields

The effect of electric fields on the electrical properties of epoxy nanocomposites was investigated by measuring their electrical resistance with two different techniques:

1. with a multimeter after the curing process (*ex situ*)
2. by tracking the direct current (DC) flowing through the specimen during the application of the electric field (*in situ*)

In situ resistance measurements were performed to investigate the dynamics of particle interconnection and network formation during the curing process. A suitable approach to follow the DC resistivity was to add an offset of 1 V_{DC} to the AC voltage applied and measure the respective current (DC) with a multimeter connected in series (A in figure 3.5a). An extra multimeter connected in parallel (V in figure 3.5b) recorded the DC voltage offset. Both multimeters are able to filter out the AC voltage and current when measuring

in DC mode. Adding 1 V_{DC} to the AC signal (fig. 3.5b) only changes the total RMS voltage by 1% (in this example from 10.6 V_{RMS} to 10.7 V_{RMS}, which is a negligible difference. These measurements resulted in a time vector of DC voltage (1 V) and DC current. DC resistivity was computed using Ohm's law $U = R \times I$, along with the relation for volume resistivity $\rho = R \times \frac{A}{d}$, where U is voltage, R resistance, I current, ρ volume resistivity, A the area and d the sample thickness, respectively.
The measured electrical current was in different ranges according to the SWCNT concentration: 0 to 700 nA (for 0.001 wt%); 20 nA to 6 µA (0.005 wt%); 30 µA to 3 mA (0.01 wt%) and 7 mA to 180 mA (0.1 wt%).
This method for *in situ* measurement of electrical resistivity while applying an electric field to the samples was validated using electrical resistances. The results are displayed in annex A.2. Additionally, the effect of using a DC offset on the final resistivity of samples cured under AC electric fields was also evaluated (annex A.3).

3.5.2 Rheological characterisation

The rheological properties of epoxy and SWCNT/epoxy suspensions, as well as of the reacting system mixed with curing agent, were investigated at 20 °C (RT), 80 °C and 100 °C using an Anton Paar MCR 501 rheometer. The complex viscosity was measured in a 25 mm diameter cell by operating the rheometer in oscillatory shear mode with parallel plate configuration.

3.5.3 Scanning electron microscopy

Composite specimens were investigated using a Carl Zeiss Supra 55-VP SEM equipped with an in-lens detector and operating at 3 kV. Before the measurements, samples were gold-sputtered for 10 s using a Cressington 208HR high-resolution sputter coater.

3.5.4 Further characterisation techniques

Apart from the aforementioned methods used to investigate the morphology of the CNT networks in the composite samples, also the following techniques were employed:

- Raman spectroscopy - in collaboration with Sandy Fisher at Imperial College London (part of TheLink network)
- Optical coherence tomography - in collaboration with Denis Ganin at the Karlsruhe Institute of Technology (part of TheLink network)
- Atomic force spectroscopy - with Hubert Weyrauch at the department for Applied Electrochemistry at Fraunhofer ICT
- X-ray micro computer tomography - with Hartmut Kröber at the department for Energetic Materials at Fraunhofer ICT

However, no relevant information about the morphology of the nanoparticle networks (eventual alignment) could be obtained from these experiments. The difficulties encountered were mainly due to the following factors:

- Very low concentration of SWCNT - down to 0.01 wt%
- Very low dimensions of the SWCNTs used - diameter of 1.6 nm and length of around 5 µm
- Molecular similarity between the particle and matrix (both carbon based)

4 Experimental Results and Discussion

This chapter presents the results of experiments performed according to the methodology described in chapter 3 together with a discussion of the observed outcomes. Firstly, the dispersion results of SWCNT and GNP in epoxy are presented (4.1). The effect of electric field on SWCNT/epoxy dispersions during curing under different conditions is then discussed in section 4.2. Section 4.3 contains the results of rheological measurements of epoxy resins with different SWCNT concentrations and cured at different temperatures for 0.01 wt%, following by a discussion on the morphological characterisation of SWCNT/epoxy composites with SEM. Finally, in section 4.4, some results of electric field experiments with GNP/epoxy are presented.

4.1 Dispersion and electrical properties of epoxy nanocomposites

Gap mode in three-roll mill

Two mixing modes were investigated in the three-roll mill:

- Constant gap - the suspension was passed 8 times with a fixed gap 1 of 15 µm (between the feed and centre rolls - refer to fig. 3.2) and a gap 2 of 5 µm (between the centre and apron rolls).[1]

[1] For simplicity, this gap configuration will be here designated as 15-5 and the following gap configurations will be referred accordingly

- Regressive gap - starting with a larger gap between rolls (60-20), and then every two passes halving the distance until reaching the physical limit used on constant gap mode, 15-5 µm.

The 8 total suspension pass gaps are resumed in table 4.1.

Table 4.1: Three-roll mix mixing modes investigated

Pass	1	2	3	4	5	6	7	8
Constant gap [µm]	15-5	15-5	15-5	15-5	15-5	15-5	15-5	15-5
Regressive gap [µm]	60-20	60-20	30-10	30-10	15-5	15-5	15-5	15-5

To avoid an excessive promotion of rupture mechanism that could damage the aspect ratio of the nanoparticles [21], the speed of 180 rpm was always set (on the apron roll).

4.1.1 Single-wall carbon nanotubes (SWCNTs)

Gap mode in three-roll mill

Resistivity measurements for the two gap modes investigated are plotted in figure 4.1. While the difference in first passes is still not perceivable, it reaches one order of magnitude after 8 passes. Using the regressive gap mode seems to promote lower electrical resistivity of SWCNT/epoxy composites for the same curing process parameters and without increasing the particle concentration.
This is expected to result from the different agglomerate dispersion mechanisms [21]. The constant mode (gaps of 15-5 µm for all passes) imposes high shear forces to the (big) initial CNT agglomerates, promoting their rupture and, most likely, of the nanotubes. On the other hand, starting with wider gaps in the regressive mode favours erosion of the agglomerates over rupture, limiting the breakage of CNTs. A higher CNT aspect ratio for the same concentration seems to help the formation of more efficient secondary

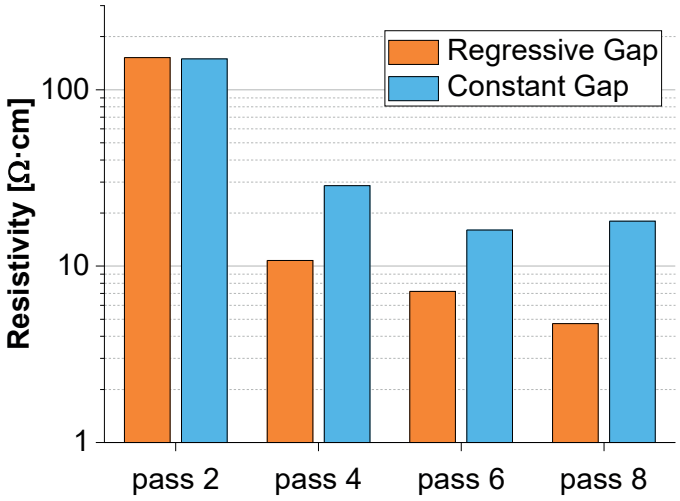

Figure 4.1: Electrical resistivity of SWCNT/epoxy 0.1 wt% produced with two gap modes in the three-roll mill (samples cured in mould A at 80 ℃)

networks for electrons to flow across the bulk composite, by enhancing the chances of contact between adjacent particles.

Percolation behaviour

Figure 4.2a shows the evolution of electrical resistivity of SWCNT/epoxy composites above the concentration of 0.01 wt% along the dispersion process in the three roll mill, i.e. for samples collected after each pass in the machine (operated in 15-5 µm constant gap mode). Here it is noticeable that the difference after each pass is more significant for the lowest concentrations and becomes less relevant above 0.5 wt% (difference between the lines for the same concentration). This is an indication of the importance of the dispersion state closer to the percolation range, where the resistivity is very sensitive to the dispersion quality. Above 1 wt%, the resistivity does not decrease considerably. In particular, despite a difference of 50% in concentration, SWCNT/epoxy 1 wt% and 1.5 wt% display very similar electrical properties. Concentrations higher than 1.5 wt% were not investigated due to difficulty of incorporation of curing agent in the SWCNT/epoxy resin, given its high viscosity.

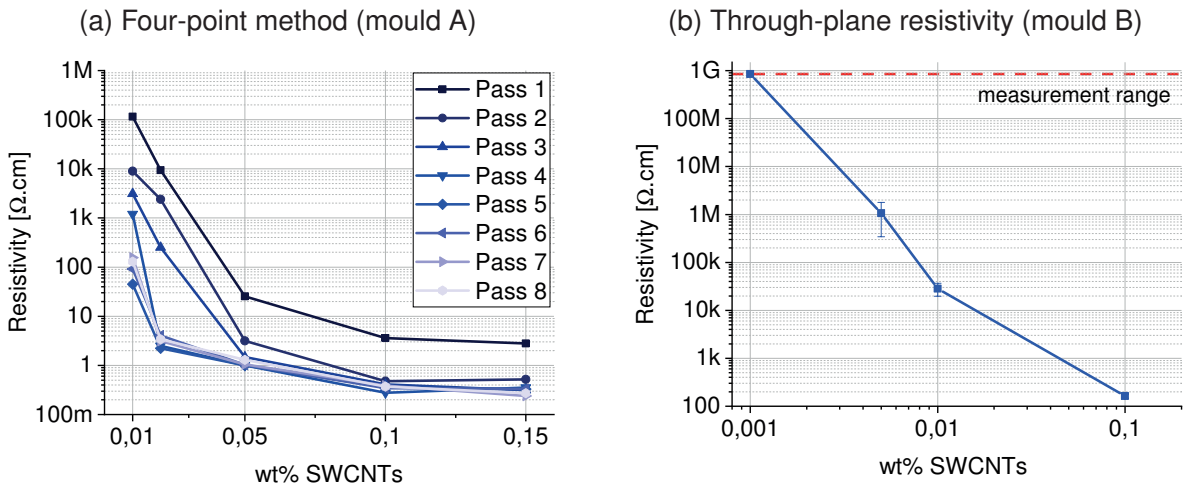

Figure 4.2: Electrical resistivity of SWCNT/epoxy as a function of particle concentration for (a) different dispersion states (cured at RT in mould B) and (b) 8 passes cured at 80 °C in mould B (all produced with gap mode in three-roll mill)

Additionally, figure 4.2b depicts the through-plane electrical resistivity of SWCNT/epoxy nanocomposites at different concentrations produced in mould B. For the lowest amount of SWCNTs, 0.001 wt%, the electrical resistivity was too high to be measured by the multimeter in resistance mode (limited to 50 MΩ) and hence the value presented corresponds to the multimeter range limit. This means that the percolation concentration lies between 0.001 wt% and 0.005 wt% for samples cured at 80 °C. The same trend was found for specimens cured at room temperature, with SWCNT/epoxy 0.005 wt% also being conductive.

Curing Temperature

The influence of curing temperature of SWCNT/epoxy composites on the final electrical resistivity was investigated for samples collected after different passes in the three-roll mill. Specimens of SWCNT/epoxy at a concentration of 0.1 wt% (mixed in constant gap mode) and at 4 different passes number were cured both at room temperature and in the oven at 80 °C. The resistivity measurements are depicted in figure 4.3a.

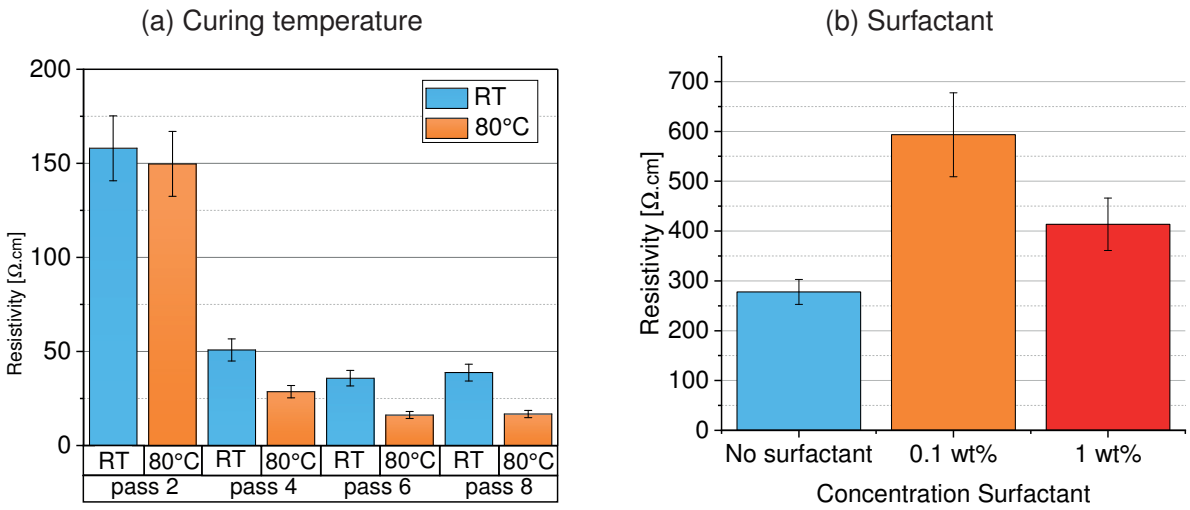

Figure 4.3: SWCNT/epoxy 0.1 wt%: (a) influence of curing temperature (mould A) and (b) surfactant concentration (mould C 80 ℃) on the electrical resistivity

By increasing the curing temperature in the oven, the electrical resistivity of the SWCNT/epoxy 0.1 wt% composites appears to decrease around 50%. Moreover, the constant gap mode confirms the beginning of a plateau at 6 passes, after which no improvements come from additional mixing in the three-roll mill. Further results and discussion on the effect of temperature on the electrical resistivity of SWCNT/epoxy follows in section 4.2.2, for experiments in the silicone mould for application of electric fields, and in section 4.3.1, for rheological measurements.

Addition of surfactant

Three different combinations of surfactant/suspension were examined: no surfactant, 0.1 wt% (same quantity of SWCNT) and 1 wt% of the suspension (10 times the content of SWCNT).
The resistivity results in figure 4.3b show that both high and low concentration of surfactant lead to less conductive material. A low concentration (0.1 wt%) of surfactant rises the average sample resistance up to 215% of the starting value. This suggests that the surfactant does not infiltrate CNT clusters, helping their dispersion, but instead acts only on already dispersed

bundles of nanotubes. One possible explanation could be the surfactant causing repulsion and pushing away entangled bundles of nanotubes, limiting the contact points that allow electrical current to flow [59]. At higher concentration (1 wt%) the resistivity increment is smaller but still considerable. This may be caused by the excess of surfactant forming aggregations and interacting with the SWCNT network [59].

4.1.2 Graphene nanoplatelets GNPs

Gap mode in three-roll mill

Electrical resistivity measurements of GNP/epoxy samples after 2, 4, 6, and 8 passes are represented in figure 4.4a. Both gap modes demonstrated a linear decrease of the resistivity for each 2 additional passes. Regressive gap mode produced a suspension that once cured has a lower electrical resistivity compared to the same suspension processed in constant gap mode; this difference is more significant after 6 or 8 passes. This is likely caused by a dispersion mechanism that preserved more efficiently the high aspect ratio of the GNPs, similarly to what happened with the SWCNT/epoxy suspensions. A higher particle aspect ratio is expected to promote an improved network of graphene nanoplatelets during the curing process, leading to more conductive paths for electrical current to flow.

Percolation behaviour

Figure 4.4b depicts the electrical resistivity of GNP/epoxy nanocomposites at different concentrations. Samples were all produced in 8 passes in the three-roll mill in regressive gap mode and cured overnight at room temperature. The electrical resistivity of samples with 0.5 wt% GNPs was too high to be measured (overflow), meaning that it reached values over $3 \times 10^7\,\Omega\,\mathrm{cm}$ and thus was regarded as non-conductive. The percolation threshold for this system was therefore estimated to be between 0.5 wt% and 0.75 wt%. Concentrations higher than 2 wt% were not investigated due to the impossibility

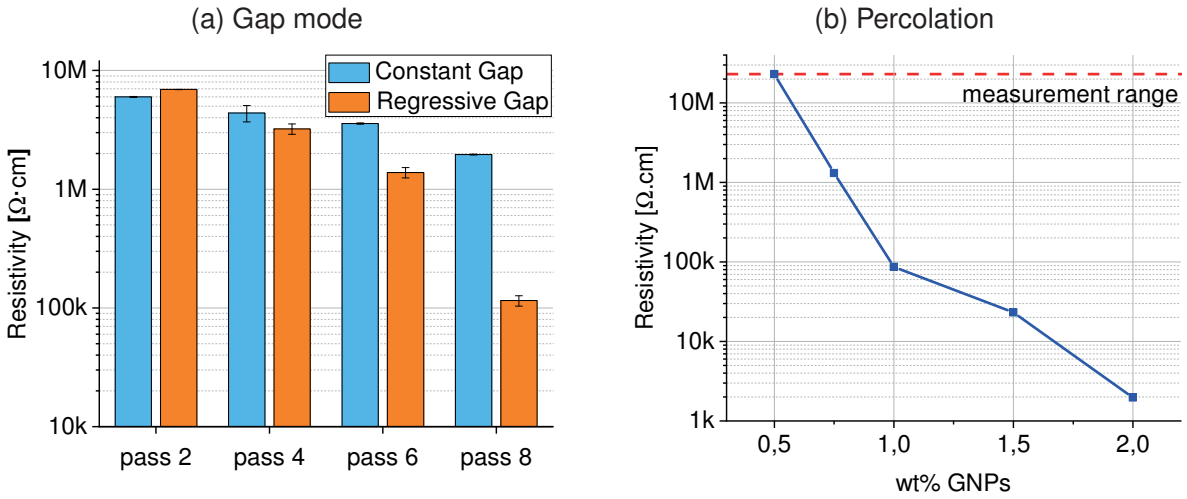

Figure 4.4: Electrical resistivity of GNP/epoxy composites: (a) influence of gap mode in three-roll mill dispersion for 1 wt% (mould A) and (b) dependancy on concentration for samples produced in regressive gap mode and cured in mould A at RT

of efficiently incorporating the curing agent in the GNP/epoxy resin because of the viscosity.

Curing Temperature

The effect of processing temperature on the resistivity of GNP/epoxy 2 wt% composites was explored by curing in the oven at the temperatures of 20, 80 and 100 °C. The results, measured with the four-point method, are presented in figure 4.5a and confirm the tendencies also found for SWCNT/epoxy composites: higher curing temperature leads to nanocomposites with decreased resistivity. On the other hand, this improvement seems to be similar for both 80 °C and 100 °C.

Figure 4.5b shows the influence of curing temperature for GNP/epoxy nanocomposites at the concentrations of 0.75 wt%, 1.5 wt% and 2 wt%. Given the negligible difference between 80 °C and 100 °C (figure 4.5a), only RT and 80 °C were further investigated.

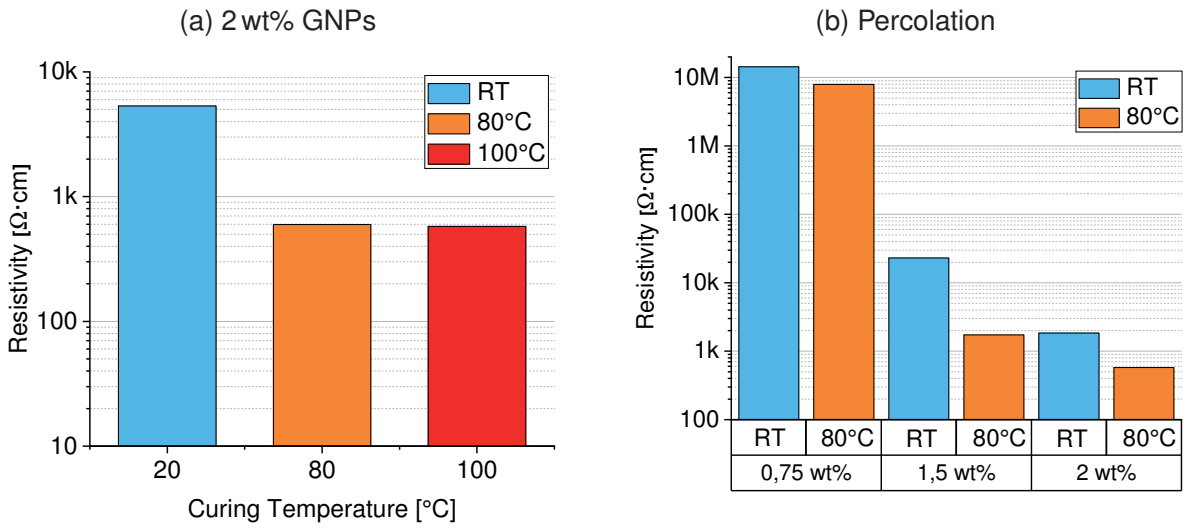

Figure 4.5: Electrical resistivity of GNP/epoxy composites (8 passes in regressive gap mode, mould A): influence of curing temperature for (a) 2 wt% GNPs and (b) for different concentrations

In general, samples cured in the oven at 80 °C showed a lower resistivity than RT cured ones. A decrease of around one order of magnitude was measured for the concentrations of 1.5 wt% and 2 wt%.
This behaviour is likely related to the viscosity development with temperature, achieving the lowest values (and hence highest particle mobility) at high temperatures. Further results and discussion on the effect of temperature on the electrical resistivity of epoxy nanocomposites can be found in sections 4.2.2 (SWCNT/epoxy) and 4.3.1 (rheological measurements).

4.2 Electric field application to SWCNT/epoxy nanocomposites

Electric fields were applied to epoxy nanocomposites during curing according to the methodology described in section 3.4. For SWCNT/epoxy composites, the effects of varying the electric field strength, frequency, curing temperature and SWCNT concentration were studied and are presented in the next subsections.

4.2.1 Influence of electric field parameters

Electric field strength

Figure 4.6a showcases the impact of varying the electric field strength during curing at 80 ℃ on the final electrical resistivity of SWCNT/epoxy composites at 0.01 wt%, obtained by varying the applied voltage, at a frequency of 10 MHz. A clear effect of the field strength on this electrical property is verified from the comparison of the three steps. Reduced electrical resistivity of the solid nanocomposites was observed with increased field strength, being understood in terms of the induced electrical force on the nanoparticles (which is directly proportional to the square of field strength, see equation 5.2 in section 5.2).

These results (Fig. 4.6a) also suggest a decrease in scatter of resistivity values for higher field strength as the difference between maximum and minimum values decreases notoriously (see error bars). This represents another indication of the importance of this parameter for the formation of more stable and effective CNT conductive networks within the polymer, thus improving reproducibility of the results.

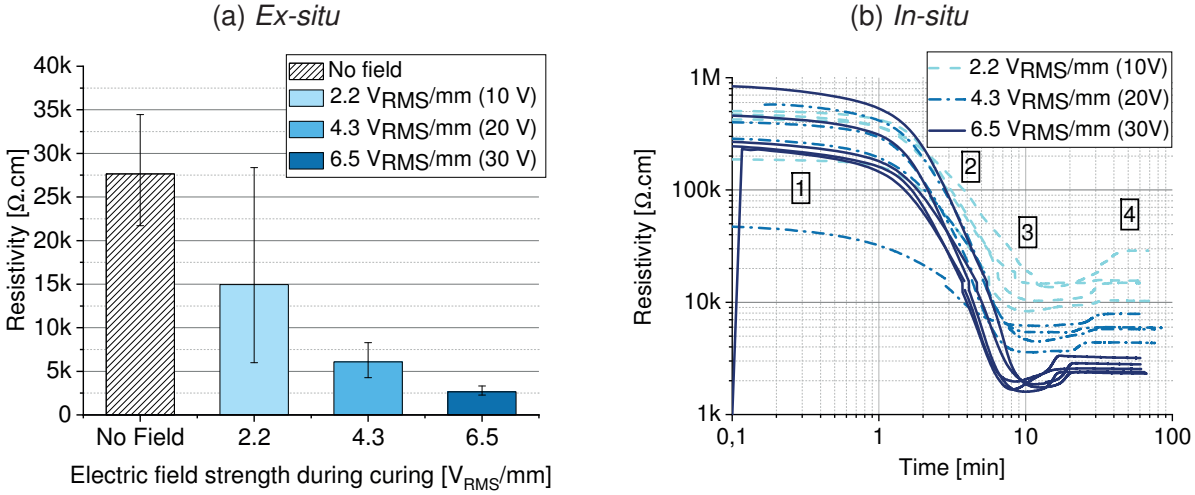

Figure 4.6: Impact of electric field strength (@10 MHz) on the final electrical resistivity of epoxy/SWCNTs 0.01 wt% solid composites cured at a set temperature of 80 ℃ (mould B)

It is important to notice that two processes are taking place simultaneously, affecting the resistivity measurements. On one hand there is the crosslinking reaction of the epoxy resin, whose dynamics might affect the nanotube dispersion state and hence the electrical resistivity. On the other hand, there is the electric field affecting the nanoparticle distribution. In addition, both of these processes are coupled with the viscosity behaviour, which is temperature dependent. *In-situ* curves provide valuable information about the time dynamics of these processes happening during the experiments.
The respective *in-situ* evolution of the DC resistivity with time for the samples in figure 4.6a is represented fig. 4.6b (time plotted in logarithmic scale in the horizontal axis). The first important remark is the agreement between the final resistivity values and the *ex situ* measurements in Fig. 4.6a. It is also possible to clearly distinguish 4 different stages for all the investigated electric field strengths (see Fig. 4.6b) that the resistivity undergoes while the resin is curing:

1. an initial gradual decrease in the first minute;
2. a pronounced drop until a minimum is reached around 10 min;
3. an additional increase lasting up to 10 min;
4. a final plateau corresponding to the final *ex situ* resistivity

This non-monotonic behaviour of resistivity (slight increase in phase 3) is likely related to the final stage of the epoxy cross-linking process: the reduction in the concentration of unreacted amine and epoxy molecules (potential charge carriers) decreases the ionic conductivity [26] and leads to shrinkage, distorting the SWCNT network [26]. Interestingly, the time that resistivity takes to stabilize around its final value decreases with the field strength. This behaviour might be an indication of a faster epoxy-amine reaction completion for the case of 6.5 V_{RMS}/mm, as opposed to a longer network consolidation for 4.3 V_{RMS}/mm and 2.2 V_{RMS}/mm, possibly induced by higher electrical currents flowing through the sample and resulting electro-thermal mechanisms such as Joule effect [60].

Electric field frequency

In a second stage, the electric field strength was fixed at 6.5 V_{RMS}/mm (corresponding to 30 V_{pp}) and the frequency was varied to investigate its impact on the through-plane electrical resistivity of the SWCNT/epoxy nanocomposites. Results are depicted in figure 4.7. While the DC field does not show significant changes on the resistivity as compared with the reference case (without electric field), a decrease in resistivity with increased frequency is clearly observed, with a resistivity plateau starting after 50 kHz. A high scatter of data for the reference samples cured without any electric field and the DC ones was observed, in contrast with the stable measurements noticed when AC electric field was used. This decreasing behaviour of the scatter might additionally point to an improvement of the carbon nanotube networks that are settled between the electrodes during the process.
Following the experiments depicted in 4.7, while DC fields did not lead to much decrease in the electrical resistivity of the final composites, AC electric fields promoted an improvement of up to one order of magnitude. Such enhanced networks could be interpreted, based on the illustration presented in figure 1.3, as follows: due to the electric field, polarisation of the SWCNTs

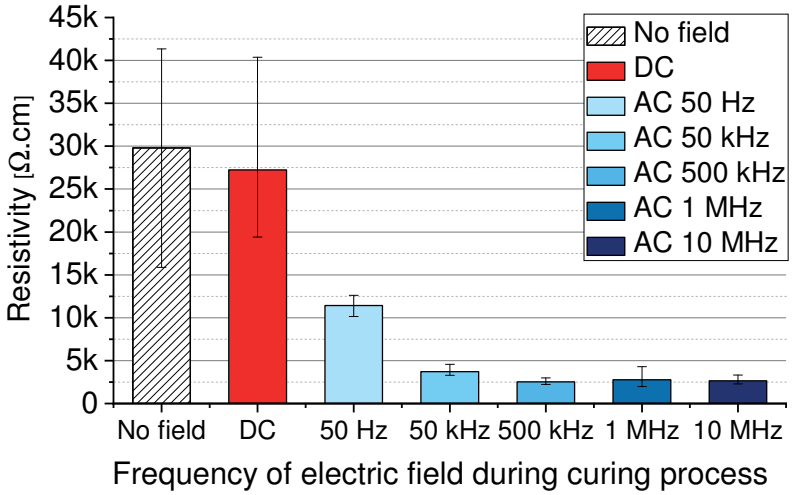

Figure 4.7: Impact of electric field frequency (6.5 V_{RMS}/mm) on the final electrical resistivity of SWCNT/epoxy 0.01 wt% composites cured at 80 °C (mould B)

takes place, leading to interactions with the field and other nanotubes, according to the theory of dielectrophoresis. When these nanotubes get close enough to the electrodes to allow the transfer of charges, they discharge and adsorb onto them. Then, the tips of the nanotubes connected to the electrodes become sources of high field strengths, constituting points for adsorption of more filler particles. The subsequent addition of more carbon nanotubes ultimately leads to a network structure extending from one electrode and reaching the other, providing conductive pathways throughout the specimen.
When DC electric fields were applied, however, no significant decrease of the electrical resistivity was observed (Fig. 4.7). This could be possibility explained by migration of charged nanotubes towards the electrodes under electrophoresis. Charging of the SWCNTs might be attributed to electrostatic interactions arising in the mixing process or due to the presence of negative surface charges on the nanotubes in an epoxy matrix. This effect was also observed in [26, 40], with nanotubes migrating towards the anode.
Further discussion on the effect of the electric field frequency can be found in section 5.2.3, in the context of the results of dielectrophoresis simulations based on this SWCNT/epoxy system. Additionally, the resistivity of SWCNT/epoxy resin without curing agent was investigated at different field frequencies (annex A.4).

4.2.2 Influence of curing temperature

To understand the role of epoxy curing dynamics on the formation of electrically conductive networks, the curing temperature was varied by changing the set temperature on the heating block in mould B. Samples were cured at RT, 80 °C and 100 °C, with final resistivities presented in figure 4.8a, for an electric field with 6.5 V_{RMS}/mm and frequency 10 MHz. For the experiments without application of electric field, increasing the curing temperature from RT to 100 °C shows a remarkable decrease in resistivity, by almost an order of magnitude, falling from more than 100 kΩ cm to almost 20 kΩ cm. The

resistivity was further reduced when cured in the presence of an AC field, as described in figure 4.8a.

As depicted in figure 4.8b, the curing temperature also seems to strongly influence the duration, the slope and resistivity interval of each of the 4 dynamic phases and, overall, there is good agreement between the four experiments for each temperature setting. For this epoxy system, higher temperatures favour states of lower viscosity (see section 4.3.1), which might allow an improved mobility of the CNTs and hence more effective action of the electric field on the induced assembly.

It is essential to realize that for reducing the electrical resistivity of the SWCNT/epoxy composites two experimental instruments were applied: the curing temperature and the electric field. As a matter of fact, Fig. 4.8a shows that a decay in the resistivity of one order of magnitude was achieved solely through increase of the curing temperature. An additional improvement of the same magnitude is thereafter attained by exposing the SWCNT/epoxy to AC electric fields during curing. This reveals two independent phenomena which, when combined, allow for a two order of

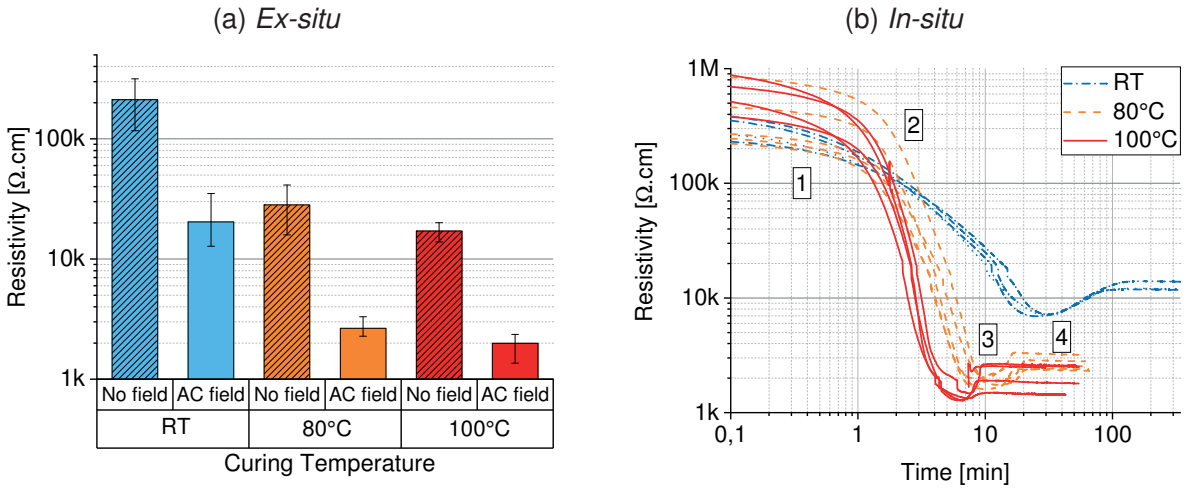

Figure 4.8: Impact of AC electric field (6.5 V_{RMS}/mm @ 10 MHz) during curing at different temperatures on the through-plane electrical resistivity of epoxy/SWCNTs 0.01 wt% nanocomposites (mould B)

magnitude decrease in electrical resistivity for composites with the same concentration of conductive nanoparticles.
One additional possibility has yet to be considered: the electric field resulting in resin heating. Indeed, a temperature difference of around 20 °C was verified between the samples cured at RT with and without electric field (using a thermal camera). This means that samples cured at 80 °C under effect of electric fields reach a temperature of around 100 °C. If the resistivity decrease was related to temperature only, then samples cured at 80 °C under effect of electric fields should have a similar resistivity value to samples cured at 100 °C without electric fields. This is not the case, as it can be observed in figure 4.8a. To further exclude the hypothesis that the resistivity decay in the samples cured under electric field is related only to temperature, further samples were cured at 140 °C (please see annex B.1). If the resistivity decrease was merely a temperature effect, then the resistivity of both samples with and without field should be more similar for a temperature high enough to prevail over the heating generated from the electric field. However, samples cured under an electric field and curing temperature of 140 °C also show a resistivity one order of magnitude lower than those without field. This fact gives additional confidence that the decrease of resistivity measured in this investigation comes from two independent effects: electric field and temperature.

4.2.3 Influence of concentration

To evaluate the effect of nanotube concentration on the resistivity, samples with CNT concentrations of 0.001 wt%, 0.005 wt%, 0.01 wt% and 0.1 wt% were fabricated at 80 °C, with and without AC electric field application. Figure 4.9a shows that the electrical resistivity decreases with increased CNT concentration. The effect of the electric field application becomes significant at 0.01 wt% and above. No differences are noticed for the composite at the lowest (0.005 wt%) concentration.

The *in situ* evolution of the DC resistivity with elapsed time for the samples produced with different concentrations is represented in figure 4.9b. Despite the fact that no *ex situ* resistivity values could be obtained from the composite samples with 0.001 wt%, *in situ* measurements are not only able to provide additional information for this concentration, but also for the pure epoxy resin. The evolution of resistivity with time is able to provide valuable insight into the curing dynamics of the resin, showing a similar behaviour with four different phases. Furthermore, this indicates that the slight increase in resistivity after the minimum - pointed out as phase 3 - must be related to the crosslinking process, since it also happens for the pure resin. In the case of pristine epoxy this is related to a reduction in concentration of unreacted amine and epoxy molecules, potential charge carriers [26].

From these results it can be inferred that the possibility of decreasing the electrical resistivity for this SWCNT/epoxy nanocomposite system is limited to CNT concentrations of 0.01 wt% and above. Moreover, this improvement seems to be less effective for 0.1 wt%. This could be caused by the significant increase in viscosity (see rheology measurements in section 4.3.1), hindering the mobility of carbon nanotubes, or due to the fact that at this

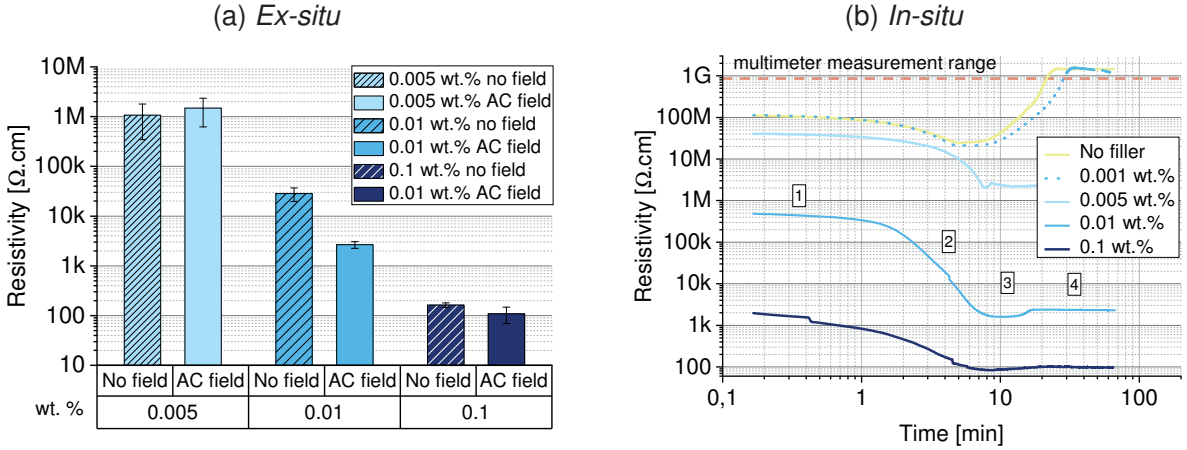

Figure 4.9: Impact of AC electric field (6.5 V_{RMS}/mm @ 10 MHz) during curing (at 80 °C) of epoxy/SWCNTs with different concentrations on the through-plane electrical resistivity (mould B)

concentration, well above percolation (between 0.001 wt% and 0.005 wt%), there are already so many contacting points between the CNTs that the final resistivity is not significantly altered by additional ones. This question is further investigated with finite element simulations in sections 5.3.2 and 5.3.3.

4.2.4 Influence of interface electrode/nanocomposite

Following the previously described experiments, mainly performed in mould B (fig. 3.3), dielectrophoresis experiments were further performed in Mould C (fig. 3.4) with SWCNT/epoxy 0.01 wt% composites. The main goal of this set-up was to produce multiple plate specimens simultaneously and with a shape defined by the silicone mould, which is a scalable process. In this case, Mould C was used to produce 6 disk samples (20 mm diameter and 1.5 mm thickness). Furthermore, the influence of distinct mould release agents was investigated (see 3.1.5).

Figure 4.10 shows the resistivity values measured between the electrodes after the curing of SWCNT/epoxy 0.01 wt% at 100 °C, with and without electric field (E=14.1 V_{RMS}/mm). The measurement was done here before opening the mould, so the values represent the total resistivity of the material connecting the electrodes. In accordance to the experiments with Mould C, one order of magnitude decrease in the resistivity was measured. However, a clear difference was noticeable when different mould release agents were used. With MR3 (silver paint), the most conductive one, both the resistivity with and without electric field were two orders of magnitude lower than that of MR1. MR2 (intermediate conductivity) appeared to be in between the two and showed a smaller difference between field and no field. This likely related to the contact resistance of the interface between the electrodes and the SWCNT/epoxy composite, which is presumably higher for MR1 and MR2. After specimen retrieval from the mould, cleaning and gold sputtering for through-plane resistivity measurements, this property was evaluated for the individual disk samples. Figure 4.11 displays the average resistivity

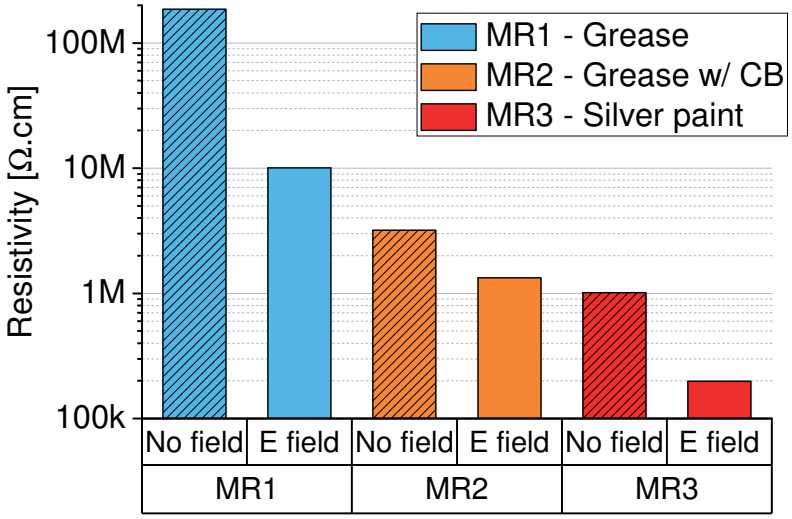

Figure 4.10: Impact of mould release agent on plate resistivity measured at the electrodes (after cure) for SWCNT/epoxy 0.01 wt% composites cured under 14.1 V_{RMS}/mm @ 10 MHz at 100 ℃ in Mould C

of individual samples corresponding to the experiments in figure 4.10. Not only seems the difference between electric field and no field to be less pronounced than in fig. 4.10, but also the resistivity values show the opposite trend: MR3 leads to the highest average resistivity and MR1 to the lowest. This behaviour can be explained by considering the properties of the individual samples after curing under the electric field, depicted in figure 4.12. In these graphs, the electrical resistivity of samples is plotted according to their fixed position in the mould, numbered from 1 to 6. For samples produced without electric field 4.12a, the electrical resistivity of six samples for each mould release agent does not vary considerably. However, when an electric field is applied (4.12b), it is possible to observe that MR3 and MR2 show a great disparity of results between the six samples. MR3, for example, has specimen 4 with a resistivity of only 1.7 kΩ cm, being the most conductive sample produced. However, samples 1,2,5 and 6 are all above 10 kΩ cm.

A possible explanation for the measurements of total resistivity in fig. 4.10 is the following phenomenon: given the very low contact resistance of silver paint (MR3), more electrical current is able to flow between the electrodes.

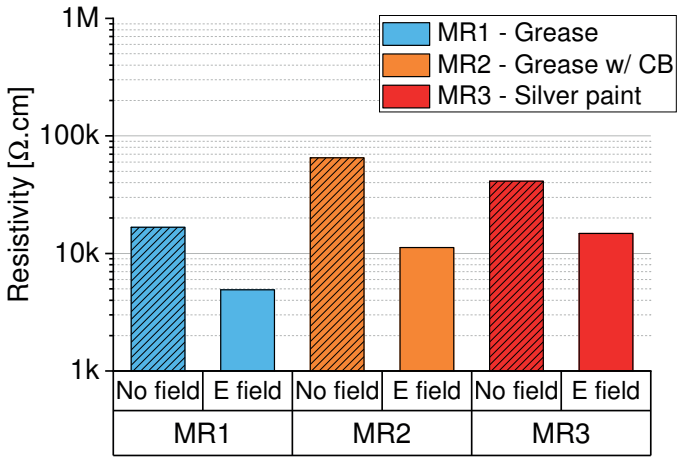

Figure 4.11: Impact of mould release agent on average resistivity of SWCNT/epoxy 0.01 wt% samples cured under 14.1 V_{RMS}/mm @ 10 MHz at 100 °C in mould C

Due to this current, the electric field propagates in the material across the sample thickness as new conductive paths are generated in the material due to CNT dielectrophoresis (see 5 for more on dielectrophoresis of CNTs). However, as soon as one of the samples becomes more conductive (sample 4 of MR3 in fig. 4.12b), more and more current starts flowing only through it, since it offers less resistivity, and less through the other samples (like 1, 2, 5 and 6 of MR3 in fig. 4.12b). This would explain the scatter in the resistivity values of samples MR3 and MR2 (fig. 4.12b) and also the lower complete resistivity presented in fig. 4.10.
These results highlight the importance of the contact interface (more specifically its resistivity) between the electrodes and the composite for influencing the electrical resistivity of SWCNT nanocomposites with electric fields.

4.3 Characterisation of SWCNT/epoxy composites

4.3.1 Rheology of SWCNT/epoxy dispersions

Figure 4.13 depicts the viscosity measurements of the epoxy and composite resin as a function of temperature. As expected, a strong dependency of

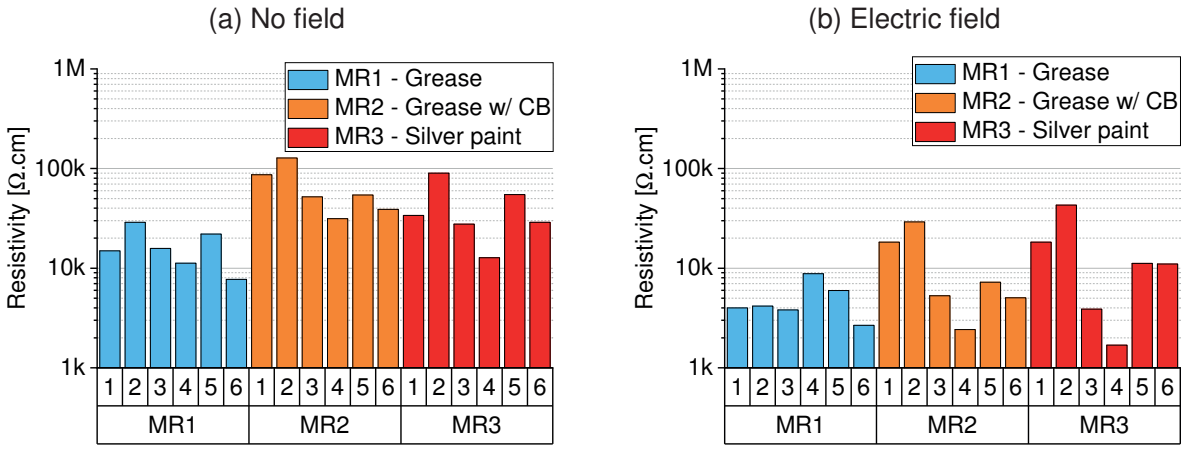

Figure 4.12: Impact of mould release agent on resistivity of SWCNT/epoxy 0.01 wt% individual samples cured under 14.1 V_{RMS}/mm @ 10 MHz at 100 °C in mould C

viscosity on temperature was found - for pure epoxy it decreased two orders of magnitude, from around 1 Pa s at 20 °C to 10 mPa s at 100 °C. The addition of only 0.01 wt% SWCNTs leads to a slight increase of viscosity of the composite resin, whereas for 0.1 wt% there is a remarkable difference (one order of magnitude higher at 100 °C). Given the fact that viscosity of a fluid provides an indication of its mobility and that of the particles immersed in it, these results might explain the tendencies found when curing the materials at different temperatures (figs. 4.8a and 4.8b). Higher temperatures lead to a lower viscosity and hence increased mobility of the SWCNTs, promoting reduced CNT-to-CNT separation distances and CNT chaining and therefore lower resistivity. As such, the viscosity of the SWCNT/epoxy system (with the curing agent) was evaluated. The complex viscosity (η^*) of the reacting system was investigated for the three different temperatures (20 °C, 80 °C and 100 °C) by curing it on a rheometer in oscillatory shear mode at 1 Hz.
In figure 4.14, the modulus of the complex viscosity $|\eta^*|$ and the loss factor $\tan\delta$ of the three curing processes are presented as a function of time. The initial value of $|\eta^*|$ was found similar for 80 °C and 100 °C, while a higher value was observed at 20 °C. In accordance with the *in situ* resistivity measurements depicted in fig. 4.8b, it was observed that the onset of the reaction

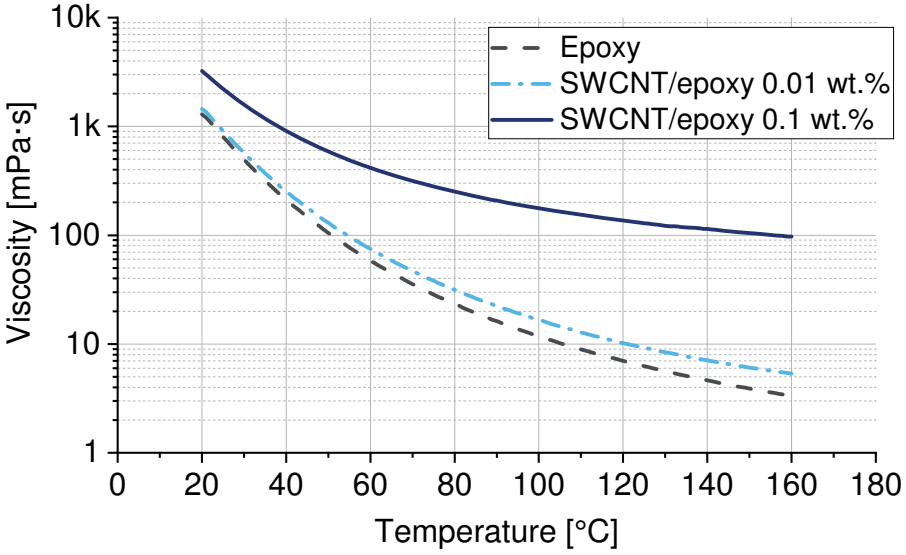

Figure 4.13: Viscosity measurements of the pristine epoxy and SWCNT/epoxy composite resin with temperature (without curing agent)

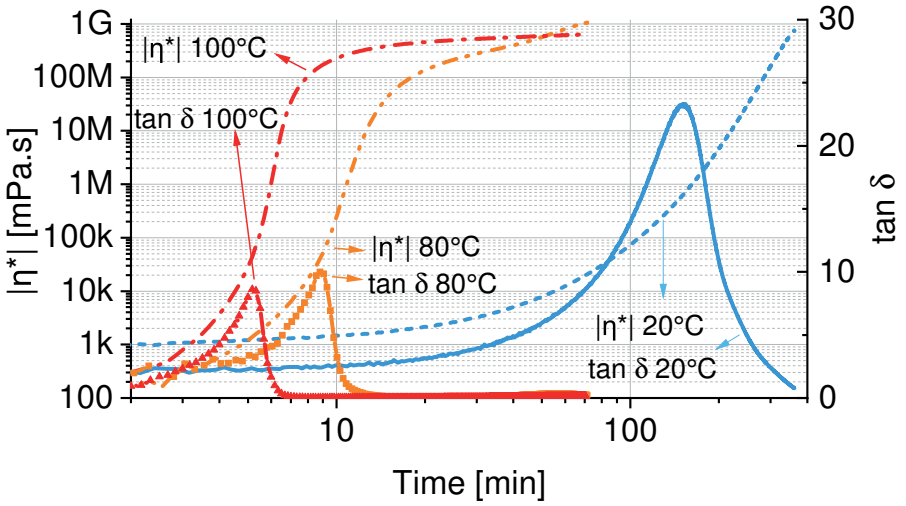

Figure 4.14: Modulus of complex viscosity $|\eta^*|$ and loss factor $\tan\delta$ of SWCNT/epoxy 0.01 wt% during curing reaction

takes place before and its duration becomes shorter at higher temperatures: at 100 ℃ (red curves), $|\eta^*|$ starts increasing and stabilizes faster and so does the corresponding peak of $\tan\delta$ (an indication of the energy dissipation during the reaction).

These rheological data provide valuable insight for understanding the behaviour of the electrical resistivity of SWCNT/epoxy composites when cured at different temperatures. Indeed, accounting for the curing dynamics and the onset of the reaction only, lower curing temperature would theoretically allow more time for the electric field to influence the CNTs and hence promote lower electrical resistivity of the final composite. Nonetheless, despite faster reaction times, higher curing temperatures have shown to promote lower electrical resistivity, as distinctly observed in the *in situ* resistivity curves plotted in fig. 4.8b. This can be noticed also for the difference between the samples cured at 80 °C and 100 °C. Even though the reaction is faster at the higher temperature - $tan\delta$ peak takes place around 4 min before (fig. 4.14) - i.e. the time window for the electric field to act reduces from 9 min to 5 min (almost 50 %) - the final resistivity values are still slightly lower for 100 °C (figs. 4.8a and 4.8b). One likely explanation for this phenomenon is the decreasing viscosity with increased temperature, as depicted in fig. 4.13, allowing for particle mobility and therefore van der Waals and $\pi - \pi$ interactions [40, 45, 44]. In general, low viscosity systems promote more CNT-CNT connections due to the particle interactions and enhanced CNT mobilities, rendering lower resistivities and percolation thresholds on such systems [61]. Another possibility is the temperature dependency of Brownian motion, which also plays a role in particle dynamics [26, 45, 28, 29].

4.3.2 Morphology characterisation

To evaluate the morphology of SWCNT networks in SWCNT/epoxy samples, specimens were both cryo-fractured and cut using a diamond blade and investigated using SEM and atomic force microscopy. Unfortunately, due to the very low filler content (0.01 wt%), it was very challenging to get meaningful results. For SEM, it was found that samples had to be gold sputtered for exactly 10 s only: either without sputtering, or with longer than 10 s (20 s) it was impossible to visualize the SWCNTs. AFM investigations of diamond

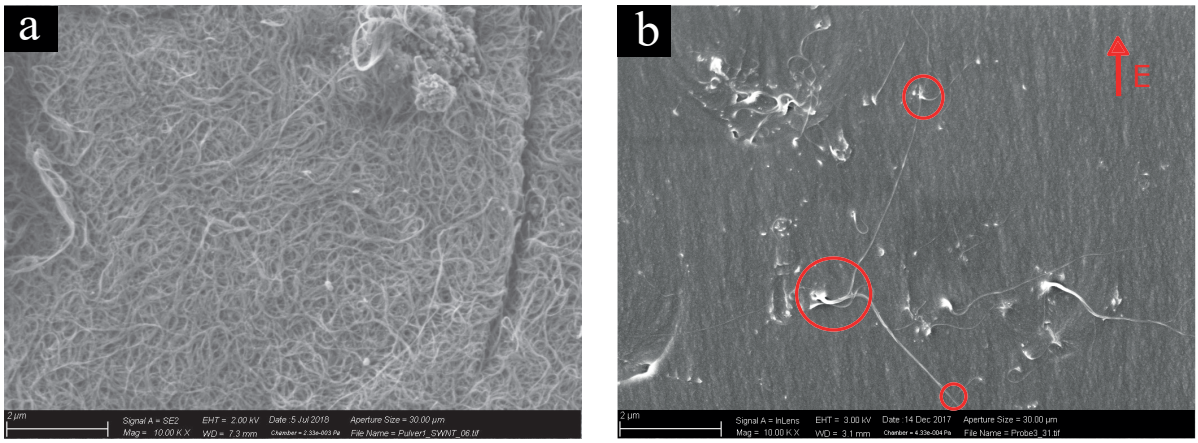

Figure 4.15: SEM images of a) the pristine SWCNT powder and b) cryo-fractured SWCNT/epoxy 0.01 wt% specimen produced under effect of electric field (direction indicated by red arrow) - red circles indicate possible bridging point between adjacent SWCNTs

cuts from the same samples did not allow for further inferences on the nanostructure of SWCNTs.

Figure 4.15 shows the SWCNTs in their as-received powder form (a) and a cryo-fractured surface of a SWCNT/epoxy 0.01 wt% specimen cured under the effect of an AC field (b). Thin and long individual structures can be clearly seen in fig. 4.15b, confirming the SWCNTs dispersion by the three-roll mill technique and subsequent composite fabrication process. According to transmission electron microscope observations of the SWCNTs from literature [62], it is generally expected that the individual structures are actually strands (microcrystals) of SWCNTs with a thickness of around 20 nm as a consequence of the manufacturing process. As it is possible to observe in 4.15, these strands display a wavy and flexible shape quite distinct from the ideal conception of rigid tubes at the macro scale.

Moreover, on the samples treated with an electric field, SWCNTs do not appear to present a defined preferential orientation along the field's direction (indicated on the top right-hand side corner), despite the clear decay in electrical resistivity measured. This could be due to the nanotubes' long aspect ratio and curvy shape: due to the electric field, SWCNTs become polarized and the local dipoles interact with each other. As soon as a nanotube finds another one in its vicinity and a contact between them is established, the

interaction is ceased and their displacement stops before each of them has the chance to adopt a clear oriented placement within the epoxy matrix.
It should be noted that these images represent only a reduced two-dimensional perspective of the bulk material and that the chance of getting representative results in exactly the fracture surface is extremely low. Nevertheless, one can presume to recognize some contacting points between neighbouring particles (marked in red in 4.15b). An improvement on the electrical conductivity of the final bulk material could be thereby explained by changes in these CNT-to-CNT contacts. This hypothesis is investigated in section 5.3 with a finite element model of CNTs for computation of their electrical properties.

4.4 Electric field application to GNP/epoxy nanocomposites

Figure 4.16 compares electrical resistivity values of GNP/epoxy nanocomposites at different concentrations produced with and without electric field (7 V_{RMS}/mm @ 1 MHz). For each of concentration, 4 disc-shaped samples under electric field effect and 4 reference samples with no field applied were cured in an oven at 80 °C.
The enhancement of through-plane electrical conductivity is present at all concentrations, with a slightly lower effect for the highest load of GNPs (2 wt%). Even if the resistivity decrease is lower than expected, when considering the order of magnitude difference verified for SWCNT/epoxy 0.01 wt%, in the case of GNPs it appears to span over a broader range of concentrations.

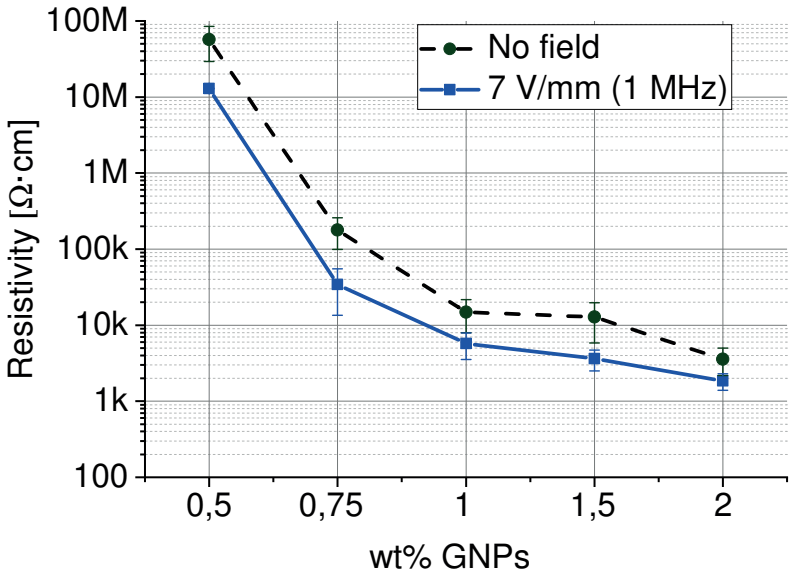

Figure 4.16: Resistivity of GNP/epoxy nanocomposites under effect of electric field (7 V_{RMS}/mm @ 1 MHz) for different concentrations

5 Simulations

5.1 Acknowledgements

This chapter presents some results of a collaborative effort with two scientists which ultimately led to the submission of a joint article for the journal Carbon. Inspired by his work on dielectrophoresis of CNTs [63, 40, 44, 64], I contacted Dr. Andrés Oliva-Avilés and told him about my ideas and plans to do experiments with SWCNT/epoxy dispersions in electric fields. This was the beginning of a very successful joint work and I am deeply grateful for all his help, patience and advice. He used a dielectrophoresis model to simulate a system under similar conditions to my experiments at the Fraunhofer ICT. Some of the work done by Dr. Andrés Oliva-Avilés published in [65] is presented in section 5.2.
The second collaboration started within the European project TheLink, which funded this research, with fellow researcher Miguel Matos. For his PhD, he has used finite element analysis to simulate CNT networks and compute macroscopic properties as electrical resistivity and its change with mechanical deformation. Taking his simulation as a starting point, we decided to investigate the theoretical implications of changing the minimum contact distance between CNTs dispersed in an epoxy matrix on the electrical resistivity of the bulk composites. This could help us understanding the changes in resistivity observed in the experiments with SWCNT/epoxy. Miguel's ideas, hard work, and willingness to help were extremely valuable for this work and for that I am really thankful. Some of the work of Miguel Matos published in [65] is presented in section 5.3.

5.2 Dielectrophoretic model of interacting SWCNTs in a fluid

As introduced in section 2.1, applying an electric field to a non-charged particle in a liquid medium might lead to the generation of a dielectrophoretic force, depending on the particle's and medium's dielectric and electric properties. If the particle has an aspect ratio, this force can cause rotation and translation of the particle in the medium depending on the frictional resistance between the two.
In section 4.2, several electric field and processing parameters have been investigated for the production of electrical conductive SWCNT/epoxy composites. In an attempt to further understand the observed decrease of the electrical resistivity of these materials due to the electric field, its influence on the rotation and interconnection was studied by modelling the interaction between two SWCNTs using classical mechanics and dielectrophoresis theory. The main goal was to investigate the dependency on field strength and frequency, and viscosity of the resin.

5.2.1 Theoretical considerations

To elucidate the role of the main experimental parameters involved in the curing of SWCNT/epoxy composites under an electric field, an analytical simplified approach based on classic mechanics and on the dielectrophoretic theory was used [44, 64]. According to the theory of dielectrophoresis, when an electric field is applied to a system of particles immersed in a fluid, the charge distribution is rearranged at the interphase of the particle/medium system due to their different dielectric properties (electrical conductivity and permittivity) [28, 29]. Furthermore, the effective dipole moment approach [28, 29] considers that such a rearrangement of charge induces a dipole moment on the CNTs, which would interact with the electric field causing the rotation (alignment) and translation of CNTs. As such, the model conceives the CNTs as electrical dipoles, with positive and negative induced charges

at their opposite ends, see figure 5.1. The model considers two metallic CNTs (CNT-1 and CNT-2) as straight and rigid prolate ellipsoids in an one-dimensional framework, with centres of charge in coordinates x_1 and x_2 and deviation angles of θ_1 and θ_2, being these the angles comprised between the CNT axis and the direction of the electric field (E) (horizontal in fig. 5.1). It is important to mention that the assumption of CNTs as straight and rigid is an idealization; CNTs are wavy and generally entangled. However, such an assumption allows the development of a simplified model exploring coupled rotational and translational motion which helps to understand the CNT response under AC electric fields and therefore the formation of interconnected conducting networks [44, 64]. The model also considers a CNT/medium interphase layer (not illustrated in fig. 5.1) which captures the effect of the electric field frequency (f) on the magnitude of the induced dipole on the CNTs [44].

To evaluate the CNT rotation and translational motion, a set of coupled non-linear differential equations based on Newton's Second Law are considered for each case. For the rotational motion, the governing motion equation for each CNT is given by:

$$I\frac{d^2\theta}{dt^2} + T_{DEP} + T_{fr} + T_{coup} = 0 \tag{5.1}$$

The first term in equation 5.1 is a rotational diffusion induced by the electric field, a term that is commonly seen in fiber orientation models where the

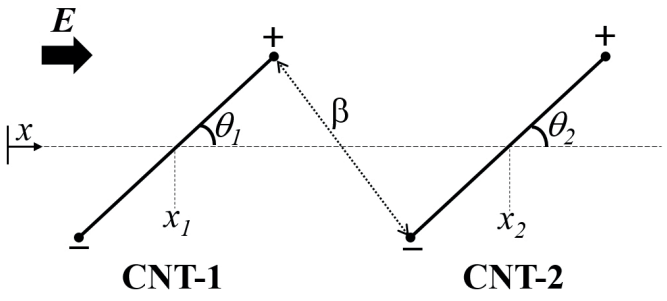

Figure 5.1: Schematic of the CNTs and illustration of variables of dielectrophoresis model

rotation is hydrodynamically induced. $I = \frac{m(a^2+b^2)}{5}$ where $m = d_{CNT} \times V$, is the mass of CNTs, d_{CNT} is the CNT density, V is the volume ($V = \frac{4}{3}\pi a b^2$), and a and b are the major and minor CNT semi axes, respectively. The second term in Eq. 5.1, T_{DEP}, corresponds to the dielectrophoretic torque exerted by the CNT due to the presence of an electric field and is given by the expression:

$$T_{DEP} = \frac{1}{4} V \epsilon_m E^2 Re[\alpha^*] \sin 2\theta \tag{5.2}$$

$$\alpha^* = \frac{(\epsilon^*_{eq} - \epsilon^*_m)^2}{[\epsilon^*_m + (\epsilon^*_{eq} - \epsilon^*_m)L](\epsilon^*_{eq} + \epsilon^*_m)} \tag{5.3}$$

$$\epsilon^*_{eq} = \epsilon^*_{lay} \left[\frac{\epsilon^*_{CNT} + \frac{\delta}{2a}(\epsilon^*_{CNT} - \epsilon^*_{lay})}{\epsilon^*_{lay} + \frac{\delta}{2a}(\epsilon^*_{CNT} - \epsilon^*_{lay})} \right] \tag{5.4}$$

$$\epsilon^* = \epsilon - j\frac{\sigma}{2\pi f} \tag{5.5}$$

where E is the electric field magnitude, δ is the thickness of the interphase layer, $L = \left[ln\left(\frac{2a}{b}\right) - 1 \right] \Big/ \left(\frac{a}{b}\right)^2$ is the CNT longitudinal depolarisation factor [44, 29], ϵ is the permittivity, σ the electrical conductivity and subscripts CNT, m and lay stand for carbon nanotube, surrounding medium and interphase layer, respectively. From Eq. 5.3, it can be observed that α^* depends on the electric field frequency f, and the real part (Re) of α^* impacts on the magnitude of T_{DEP} . For more detailed explanations and rationale regarding the expression of T_{DEP}, please refer to [44, 64]. In Eq. 5.1 T_{fr} refers to the frictional (viscous) torque and T_{coup} represents the torque exerted by the CNT due to the presence of the other CNT. Expressions for T_{fr} and T_{coup} terms in Eq. 5.1 can be found in [64]. Initially, the CNTs were considered misaligned in respect to the electric field, with initial angles set to $89°$ (instead of $90°$) to avoid numerical issues during the computational solution process due to the non-linearity of the equations. The initial angular velocity was set to zero. The evolution of the rotational angles of the CNTs is obtained by

solving Eq. 5.1 numerically. Using a similar rationale, the governing equation for the translational motion is given by,

$$m\frac{d^2x}{dt^2} + F_{fr} + F_{coup} + F_{rep} = 0 \tag{5.6}$$

where, similarly to equation 5.1, the first term is a translational diffusion that in common fibre reinforced composites is induced by the flow field itself. F_{fr} and F_{coup} refer to the frictional and coupling forces exerted by each CNT, see [64]. F_{rep} in Eq. 5.6 refers to a short-range repulsive force that decays quickly with the CNT-to-CNT separation distance (β, see fig. 5.1), which is incorporated in the model to prevent the CNT overlapping [64]. By numerically solving 5.6 the time evolution of the position of both CNTs' centres of mass, and therefore β, can be computed. The initial positions of CNTs were set in such a way that the horizontal distances between their centres of mass ($x_2 - x_1$ in fig. 5.1) was 7 µm, and their initial translational velocity was zero. It is important to note that equations 5.1 and 5.6 are coupled by the direct dependence of T_{coup} on F_{coup} terms [28].

Table 5.1 shows the fixed value parameters used in the model, selected based on the experimental conditions used in this study and previous works [44, 64]. It should be noted that a CNT/epoxy curing under electric fields is a complex system with several influencing factors Viscosity, electric field magnitude and frequency were varied in the model using experimentally used values, and the influence of such changes is evaluated in the model predictions. The permittivity of the fluid (liquid epoxy) is assumed to be 11, which was measured with dielectric spectroscopy at RT. In general, the permittivity of the resin depends on the temperature but is expected that the moderate increase of the T (up to 100 °C) does not change significantly such a value. Additionally, the very high difference between permittivity of fluid and particle makes the slight changes on the fluid permittivity almost negligible for the effective dielectrophoretic forces and torques [28, 64].

Table 5.1: Numerical parameters used for the simulations

	Physical property	Fixed value
CNT	Permittivity, ϵ_{CNT} [-]	1×10^5 [64]
	Electrical conductivity, σ_{CNT} [S m^{-1}]	1×10^4 [66]
	Density, d_{CNT} [kg m^{-3}]	2000 (est. from [67])
	Major semi-axis, $a = L_{CNT}/2$ [µm]	2.5 [55]
	Minor semi-axis, $b = D_{CNT}/2$ [nm]	1 [55]
	Aspect ratio [–]	2777
Fluid	Permittivity, ϵ_m [-]	11 [exp, RT]
	Electrical conductivity, σ_m [S m^{-1}]	3×10^{-5} [exp]
	Viscosity, μ [mPa s]	30 and 1500 [exp]
CNT/fluid interphase layer	Permittivity, ϵ_{lay} [-]	1×10^4 [64]
	Electrical conductivity, σ_{lay} [S m^{-1}]	1×10^{-4} [64]
	Thickness, δ [nm]	10 [64]
Electric field	Magnitude, E [V mm^{-1}]	2.1 and 6.5 [exp]
	Frequency, f [Hz]	50 and 1×10^6 [exp]

5.2.2 Results of dielectrophoresis modelling

The dependence of the polarisation factor α^* on the electric field frequency was first explored by means of Eq. 5.3 with the values from table 5.1 and the results are presented in 5.2. It can be observed that $Re[\alpha^*] \approx 265$ is computed for frequencies up to 100 Hz and then the magnitude increases for higher frequencies, reaching a plateau value of $Re[\alpha^*] \approx 2300$ at approximately f = 10 kHz. According to the dielectrophoresis model, a higher polarisation factor indicates higher magnitudes for the electric field-induced torques and forces exerted by the CNT, which would impact in more accelerated dynamics [44, 64]. This trend has also been validated by experiments, where authors reported faster and better-aligned structures when the electric field is increased [32, 68, 69].

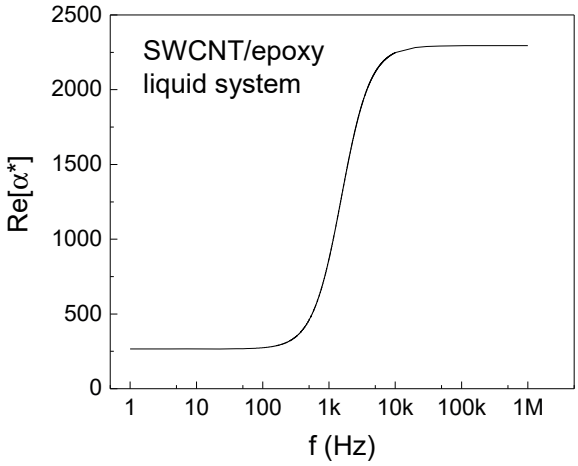

Figure 5.2: Real part of the polarisation factor α^* (see Eq. 5.3) as a function of electric field frequency for a SWCNT immersed in liquid epoxy

From the solution of Eqs. 5.2 and 5.6, the temporal evolution of the CNTs angle (θ, black lines) and the CNT-to-CNT separation distance (β, red lines) is presented in fig. 5.3 for cases where the frequency, electric field and viscosity were varied (as in the experiments), in order to explore their influence on the CNTs motion. For all cases, the CNT alignment (i.e. when$\theta \approx 0$) is the first event to be completed and then the CNTs horizontally translate until reaching contact (i.e. when $\beta \approx 0$). For both frequencies, β experiences a sudden decrease (see red lines) which is related to the CNT rotation, i.e. β is lowered as the CNTs rotate towards the alignment condition (see fig. 5.3). Once alignment of the CNTs is reached, it can be observed that the translational motion follows a slower rate, experiencing a sudden decrease towards the chained condition ($\beta \approx 0$) once the CNTs are close enough. Fig. 5.3a shows that faster CNT alignment occurs when the frequency is increased from 50 Hz (black dashed line) to 1 MHz (black solid line). A similar trend is also appreciated for the elapsed time for the CNT-to-CNT chaining (red lines), with shorter elapsed times of chaining when the frequency is increased. As expected from the behaviour of the polarisation factor in fig. 5.2,

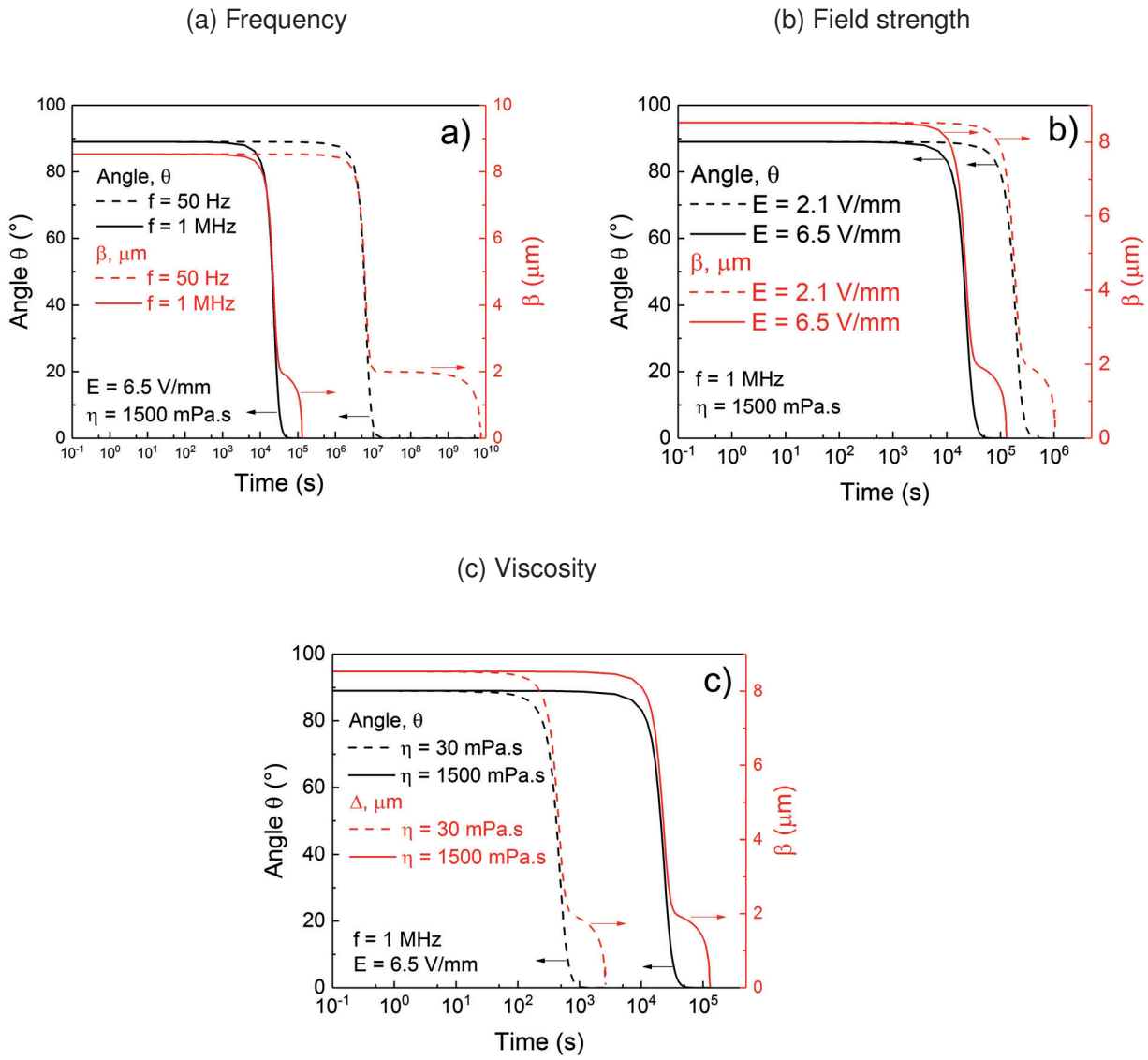

Figure 5.3: Rotational angle (left vertical axis) and CNT-to-CNT separation distance (β, right vertical axis) as a function of time for a SWCNT/epoxy system. a) Influence of electric field frequency, b) electric field magnitude, and c) medium

the dynamic of rotation and translation is accelerated due to the increased dielectrophoresis-induced torques and forces.

A similar trend regarding the influence of the electric field magnitude (fig. 5.3b) and medium viscosity (fig. 5.3c) on the alignment and chaining times can be noticed. From fig. 5.3b it is seen that the rotational and translational

dynamics are accelerated when the electric field magnitude is increased, which can be somehow expected from the quadratic dependence of T_{DEP} on E^2 in Eq. 5.2. In addition, higher viscosity promotes a slower rotational and translational motion of the CNT, which can be observed in figure 5.3c. It is important to consider that the dielectrophoresis model has certain simplified assumptions which may impact in the order of magnitude of the predicted times, which may seem very long. For example, CNTs are considered isolated with influence of solely their first neighbour CNT. This fact neglects other type of interactions that would contribute to accelerated processes. Also, no electric field gradients are considered, which also underestimates the effect of dielectrophoresis-forces promoting CNT motion. However, despite these assumptions, the main aim of this simple model is to capture specific trends regarding the influence of experimental parameters associated with the experiments. The connection of the trends predicted by the dielectrophoresis model with the experimental results is discussed in following section.

5.2.3 Correlation of experimental results and dielectrophoresis simulations

In the experiments with SWCNT/epoxy under electric fields presented in section 4.2, a clear dependency on the frequency was verified. Such effect stabilized above ca. 50 kHz (fig. 4.7), i.e. for the frequencies tested above this value (500 kHz, 1 MHz, 10 MHz) the electrical resistivity stayed in the same range. One way of interpreting these results using dielectrophoresis theory is to analyse the development of the polarisation factor α^* with the electric field frequency. In fact, according to equation 5.2, the dielectrophoresis-induced torque on the CNTs is directly proportional to $Re[\alpha^*]$, meaning the higher $Re[\alpha^*]$, the stronger the momentum on the CNTs causing them to reorient. Interestingly, from the dielectrophoresis model of this SWCNT/epoxy system, $Re[\alpha^*]$ increases for higher frequencies up until a plateau at around 10 kHz (fig. 5.2). This implies that the frequency contribution for the dielectrophore-

sis torque (and hence for the conductive network formation) is maximized at this frequency range, thereby providing a possible explanation for the frequency dependency of resistivity improvement observable on figure 4.7.
From figs. 4.6a and 4.6b, the higher the electric field strength (E) applied (or voltage) the lower the resistivity of the SWCNT/epoxy composites produced. This is related to dependency of the dielectrophoresis-induced torque (T_{DEP}) on E^2 (Eq. 5.2) and this effect is verified by the dielectrophoresis simulations where E was varied according to the experimental parameters. In fact, increasing the field strength from 2.1 kV mm^{-1} to 6.5 kV mm^{-1} in the modelling scenario of the two interacting CNTs leads to a decrease of the alignment time of around one order of magnitude (fig. 5.3b).
The third parameter investigated using the dielectrophoresis model was the viscosity of the medium. Fig. 5.3c presents the CNT angle and chaining for the viscosities of 30 mPa s and 1500 mPa s. As predicted, at higher viscosity the rotational and translational motion of the CNT becomes slower. This can be of critical importance given the fact that the system under investigation is a reactive one, and so there is only a limited amount of time for a rearrangement of the CNTs to take place, as evident by the rheological behaviour of this SWCNT/epoxy system studied in section 4.3.1.

5.3 Finite element (FE) modelling of the bulk conductivity of CNT-polymer networks

Finally, the impact of the distance between adjacent CNTs in the bulk on the electrical properties was explored using FE analysis for a variety of particle concentrations, revealing resistivity changes compatible with the experimental observations.

5.3.1 Theoretical considerations

With the objective of quantifying the effect of the distance between CNTs on the bulk electrical properties of the composite materials, the methodology

presented in Ref. [70] was applied. This allows modelling of all the main mechanisms of conductivity in these systems:

1. conductivity of the CNTs,
2. conductivity across CNT-CNT junctions and
3. conductivity of the polymeric matrix

Electrical conductivity was calculated based on simulations of representative volume elements (RVE) where CNTs are randomly distributed in a cubic matrix.
For this approach, CNTs were described by continuum cylinders with prescribed length L_{CNT} and external diameter D_{CNT}. These were seeded at random locations within the RVE of side L_{RVE} and at random azimuthal and latitudinal angles. Since the nanotubes are impenetrable, a search for intersections was performed. When an intersection was detected, the respective nanotubes were locally deformed so that the minimum distance that separates them d_{min} was never inferior to the van der Waals equilibrium distance of 0.34 nm [71]. Once the desired volume fraction is reached, geometric periodicity is enforced so that the macroscopic material can be idealized as a periodic repetition of the RVE along all Cartesian directions, as represented in fig. 5.4.
The electrical analysis is performed using Abaqus steady-state heat-transfer analysis [72], replacing all thermal properties with the adequate electrical equivalents [73]. The CNTs are modelled by DC1D2 2-noded link heat transfer elements that are embedded in the polymeric matrix, discretized by a regular mesh of DC3D8 8-noded brick elements. The conductivity between adjacent CNTs is modeled with a user element [70] integrated into a Fortran UEL subroutine in Abaqus [74] that reproduces the fluctuation-induced tunneling electron transport [75] using Simmons's generalized formula [76]. The tunnel current density J across the contacting CNTs that are separated by a thin insulating layer of permittivity ϵ can be expressed as a function of the separation s between them, as

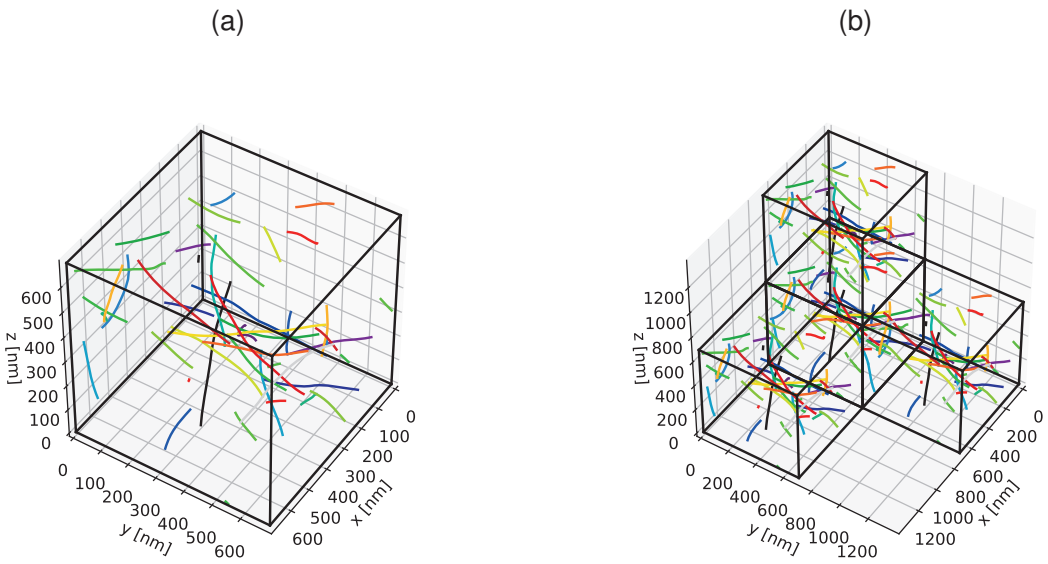

Figure 5.4: Example of a) an RVE and b) its periodicity

$$J = J_0 \left\{ \bar{\varphi} \mathrm{e}^{-A\sqrt{\bar{\varphi}}} - (\bar{\varphi} + eV)\mathrm{e}^{-A\sqrt{\bar{\varphi}+eV}} \right\} \tag{5.7}$$

$$J_0 = \frac{e}{2\pi h(\Delta s)^2} \tag{5.8}$$

$$A = \frac{4\pi\Delta s}{h}\sqrt{2m_e} \tag{5.9}$$

where the constants e and m_e represent the charge and mass of the electron, respectively, and h is Planck's constant. $\bar{\varphi}$ is the mean value of the potential barrier, which has two roots at positions $s_1$and s_2, with $\Delta s = s_2 - s_1$. For a potential barrier of magnitude φ_0, here taken as the CNT work function, these can be approximated by [76]

$$\bar{\varphi} = \varphi_0 - \frac{eV}{2s}(s_1 + s_2) - \left[\frac{1.15\omega s}{s_2 - s_1}\right] \ln \frac{s_2(s - s_1)}{s_1(s - s_2)} \tag{5.10}$$

$$s_1 = \frac{1.2\omega s}{\varphi_0} \tag{5.11}$$

$$s_2 = \begin{cases} s_1 + s\left[1 - \frac{9.2\omega}{3\varphi_0 + 4\omega - 2eV}\right], & eV < \varphi_0 \\ (\varphi_0 - 5.6\omega)\left(\frac{s}{eV}\right), & eV \geq \varphi_0 \end{cases} \tag{5.12}$$

$$\omega = \frac{e^2 \ln 2}{8\pi\epsilon s} \tag{5.13}$$

This effect is here described as an equivalent parallel-plate capacitor of area D_{CNT}^2 and separation s. The element is applied to every contact point between distinct nanotubes within a distance inferior to $d_{cut-off} = 4\,\text{nm}$. Periodic boundary conditions are enforced at every boundary of the RVE and 3 load steps are created, each representing a homogenized electric field along each of the 3 Cartesian directions, allowing the retrieval of the conductivity all directions (which should tend to the same number for an isotropic dispersion).

5.3.2 Results of finite element modelling

The FE methodology described in the previous section was used to investigate the effect of infinitesimal changes of the minimum contact distance between CNTs within the polymer matrix, and its relation to the measured improvements in conductivity. We considered a test case based on the CNT dispersion in epoxy as investigated in [70, 77]. CNT dimensions and properties considered by Hu et al. [77] are presented in table 5.2. As before, we considered a nanotube resistivity $\rho_{CNT} = 1/\sigma_{CNT} = 1 \times 10^{-4}\,\Omega\,\text{m}$, and an epoxy resistivity of $1 \times 10^6\,\Omega\,\text{m}$. For the tunnelling junctions, a relative permittivity of 3.98 (representative of epoxy) and a work fraction of 4.95 eV [78] were used.

To allow generalization to any CNT-epoxy system, results are presented in adimensional form (similar to the dimensional analysis in [79]). Moreover, according to the percolation theory [17], the composite conductivity around

Table 5.2: Relevant material properties and CNT geometry for FEM simulations [77]

Material	Electrical resistivity $[\Omega\,\mathrm{m}]$	Diameter $[\mathrm{nm}]$	Length $[\mu\mathrm{m}]$
CNT	1×10^{-4}	50	5
Epoxy	1×10^{6}	-	-

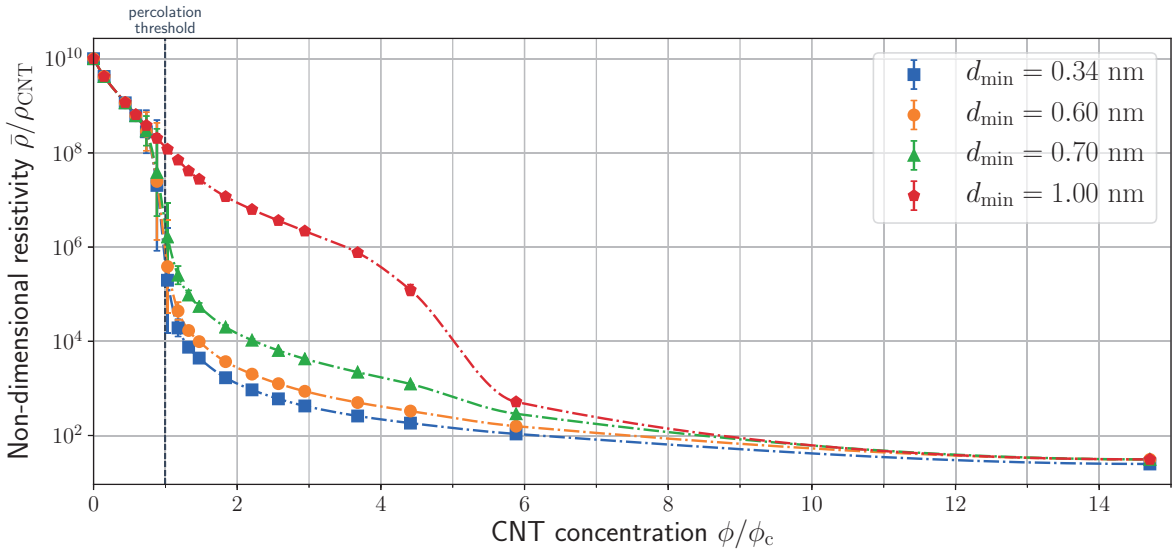

Figure 5.5: Homogenized electrical resistivity as function of the CNT concentration divided by its percolation threshold, considering different values of the minimum distance between CNTs (bars represent the standard deviation)

percolation is proportional to $(\frac{\phi}{\phi_c} - 1)^t$, where ϕ and ϕ_c are the CNT concentration and percolation threshold, respectively, and t is the power law exponent. Therefore, the composite homogenized resistivity $\bar{\rho}$ adimensionalised by the CNT resistivity is presented against the concentration ratio $\frac{\phi}{\phi_c}$.
For this system, the critical percolation threshold was found around a volume fraction of 0.68%, agreeing with the prediction obtained by the excluded volume theory [70, 80]. Results are presented for a converged RVE size of $L_{RVE} = 2 \times L_{CNT}$ and results were averaged over 20 realizations and the 3 Cartesian directions. The effect of the minimum distance between CNTs was studied by changing d_{min} varying from the van der Waals distance of 0.34 nm up to 1 nm, and the resulting composite conductivity is presented in fig. 5.5.

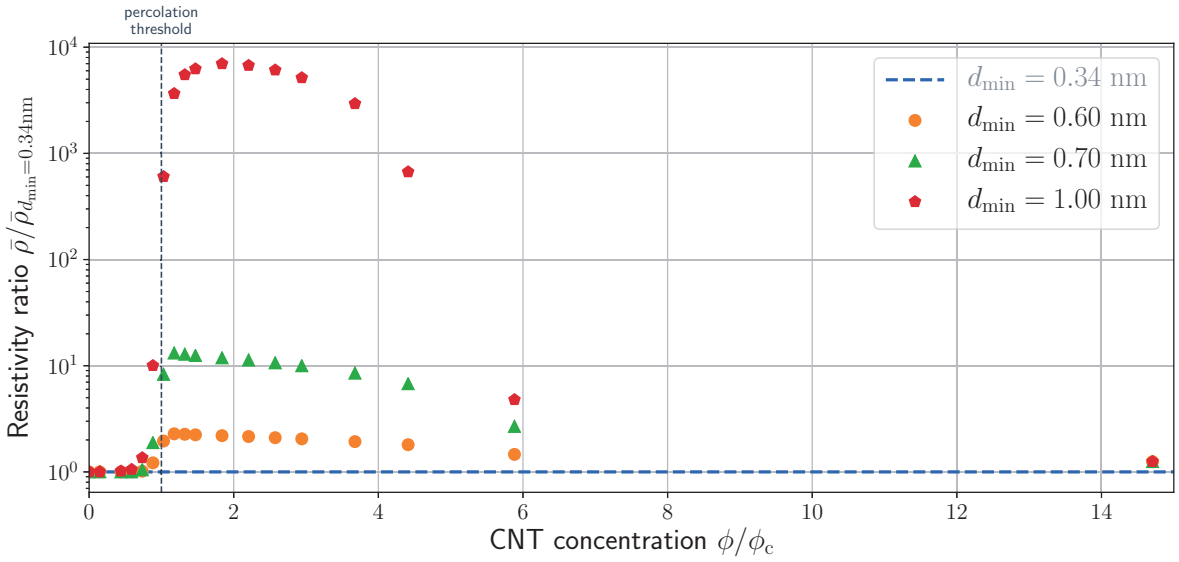

Figure 5.6: Ratio of the homogenized resistivity with respect to the minimum distance d_{min}=0.34 nm

All curves represented in figure 5.5 show the typical response of a percolation problem [81], departing from the matrix conductivity at null concentration and rapidly decreasing in resistivity (or increasing conductivity) with the CNT concentration around the percolation threshold ϕ_c. However, the decrease in resistivity around the percolation threshold becomes less abrupt for higher values of d_{min}. This is due to the fact that the junction resistivity is very high, increasing exponentially with the spacing between nanotubes [82].

The ratios between these conductivities and the one for the minimum considered (d_{min} =0.34 nm) are reproduced in fig. 5.6, illustrating the potential increase in conductivity resulting from a decrease in nanotube separation. Comparing the conductivity of the two extremes d_{min} = 0.34 nm and d_{min} =1 nm, their ratio is maximum around 90 % above the critical concentration (1.90 wt%) with a value of approximately 7×10^3. For the highest analysed concentration, this ratio decreases to 1.25.

These observations suggest that altering the processing method in a fashion that can bring dispersed CNTs together will have a much more significant effect on the resistivity change near the percolation region. At the same

time, the potential improvement in conductivity and its sensitivity to CNT concentration follows the trends observed experimentally when curing under an electric field, suggesting that this processing method alters the CNT network by influencing the CNT-CNT contact points.

5.3.3 Correlation of experimental results and finite element simulations

In the experiments with SWCNT/epoxy under electric fields presented in section 4.2, an obvious dependency of the electrical resistivity of the composites as a result of the processing method was verified. To validate the assumption that a decreased resistivity was due to an improvement of the contact between the CNTs, finite element simulations of CNT networks in a polymeric matrix were performed and their electrical resistivity was computed for several configurations (contact distances) and concentrations. By investigating the impact of infinitesimal changes on the minimum contact distance between CNTs, presented in fig. 5.5, one can conclude that a variation from 0.34 nm to 0.70 nm can promote a decrease of one order of magnitude on the overall bulk resistivity. From 0.70 nm to 1 nm, the change is even more remarkable - between two and three orders of magnitude. In other words, a sub-nanometer change on the anchoring points separating the CNTs can lead to a bulk effect of up to three orders of magnitude on the electrical properties. This provides a possible interpretation for the separate and combined effects of the curing temperature (and hence viscosity) and electric field in fig. 4.8a: both impact the distance between individual particles (i.e. contact points) leading to measurable bulk effects.
For instance, curing SWCNT/epoxy composites under the effect of AC electric fields at room temperature (second blue column in fig. 4.8a) promotes a final bulk resistivity similar to the composites without electric field but cured at higher temperatures (left orange and red columns), with a larger dispersion of results indicated by the error bar. This could reflect a comparable average contact distance between the CNTs. Yet, for the samples produced with both

AC electric fields and higher temperature (red orange and red columns), the chaining distance is further decreased at the sub-nanometer level, rendering an additional improvement of one order of magnitude on the resistivity.
Moreover, another interesting question that FE simulations allowed to explore is the impact of the contacting distance variation at different CNT concentrations. Clearly, this is related with the relative importance of the different conduction mechanisms, dominated by conductive pathways and conductivity between contacting CNTs, at different concentrations. As displayed in fig. 4.9a, even though specimens with 0.01 wt% SWCNTs have shown a decrease of one order of magnitude solely due to the effect of the electric field, such behaviour was not verified for the concentrations of 0.005 wt% and 0.1 wt%. Naturally, the questions arise: can the electrical resistivity of such composites be influenced even if the particle network is still not percolated? Moreover, if there is already a network with enough contacts for electricity to flow (i.e. above the percolation threshold), can we still improve its conductivity by promoting further chaining points? According to the FE simulations of conductive networks for different concentrations, presented in fig. 5.6, there is in fact a lower as well as an upper concentration limit where a change of the contacting distances between the CNTs has a much less pronounced effect on the bulk resistivity. This means that if the particle amount is too low, as it was the case of 0.005 wt% samples produced, improving the contact points between the particles still brings no significant improvement. On the other hand, for higher concentrations, as for the 0.1 wt% SWCNT/epoxy specimens, the particle network has already so many anchoring points that further changes do not impact much the final resistivity.
It should be emphasized that this modelling approach was meant to identify tendencies on the electrical properties of the bulk composites for changes on the above-mentioned parameters. The aspect ratio of the CNTs modelled (100) was considerably shorter than that of the CNTs used in experiments (2777) due the limiting computation effort of the simulations. Regardless, the results are presented in non-dimensional form to ease the generalization of these conclusions.

6 Conclusions

The aim of this thesis has been to investigate the possibility of reducing the electrical resistivity of epoxy nanocomposites by adjusting the processing method employed. For that, SWCNT/epoxy dispersions were produced and cured under the influence of electric fields. Different processing parameters were explored and correlated with two simulation approaches in order to deepen the understanding of the underlying phenomena and mechanisms. The main conclusions of this research are presented below.

6.1 Summary

6.1.1 Dispersion of SWCNTs and GNPs in epoxy

As a first step, epoxy nanocomposites were produced and the dispersion process was investigated and optimised for reduced electrical resistivity. The results of dispersion experiments were discussed in section 4.1. Two mixing modes in the three-roll mill were tested: keeping a small gap configuration (15-5 µm) throughout the eight passes of the mixing (constant gap mode) or starting with a comparatively large gap between the rolls (60-20 µm) and progressively decreasing it to the smallest configuration (regressive gap mode). It was found that the regressive gap mode was preferable for obtaining lower electrical resistivity both in SWCNT and GNP nanocomposites. Next the percolation of these two systems was studied by measuring the electrical resistivity of samples at different concentrations. The percolation threshold of SWCNT/epoxy was estimated to be around 0.005 wt%. GNP/epoxy was found electrically conductive above 0.75 wt%. Both materials were cured at different temperatures and it was found that higher processing temperatures

promote lower electrical resistivity. This is likely to be connected to the lower viscosity of epoxy, as rheological characterisation has shown (section 4.3.1). Additionally, adding surfactant to SWCNT/epoxy dispersions has negatively affected the electrical properties, rendering higher electrical resistivity.

6.1.2 Application of electric fields to epoxy nanocomposites during curing

Experimental set-ups were developed for the application of electric fields to epoxy nanocomposites during curing. Mould B permitted the simultaneous processing of two nanocomposite plates of $22.5 \times 12 \times 1.65$ mm: one test sample exposed to the electric field and the other as reference without the field (section 3.3.2). Mould C was designed to be scalable and suitable for resin injection of multiple samples with the possibility for different flat geometries. It was used for the simultaneous production of 6 disk samples under electric fields (section 3.3.3).

The influence of applying an electric field during the curing process of SWCNT/epoxy nanocomposites was investigated. In terms of electrical resistivity, the advantage of such process was successfully verified, with a reduction of up to one order of magnitude. We suggest that this improvement in the electrical properties was due to a field-induced orientation and assembly of the nanotubes into an enhanced conductive network. For the concentration of 0.01 wt%, a decrease of the electrical resistivity was observed for composites produced with increased field strength and frequency. Increasing the curing from room temperature to 100 ℃ also led to a reduction in the electrical resistivity of one order of magnitude. For SWCNTs, the effect of the electric field was stronger just above the percolation threshold (for 0.01 wt%).

Furthermore, the conductivity of the interface between the electrodes and the nanocomposite resin has also shown a crucial role in determining the final resistivity of the bulk materials produced under electric fields. A highly conductive interface (MR1) promoted more inhomogeneous samples, lead-

ing to pronounced changes in the resistivity at a local level (great differences between six samples produced simultaneously). On the other hand, a highly resistive interface (MR3) prevented such local differences and resulted in a smaller average resistivity in the samples produced.
The rheological behaviour of SWCNT/epoxy resins has shown that, despite the shorter curing time, at higher temperatures there is a considerable viscosity drop which might be behind the lower electrical resistivity for samples cured at 100 ℃ when compared to room temperature. The morphology of SWCNT networks in epoxy was investigated with SEM.
In addition, electric fields were applied to GNP/epoxy samples during curing and a decrease on electrical resistivity up to 80% was verified over concentrations from 0.5 wt% to 2 wt%.

6.1.3 Simulation of dielectrophoresis and CNT networks in epoxy

In section 5.2 the electric field effects were studied using a classical mechanics model based on dielectrophoresis to help interpret the experimental results, revealing an excellent agreement with the observed tendencies. Furthermore, in section 5.3, finite element simulations of CNT networks in epoxy were performed to investigate the effect of the minimum inter-nanotube distance on the bulk conductivity, providing a possible explication for the resistivity decrease found for different curing temperatures and electric fields. These simulations demonstrate that the possibility of affecting the resistivity by influencing the contact points between the particles is much more significant for a concentration range around the percolation threshold than for lower and higher concentrations.

6.2 Achievements

- SWCNT/epoxy nanocomposites with decreased electrical resistivity (up to one order of magnitude) for the same filler concentration were produced by influencing the nanostructure with electric fields
- The role of electric field parameters (strength and frequency) on the electrical resistivity of SWCNT/epoxy was investigated both *ex situ* and *in situ* and the experimental results compared with a model of interacting CNTs based on dielectrophoresis and classical mechanics
- The decrease of electrical resistivity was correlated with a reduction of the inter-particle contact distance by using a finite element model of CNT networks in epoxy. This model also made it possible to evaluate the effect of electric fields on the resistivity improvement at different concentrations
- A scalable resin injection mould for curing epoxy nanocomposites under electric fields was developed
- GNP/epoxy nanocomposites with decreased electrical resistivity (up to 80% reduction) for the same filler ratio were also produced using electric fields

6.3 Overall conclusions

This study focused on understanding the effects of applying electric fields to carbon nanotubes in a polymer system and, based on that, developing a scalable processing technology for obtaining conductive nanocomposites with improved electrical properties.
The central message is that electric fields are a powerful tool to improve and control the electrical resistivity properties of carbon nanocomposites by influencing the particle nanostructure during the processing step. The fundamental aspects of this technique were investigated for a system of epoxy

and single-walled carbon nanotubes and it has also shown potential with graphene nanoplatelets.
Such a technology would enable lowering the nanoparticle content required for attaining similar electrical properties, thereby allowing the tailoring and production of more cost-effective nanocomposites with a wide range of industrial applications such as battery, sensing, and heat management technologies.

6.4 Novelty and impact

This work focused on fundamental questions and challenges of using electric fields to manipulate CNTs in nanocomposites for improved electrical properties. Its main additions to the state-of-the-art are:

1. A scalable process for the application of electric fields to nanocomposites based on resin injection moulding was developed and tested, showing the potential to improving the electrical resistivity of these materials. This is the first discussion of such an industrial relevant process for production of nanocomposite plates under dielectrophoresis in the literature.

2. For the first time, *in situ* resistivity measurements of SWCNT/epoxy nanocomposites under electric fields were performed at different curing temperatures and correlated with rheological measurements.

3. The effect of electrode interface electrical conductivity on the resistivity of nanocomposites produced under electric field as described in this thesis had never been reported in the literature

4. This is the first documented experimental work on improvement of SWCNT networks in epoxy that has been correlated with dielectrophoresis modelling. This made it possible to understand the effect of field and processing parameters on the final resistivity of nanocomposites

5. The correlation of experimental results with finite element simulations of SWCNT networks to study the effect of sub-nanometer changes on inter-CNT contacts and thus to understand experimental measured bulk resistivity differences is unique in the literature

6.5 Future Work

The research presented here has explored the potential of electric fields for tailoring the electrical properties of nanocomposites and has pushed the boundaries of knowledge and experience in the implementation of this technology in an industrial relevant scenario. Fundamental questions such as the main electric field and processing parameters are now better understood, and a basis for the comprehension of more practical issues has been established.
Nevertheless, many points remain open to utilise the full potential of dielectrophoresis as a tool to improve electrical conductive nanocomposites. Hopefully, this investigation might inspire future studies to build upon the results presented here. Interesting future developments include:

- understanding the compromise between viscosity and electric field strength. Would dielectrophoresis of CNTs also work in more viscous polymers if stronger electric fields were applied?

- testing stronger electric fields for lower particle concentrations. Could it be that dielectrophoresis also works below the percolation threshold with stronger electric fields?

- exploring other kinds of nanoparticles and understanding the impact of their properties on dielectrophoresis. How would a multi-scale system of different nanoparticles react (e.g. CB and CNTs)?

- developing/applying characterisation tools for the visualisation of 3-dimensional networks of nanoparticles in composites.

- measuring the electrical properties of these nanocomposites in different directions (anisotropic resistivity) and in multiple cross-sections across the field direction (to study the evolution of the network propagating between the electrodes).
- developing simulation tools combining dielectrophoresis interactions of multiple CNTs (in a network) and a finite element framework where dynamic processes can be reproduced (e.g. curing of epoxy).

References

[1] Matula R.A. Electrical resistivity of copper, gold palladium and silver. *Journal of Physical Chemistry*, 8(4):1147–1298, 1979.

[2] Giancoli D.C. *Physics*. Prentice Hall, Englewood Cliffs, N.J, USA, 4th edition, 1995.

[3] Kaur G., Adhikari R., Cass P., Bown M., and Gunatillake P. Electrically conductive polymers and composites for biomedical applications. *RSC Adv.*, 5(47):37553–37567, 2015.

[4] Sweeney C.B., Lackey B.A., Pospisil M.J., Achee T.C., Hicks V.K., Moran A.G., Teipel B.R., Saed M.A., and Green M.J. Welding of 3D-printed carbon nanotube - polymer composites by locally induced microwave heating. *Sci. Adv.*, 3(6):1–7, 2017.

[5] Sharma M., Singh M.P., Srivastava C., Madras G., and Bose S. Poly(vinylidene fluoride)-based flexible and lightweight materials for attenuating microwave radiations. *ACS Applied Materials & Interfaces*, 6(23):21151–21160, 2014.

[6] Zeng Z., Jin H., Chen M., Li W., Zhou L., and Zhang Z. Lightweight and anisotropic porous mwcnt/wpu composites for ultrahigh performance electromagnetic interference shielding. *Advanced Functional Materials*, 26(2):303–310, 2016.

[7] Mahmoodi M., Arjmand M., Sundararaj U., and Park S. The electrical conductivity and electromagnetic interference shielding of injection molded multi-walled carbon nanotube/polystyrene composites. *Carbon*, 50(4):1455–1464, 2012.

[8] Yeetsorn R., Fowler M., and Tzoganakis C. A review of thermoplastic composites for bipolar plate materials in PEM fuel cells. *Nanocomposites with Unique Properties and Applications in Medicine and Industry*, pages 317–344, 2011.

[9] Lan Y., Wang Y., and Ren Z.F. Physics and applications of aligned carbon nanotubes. *Advances in Physics*, 60(4):553–678, 2011.

[10] Gohardani O., Elola M.C., and Elizetxea C. Potential and prospective implementation of carbon nanotubes on next generation aircraft and space vehicles: A review of current and expected applications in aerospace sciences. *Progress in Aerospace Sciences*, 70:42–68, 2014.

[11] Inam F., Bhat B.R., Luhyna N., and Vo T. Comparison of structural health assessment capabilities in epoxy - Carbon black and epoxy - Carbon nanotube nanocomposites. *Express Polymer Letters*, 8(1):55–61, 2014.

[12] Sharma S., Hussain S., Singh S., and Islam S.S. Mwcnt-conducting polymer composite based ammonia gas sensors: A new approach for complete recovery process. *Sensors and Actuators B: Chemical*, 194:213 – 219, 2014.

[13] Li Z., Moon K.S., Yao Y., Hansen K., Watkins K., Morato L., and Wong C. P. Carbon nanotube/polymer nanocomposites: Sensing the thermal aging conditions of electrical insulation components. *Carbon*, 65:71–79, 2013.

[14] Erik T.T., Zhifeng R., and Tsu-Wei C. Advances in the science and technology of carbon nanotubes and their composites: a review. *Composites Science and Technology*, 61(13):1899 – 1912, 2001.

[15] Sathyanarayana S. and Hübner C. *Structural Nanocomposites, Perspectives for Future Applications*, chapter Thermoplastic Nanocomposites with Carbon Nanotubes, pages 19–61. Berlin Heidelberg Springer-Verlag, 2013.

[16] Bauhofer W. and Kovacs J.Z. A review and analysis of electrical percolation in carbon nanotube polymer composites. *Composites Science and Technology*, 69(10):1486–1498, 2009.

[17] Stauffer D. and Aharony A. *Introduction to Percolation Theory*. Taylor & Francis, London, 2003.

[18] Seidel G.D. and Lagoudas D.C. Micromechanical analysis of the effective elastic properties of carbon nanotube reinforced composites. *Mechanics of Materials*, 38(8):884 – 907, 2006.

[19] Alig I., Pötschke P., Lellinger D., Skipa T., Pegel S., Kasaliwal G.R., and Villmow T. Establishment, morphology and properties of carbon nanotube networks in polymer melts. *Polymer*, 53(1):4–28, 2012.

[20] Müller M.T., Krause B., Kretzschmar B., and Pötschke P. Influence of feeding conditions in twin-screw extrusion of PP/MWCNT composites on electrical and mechanical properties. *Composites Science and Technology*, 71(13):1535–1542, 2011.

[21] Olowojoba G., Sathyanarayana S., Caglar B., Kiss-Pataki B., Mikonsaari I., Hübner C., and Elsner P. Influence of process parameters on the morphology, rheological and dielectric properties of three-roll-milled multiwalled carbon nanotube/epoxy suspensions. *Polymer (United Kingdom)*, 54(1):188–198, 2013.

[22] Olowojoba G., Sathyanarayana S., Caglar B., Mikonsaari I., Hübner C., and Elsner P. Influence of processing temperature, carbon nanotube agglomerate bulk density and functionalization on the dielectric and morphological properties of carbon nanotube / epoxy suspensions. *Proceedings of the Polymer Processing Society 29th Annual Meeting PPS-29*, 2013.

[23] Arjmand M., Apperley T., Okoniewski M., and Sundararaj U. Comparative study of electromagnetic interference shielding properties of injection molded versus compression molded multi-walled carbon nanotube/polystyrene composites. *Carbon*, 50(14):5126–5134, 2012.

[24] Yamamoto K., Akita S., and Nakayama Y. Orientation of Carbon Nanotubes Using Electrophoresis. *Japanese Journal of Applied Physics*, 35(7b):L 917– L 918, 1996.

[25] Yamamoto K., Akita S., and Nakayama Y. Orientation an durification of carbon nanotubes using ac electrophoresis. *J. Phys. D: Appl. Phys.*, 31:L34, 1998.

[26] Martin C.A., Sandler J.K.W., Windle A.H., Schwarz M.K., Bauhofer W., Schulte K., and Shaffer M.S.P. Electric field-induced aligned multi-wall carbon nanotube networks in epoxy composites. *Polymer*, 46(3):877–886, 2005.

[27] Krause B., Pötschke P., Ilin E., and Predtechenskiy M. Melt mixed SWCNT-polypropylene composites with very low electrical percolation. *Polymer (United Kingdom)*, 98:45–50, 2016.

[28] Jones T.B. *Electromechanics of Particles*. Cambridge University Press, Cambridge, 1995.

[29] Morgan H. and Green N.G. *AC Electrokinetics: Colloids and Nanoparticles*. Research Studies Press LTD, Baldock, 2003.

[30] Chen X.Q., Saito T., Yamada H., and Matsushige K. Aligning single-wall carbon nanotubes with an alternating-current electric field. *Applied Physics Letters*, 78(23):3714–3716, 2001.

[31] Krupke R., Hennrich F., Weber H.B., Beckmann D., Hampe O., Malik S., Kappes M.M., and Löhneysen H.V. Contacting single bundles of carbon nanotubes with alternating electric fields. *Applied Physics A: Materials Science and Processing*, 76(3):397–400, 2003.

[32] Kumar M.S., Kim T.H., Lee S.H., Song S.M., Yang J.W., Nahm K.S., and Suh E.K. Influence of electric field type on the assembly of single walled carbon nanotubes. *Chemical Physics Letters*, 383(3-4):235–239, 2004.

[33] Li J., Zhang Q., Peng N., and Zhu Q. Manipulation of carbon nanotubes using AC dielectrophoresis. *Applied Physics Letters*, 86:1–3, 2005.

[34] Chen Z., Yang Y.L., Chen F., Qing Q., Wu Z.Y., and Liu Z.F. Controllable interconnection of single-walled carbon nanotubes under ac electric field. *J. Phys. Chem. B*, 109(23):11420–11423, 2005.

[35] Bubke K., Gnewuch H., Hempstead M., Hammer J., and Green M.L.H. Optical anisotropy of dispersed carbon nanotubes induced by an electric fiel. *Appl Phys Lett*, 71(14):1906–8, 1997.

[36] Park C., Wilkinson J., Banda S., Ounaies Z., Wise K.E., Sauti G., Lillehei P.T., and Harrison J.S. Aligned Single-Wall Carbon Nanotube Polymer Composites Using an Electric Field. *Journal of Polymer Science: Part B: Polymer Physics*, pages 1751–1762, 2006.

[37] Zhu Y., Ma C., Zhang W., Zhang R., Koratkar N., and Liang J. Alignment of multiwalled carbon nanotubes in bulk epoxy composites via electric field. *Journal of Applied Physics*, 105(5), 2009.

[38] Yang X., Zhu Y., Ji L., Zhang C., and Liang J. Influence of AC electric field on macroscopic network of carbon nanotubes in polystyrene. *Journal of Dispersion Science and Technology*, 28(8):1164–1168, 2007.

[39] Ma C., Zhu Y.F., Yang X.Z., Ji L.J., Zhang C., and Liang J. Macroscopic networks of carbon nanotubes in PMMA matrix induced by AC electric field. *Journal of Dispersion Science and Technology*, 29(4):502–507, 2008.

[40] Oliva-Avilés A.I., Avilés F., Sosa V., Oliva A.I., and Gamboa F. Dynamics of carbon nanotube alignment by electric fields. *Nanotechnology*, 23(46):465710, 2012.

[41] Kim G., Bernholc J., and Kwon Y. Band gap control of small bundles of carbon nanotubes using applied electric fields: A density functional theory study. *Applied Physics Letters*, 97(6):063113, 2010.

[42] Osazuwa O., Kontopoulou M., Xiang P., Ye Z., and Docoslis A. Electrically conducting polyolefin composites containing electric field-aligned multiwall carbon nanotube structures: The effects of process parameters and filler loading. *Carbon*, 72:89–99, 2014.

[43] Osazuwa O., Kontopoulou M., Sabat R.G., and Docoslis A. Electrified Polyolefin/Multiwall Carbon Nanotube Composites Exhibit Dramatic Changes in Electrical Conductivity, Permittivity, and Filler Structure. *Macromolecular Materials and Engineering*, 300(4):448–457, 2015.

[44] Oliva-Avilés A. I., Avilés F., Sosa V., and Seidel G.D. Dielectrophoretic modeling of the dynamic carbon nanotube network formation in viscous media under alternating current electric fields. *Carbon*, 69:342–354, 2014.

[45] Monti M., Natali M., Torre L., and Kenny J.M. The alignment of single walled carbon nanotubes in an epoxy resin by applying a DC electric field. *Carbon*, 50(7):2453–2464, 2012.

[46] Chung J.and Lee K., Lee J., and Ruoff R. Toward Large-Scale Integration of Carbon Nanotubes. *Langmuir*, (17):3011–3017, 2004.

[47] Sarker B.K., Islam M.R., Alzubi F., and Khondaker S.I. Fabrication of Aligned Carbon Nanotube Array Electrodes for Organic Electronic Devices. *Materials Express*, 1(1):80–85, 2011.

[48] Sun W., Tomita H., Hasegawa S., Kitamura Y., Nakano M., and J. Suehiro. An array of interdigitated parallel wire electrodes for preparing a large-scale nanocomposite film with aligned carbon nanotubes. *Journal of Physics D: Applied Physics*, 44(44), 2011.

[49] Felisberto M., Arias-Durán A., Ramos J.A., Mondragon I., Candal R., Goyanes S., and Rubiolo G.H. Influence of filler alignment in the mechanical and electrical properties of carbon nanotubes/epoxy nanocomposites. *Physica B: Condensed Matter*, 407(16):3181–3183, 2012.

[50] Romyen N., Thongyai S., and Praserthdam P. Alignment of Carbon Nanotubes in Polyimide Under Electric and Magnetic Fields. *Appl. Polym. Sci.*, 123:3470–3475, 2012.

[51] Wu S., Ladani R.B., Zhang J., Bafekrpour E., Ghorbani K., Mouritz A.P., Kinloch A.J., and Wang C.H. Aligning multilayer graphene flakes with

an external electric field to improve multifunctional properties of epoxy nanocomposites. *Carbon*, 94:607–618, 2015.

[52] Remillard E.M., Zhang Q., Sosina S., Branson Z., Dasgupta T., and Vecitis C.D. Electric-field alignment of aqueous multi-walled carbon nanotubes on microporous substrates. *Carbon*, 100:578–589, 2016.

[53] Nguyen J., Contera S, and Garcia I.L. Magneto-electrical orientation of lipid-coated graphitic micro-particles in solution. *RCS Advances*, 6:46643, 2016.

[54] Knite M., Linarts A., Ozols K., Tupureina V., Stalte I., and Lapcinskis L. A study of electric field-induced conductive aligned network formation in high structure carbon black/silicone oil fluids. *Colloids and Surfaces A: Physicochemical and Engineering Aspects*, 526:8–13, 2017.

[55] OCSiAl LTD. *Tuball, Technical Datasheet*. Available: `https://ocsial.com/assets/documents/TDS_TUBALL_1.pdf`, last accessed March 3, 2020.

[56] Lange+Ritter GmbH, Gerlingen, Germany. *Epikote Resin MGS RIMR426, Technical Datasheet*, 2017.

[57] Keysight Technologies. *Make Better AC RMS Measurements with your Digital Multimeter, Application Note*. Available: `https://www.keysight.com/de/de/assets/7018-01113/application-notes/5988-6916.pdf`, last accessed August 12, 2019.

[58] Djurdjevic D. *Identifizierung geeigneter Methoden für die elektrische Charakterisierung von Dünnschichten*. Master Thesis, Fraunhofer Institut für Produktionstechnik und Automatisierung IPA und Reinhold-Würth-Hochschule, 2015.

[59] Geng Y., Liu M.Y., Li J., Shi X.M., and Kim J.K. Effects of surfactant treatment on mechanical and electrical properties of CNT/epoxy nanocomposites. *Composites Part A: Applied Science and Manufacturing*, 39(12):1876–1883, 2008.

[60] Wang J., Yu S., Luo S., Chu B., Sun R., and Wong C.-P. Investigation of nonlinear i-v behavior of cnts filled polymer composites. *Materials Science and Engineering: B*, 206:55–60, 2016.

[61] Socher R., Krause B., Müller M.T., Boldt R., and Pötschke P. The influence of matrix viscosity on MWCNT dispersion and electrical properties in different thermoplastic nanocomposites. *Polymer*, 53(2):495–504, 2012.

[62] Krestinin A.V.and Dremova N.N., E.I. Knerel'man, Blinova L.N., Zhigalina V.G., and Kiselev N.A. Characterization of swcnt products manufactured in russia and the prospects for their industrial application. *Nanotechnologies in Russia*, 10(7):537–548, 2015.

[63] Oliva-Avilés A.I., Avilés F., and Sosa V. Electrical and piezoresistive properties of multi-walled carbon nanotube/polymer composite films aligned by an electric field. *Carbon*, 49(9):2989–2997, 2011.

[64] Oliva-Avilés A.I., Zozulya V.V., Gamboa F., and Avilés F. Dynamic evolution of interacting carbon nanotubes suspended in a fluid using a dielectrophoretic framework. *Physica E: Low-Dimensional Systems and Nanostructures*, 83:7–21, 2016.

[65] Morais M.V.C., Oliva-Avilés A.I., Matos M.A.S., Tagarielli V.L., Pinho S.T., Hübner C., and Henning F. On the effect of electric field application during the curing process on the electrical conductivity of single-walled carbon nanotubes-epoxy composites. *Carbon*, 150:153 – 167, 2019.

[66] Ebbesen T. W., Lezec H.J., Hiura H., Bennett J. W., Ghaemi H.F., and Thio T. Electrical conductivity of individual carbon nanotubes. *Nature*, 382:54–56, 1996.

[67] Laurent C., Flahaut E., and Peigney A. The weight and density of carbon nanotubes versus the number of walls and diameter. *Carbon*, 48(10):2994–2996, 2010.

[68] Castellano R.J., Akin C., Giraldo G., Kim S., Fornasiero F., and Shan J.W. Electrokinetics of scalable, electric-field-assisted fabrication of vertically aligned carbon-nanotube/polymer composites. *Journal of Applied Physics*, 117(21):214306, 2015.

[69] Smith B.D., Mayer T.S., and Keating C.D. Deterministic assembly of functional nanostructures using nonuniform electric fields. *Annual Review of Physical Chemistry*, 63:241–263, 2012.

[70] Matos M.A.S., Tagarielli V.L., Baiz-Villafranca P.M., and Pinho S.T. Predictions of the electro-mechanical response of conductive CNT-polymer composites. *Journal of the Mechanics and Physics of Solids*, 114:84–96, 2018.

[71] Girifalco L.A. Hodak M. and Lee R. S. Carbon nanotubes, buckyballs, ropes, and a universal graphitic potential. *Physical Review B*, 62(19):104–110, 2000.

[72] Dassault Systèmes - Simulia, Johnston, Rhode Island, USA. *Abaqus 2018 Documentation*, 2018.

[73] Reddy J.N. *An Introduction To The Finite Element Method*. McGraw-Hill, New York, USA, 2006.

[74] Dassault Systèmes - Simulia, Johnston, Rhode Island, USA. *Abaqus User Subroutines Guide*, 2018.

[75] Ventra M.D. *Electrical Transport in Nanoscale Systems*. Cambridge University Press, Cambridge, UK, 2008.

[76] Simmons J.G. Generalized Thermal J V Characteristic for the Electric Tunnel Effect. *Journal of Applied Physics*, 9(35):2655–2658, 1964.

[77] Hu N., Karube Y., Yan C., Masuda Z., and Fukunaga H. Tunneling effect in a polymer/carbon nanotube nanocomposite strain sensor. *Acta Materialia*, 56(13):2929–2936, 2008.

[78] Shiraishi M. and Ata M. Work function of carbon nanotubes. *Carbon*, 39(12):1913–1917, 2001.

[79] Matos M.A.S., Pinho S.T., and Tagarielli V.L. Predictions of the electrical conductivity of composites of polymers and carbon nanotubes by an artificial neural network. *Scripta Materialia*, 166:117 – 121, 2019.

[80] Balberg I., Anderson C.H., Alexander S., and Wagner N. Excluded volume and its realtion to the onset of percolation. *Phsical Review B*, 30(7):3933–3943, 1984.

[81] Sahimi M. *Applications Of Percolation Theory*. Taylor & Francis, London, 2003.

[82] Simmons J.G. Generalized Formula for the Electric Tunnel Effect between Similar Electrodes Separated by a Thin Insulating Film. *Journal of Applied Physics*, 6(34):1793, 1963.

[83] Chandra H., Allen S.W., Oberloier S.W., Bihari N., Gwamuri J., and Pearce J.M. Open-source automated mapping four-point probe. *Materials*, 10(2), 2017.

[84] L. B. Valdes. Resistivity measurements on germanium for transistors. *Proceedings of the IRE*, 42(2):420–427, 1954.

[85] d'Heurle F. and Ames I. Electromigration in single-crystal aluminium films. *Applied Physics Letters*, 16(2):80–81, 1970.

[86] Romanus H. *Siliziumkarbidelektronik - Technologische und Werkstofftechnische Untersuchungen zur Metalisierung-Kontaktierung*. Dissertation, Technische Universität Ilmenau, 2003.

A Appendix - Electrical resistance measurements

A.1 Four-point method correction factors

The four-point method for calculating the resistance assumes an ideal infinitely large area and thickness of the test specimen. This is not applicable to most realistic cases, since the possible current paths in the sample are limited by the vicinity of boundaries. Therefore, the theoretical formulas should be corrected with a correction factor F [83]. This can be computed by combining three different correction factors [84]:

$$F = F_1 F_2 F_3 \tag{A.1}$$

These correction factors are dependent on (see figure 3.6):

- Thickness d of the layer (F_1)
- Ratio of the diagonal D of the surface to tip distance s_R (F_2)
- Position of the measuring tips on the sample (F_3)

F_1 depends on the conductivity of the bottom surface of the probe. For simplicity, one can assume a non-conductive bottom surface such as glass [85]:

$$F_{11} = \frac{\frac{d}{s_R}}{2\ln\left[\frac{\sinh\frac{d}{s_R}}{\sinh\frac{d}{2s_R}}\right]} \tag{A.2}$$

F_2 takes into account the sample size, being divided in F_{21} for circular wafers of diameter D and F_{22} for rectangular shapes with diagonal D:

$$F_{21}, F_{22} = \frac{\ln 2}{\ln 2 + \ln\left[\frac{\left(\frac{D}{s_R}\right)^2 + 3}{\left(\frac{D}{s_R}\right)^2 - 3}\right]} \tag{A.3}$$

F_3 is calculated using distances s_R between pins and a_R from pins to edge of the specimen. From the linear arrangement of the measuring tips, the distance from the edge can be determined in two different directions. This is represented in figure A.1.

For a non-conductive substrate, the two related correction factors F_{31} and F_{32}, for an arrangement according to figures A.1a and A.1b, respectively, can be computed with:

$$F_{31} = \frac{1}{1 + \frac{2}{\sqrt{1+\left(\frac{2a_R}{s_R}\right)^2}} - \frac{1}{\sqrt{1+\left(\frac{a_R}{s_R}\right)^2}}} \tag{A.4}$$

$$F_{32} = \frac{1}{1 + \frac{1}{1+\frac{2a_R}{s_R}} - \frac{1}{2+\frac{2a_R}{s_R}} - \frac{1}{4+\frac{2a_R}{s_R}} - \frac{1}{5+\frac{2a_R}{s_R}}} \tag{A.5}$$

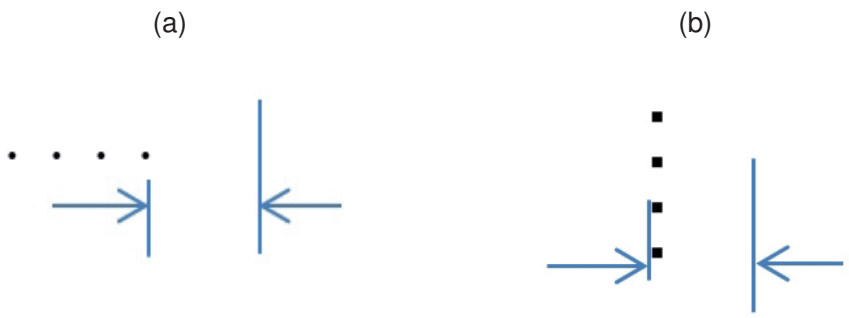

Figure A.1: Two different arrangements for definition of distance a_R from the pins to the edge of sample

Samples analysed with the four-point method (produced with mould A) had a thickness of d= 2 mm, and a distance between the sensing pins of s_R= 2 mm. Substituting d and s_R in equation A.2 leads to:

$F_1 = F_{11} = 0.6148$

As for factor F_2, a rectangular shape scenario with diagonal D= 40 mm was considered. From equation A.3 one obtains:

$F_2 = 0.9788$

According to [86], in most four-point probe measurements factor F_3 is negligible since it reduces to unity. In this case, substituting the values in equations A.4 and A.5 one gets:

$F_{31} = 0.9999$

$F_{32} = 0.9587$

$F_3 = F_{31}F_{32} = 0.9576$

And hence the correction factor F results:

$F = F_1F_2F_3 = 0.6148 \times 0.9576 \times 0.9788 = 0.5762$

Finally, the bulk resistivity in Ω cm of samples measured using the four-point method can be computed using the relation $\rho = R \times F$, where R is the resistance measured.

A.2 Validation of resistivity measurements with known resistances

For validating the *in-situ* conductivity measurements, resistors of 10 kΩ, 99.1 kΩ and 1.2 MΩ were connected to the alignment/measuring electronic setup in order to verify the significance of the resistance values measured *in situ*. For this, a signal of 30 V_{pp} @ 45 MHz with 1 V_{DC} was tested (highest frequency possible with the power amplifier used)). Figure A.2 shows the good accordance of the measured and actual values of the resistors tested as well as the stability of the measurement.

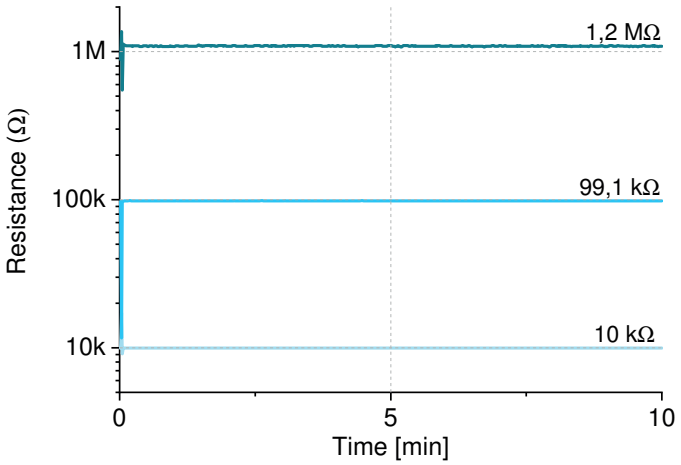

Figure A.2: *In situ* conductivity measurements - plot of different resistances measured with 1 V_{DC} offset during application of 30 V_{pp} @ 45 MHz

A.3 Influence of DC offset on resistivity of SWCNT/epoxy composites

Figure A.3 shows the comparison of the final resistivity of samples cured under the influence of a 6.5 V_{RMS}/mm @10 MHz electric field with and without the DC offset, together with the respective reference samples with no electric field. Both specimens cured under electric field show a clear decrease in the final resistivity in comparison with reference counterparts, with only a slight difference between them. This suggests that adding the DC offset to an AC test signal does not significantly affect the results, as suggested through the computed total RMS voltage in section 3.4, and hence provides a practical method to follow the behaviour of *in-situ* resistivity during electric field experiments.

A.4 Influence of frequency on resistivity of SWCNT/epoxy composites

For further understanding the impact of electric field frequency on the DC resistivity of SWCNT networks in epoxy (see fig. 4.7), a frequency sweep

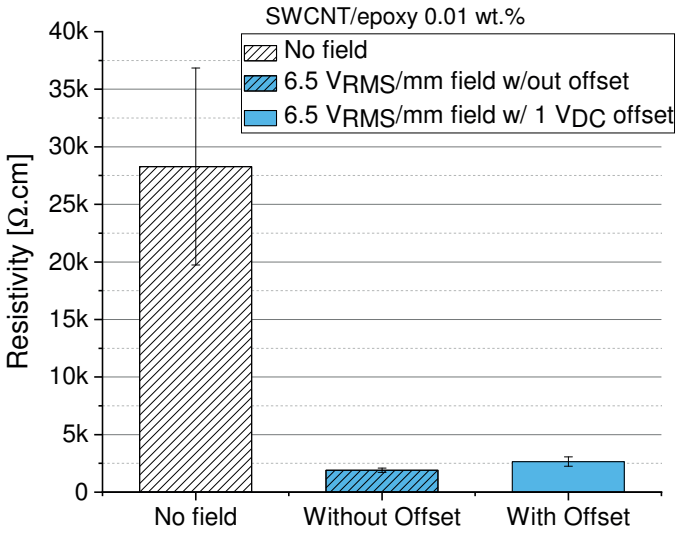

Figure A.3: Resistivity of samples subjected to an alternated electric field of 6.5 V_{RMS}/mm @10MHz (30 V_{pp}) during the curing process with and without 1 V_{DC} offset

(6.5 V_{RMS}/mm with 1 V_{DC} offset was performed 10 times on SWCNT/epoxy 0.01 wt%. Figure A.4 displays the DC resistance of SWCNT/epoxy 0.01 wt% resin without curing agent as the frequency of the AC field (to influence the particle network) is varied. The lighter curve (#1) represents the first sweep and the darkest (#10) the last. The red curve stands for the frequency sweep performed. Here it is clear that the DC resistivity of SWCNT/epoxy resin highly depends on the frequency of the applied electric field. Lower frequencies led to lower resistance values, as it is noticeable by the step increase in frequency from 1 Hz to 100 kHz. Above 100 kHz, for 1 MHz, 10 MHz and 45 MHz, no apparent difference on the resistance was verified.

This is believed to be due to the ionic conductivity of the epoxy matrix at lower frequencies, allowing for charges to flow across the resin and hence rendering a lower resistance of the whole system. As frequency is increased, less charges are able to flow through the epoxy matrix, leading to a higher resistance of the whole SWCNT/epoxy system. Interestingly, this threshold between 10 kHz and 100 kHz perfectly matches the plateau frequency observed for the resistivity measurements of SWCNT/epoxy 0.01 wt% cured at different frequencies (see figure 4.7). At higher frequencies (i.e. above

10 kHz), the epoxy matrix does not contribute to the conductivity, meaning all the electrical energy applied is transferred through the SWCNTs, promoting interactions between them as described in section 5.2. This experimental result is in perfect accordance with the evolution of the real part of the polarisation factor α^*, which also reaches a plateau at around 10 kHz (see figure 5.2).

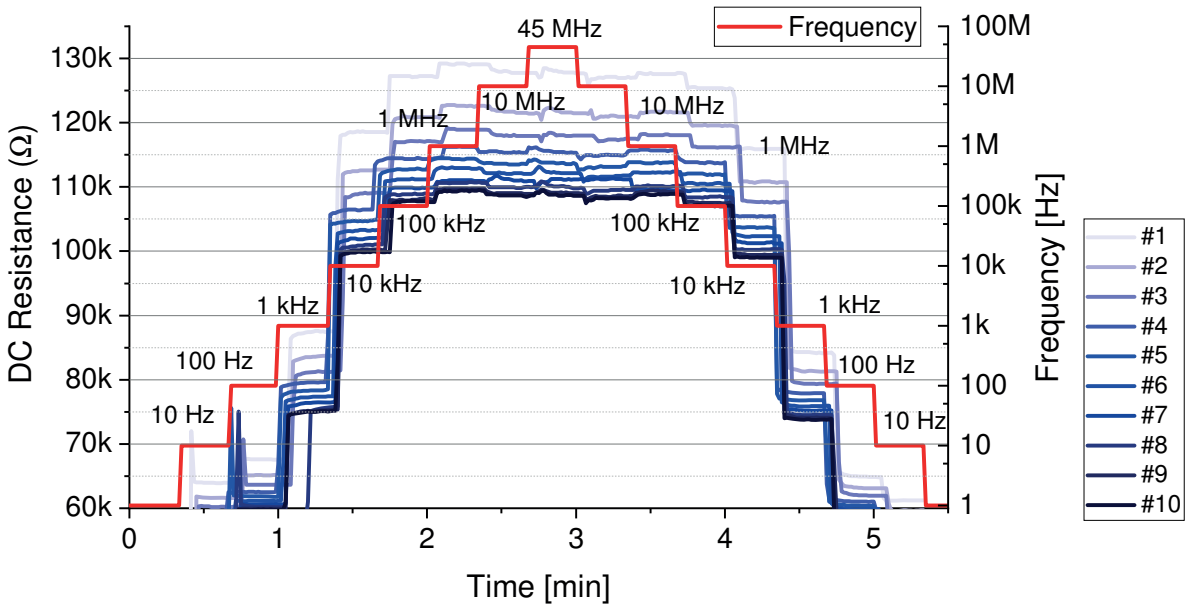

Figure A.4: Frequency dependant resistance of SWCNT/epoxy resin (without curing agent) - frequency sweep performed 10 times (lighter to darker lines)

B Appendix - Temperature effects

B.1 Isolation of temperature effects

Figure B.1 displays the results of further electric field experiments performed with epoxy/SWCNTs 0.01 wt% nanocomposites at 140 °C (in mould B).

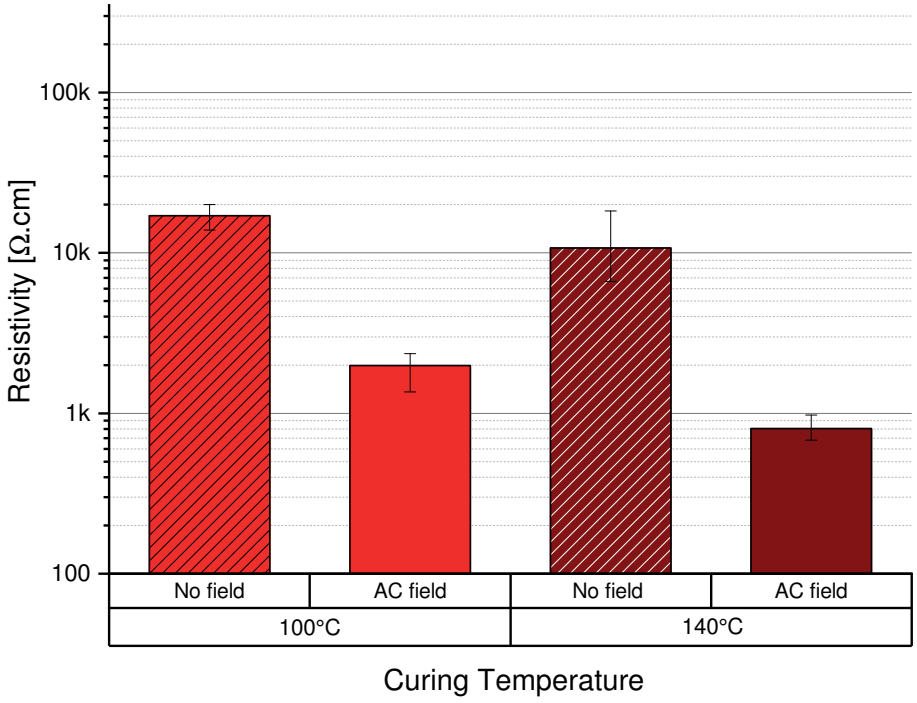

Figure B.1: Impact of AC electric field (6.5 V_{RMS}/mm @ 10 MHz) during curing at 100 °C and 140 °C on the through-plane electrical resistivity of epoxy/SWCNTs 0.01 wt% nanocomposites (mould B)

List of publications & dissemination

Peer-reviewed journal publications

[1] Morais M.V.C., Reidel R., Weiss P., Baumann S., Hübner C., and Henning F. Integration of electronic components in the thermoplastic processing chain: possibilities through additive manufacturing using conductive materials. *2018 13th International Congress Molded Interconnect Devices (MID)*, Würzburg, 1–4, 2018

[2] Morais M.V.C., Oliva-Avilés A.I., Matos M.A.S., Tagarielli V.L., Pinho S.T., Hübner C., and Henning F. On the effect of electric field application during the curing process on the electrical conductivity of single-walled carbon nanotubes-epoxy composites. *Carbon*, 150:153–167, 2019

[3] Morais M.V.C., Marcellan M., Sohn N., Hübner C., and Henning F. Process Chain Optimization for SWCNT/Epoxy Nanocomposite Parts with Improved Electrical Properties. *J. Compos. Sci., 4*, 114, 2020

Conference abstracts

[1] Morais M.V.C., Schönwald M., Mikonsaari I. and Hübner C., Alignment of carbon nanoparticles in composites with electric fields, *Third NanoCarbon Annual Conference 2017*, Würzburg, Germany, February 21 and 22, 2017 – poster – second place for best poster award

[2] Morais M.V.C., Schönwald M., Mikonsaari I. and Hübner C., Alignment of carbon nanoparticles in composites with electric fields, *PPS2017, Europe Africa Conference 2017 of the Polymer Society*, Dresden, Germany, June 26 to 29, 2017 – poster

[3] Morais M.V.C., Schönwald M., Mikonsaari I. and Hübner C., Manipulation of carbon nanotubes in composites with electric fields, poster and presentation *Fourth NanoCarbon Annual Conference 2018*, Würzburg, Germany, February 27 and 28, 2018 – oral presentation and poster – **best poster award**

[4] Morais M.V.C., Reidel R., Weiss P., Baumann S., Hübner C., and Henning F. Integration of electronic components in the thermoplastic processing chain: possibilities through additive manufacturing using conductive materials. *2018 13th International Congress Molded Interconnect Devices (MID)*, Würzburg, 1–4, 2018 – oral presentation

[5] Morais M.V.C., Reidel R., Weiss P., Baumann S., Hübner C., and Henning F. Integration of electronic components in thermoplastic processing chain: possibilities through additive manufacturing. *Fifth NanoCarbon Annual Conference 2019*, Würzburg, Germany, February 26 and 27, 2019 – oral presentation and poster

[6] Morais M.V.C, Hübner C. and Henning F., Manipulation of single-walled carbon nanotubes in composites with electric fields. *CNPCOMP2019: The 8th International Conference on Carbon NanoParticle Based Composites*, London, United Kingdom, June 16, 2019 – oral presentation

[7] Morais M.V.C, Matos M., Hübner C. and Henning F., Manipulation of carbon nanoparticles in composites during processing for improved electrical properties. *Deutsche Gesellschaft für Materialkunde (DGM) - MSE Congress 2020*, Online Conference, September 22, 2020 – oral presentation

Invited lectures

[1] Alignment of carbon nanoparticles in composites with electric fields – Lecture at the Leibniz-Institute of Polymer Reserch Dresden (IPF), Dresden, Germany, June 20, 2017

Outreach

[1] Accelerating R&D: Synergies between disciplines in nanomaterial research – Interactive workshop organised by TheLink project, *PPS2017, Europe Africa Conference 2017 of the Polymer Society*, Dresden, Germany, June 27, 2017

In this work, the electrical properties of epoxy nanocomposites with carbon nanoparticles as conductive filler are investigated for different processing conditions.

Compared to a classical shaping process for epoxy materials, the application of electric fields during the curing process is used as an additional process parameter. Electric fields are applied to the nanocomposites during curing, influencing the electrical properties of the final material. This phenomenon is studied for a system of single-wall carbon nanotube and the impact of processing parameters on the electrical response of the system is evaluated.

A scalable process based on resin transfer moulding for producing nanocomposites under electric fields is developed.

This processing technique presents promising results for enhancing and tailoring the electrical conductivity of polymer nanocomposites.

ISSN 0933-0062

Editor:
Fraunhofer Institute for Chemical Technology ICT
Joseph-von-Fraunhofer-Strasse 7
76327 Pfinztal (Berghausen)
Phone +49 721 4640-0
Fax +49 721 4640-111
info@ict.fraunhofer.de
www.ict.fraunhofer.de

ISBN 978-3-8396-1685-7